MASTER

Feasibility study for the use of a Floating-Electrode Dielectric Barrier Discharge for skin disinfection in the context of neonatal sepsis

Kruyen, A.H.J.

Award date:
2013

Link to publication

Eindhoven University of Technology
Department of Applied Physics
Elementary Processes in Gas Discharges (EPG)
&
Maxima Medisch Centrum Veldhoven
Vrouw Moeder Kind-Centrum
Neonatale Intensive Care Unit (NICU)

Feasibility study for the use of a Floating-Electrode Dielectric Barrier Discharge for skin disinfection in the context of neonatal sepsis

A.H.J. Kruyen

July, 2013 EPG 13-

Supervisors:

prof. dr. Gerrit Kroesen
prof. dr. Peter Bruggeman
prof. dr. Sidarto Bambang Oetomo
Bouke Boekema PhD

Abstract

A preliminary in vitro feasibility study for the use of a Floating-Electrode Dielectric Barrier Discharge (FE-DBD) plasma source to induce skin disinfection in the context of preventing neonatal sepsis is performed. The FE-DBD is a copper electrode, enclosed in an insulating material and a thin plate of quartz. The quartz is placed parallel above the substrate which is to be disinfected and is used as secondary electrode. Short damping kHz voltage pulses are fed to the electrode, which leads to filamentary microdischarges between the quartz and the substrate. By changing the pulse frequency, pulse width, duty cycle, gap distance and the to be treated surface, the properties of the plasma formed between the quartz and the substrate are affected. For different settings of these five variables, the relative light intensity, maximum voltage in one pulse and power dissipation in the plasma are studied. FTIR spectrometry is used to get quantitative insight in the chemistry in the discharge, but the path length was too short to obtain species densities.

The effect of treatment of a FE-DBD on bacteria and skin is investigated. *Staphylococcus aureus* are placed with small drops on cover glass and treated for different settings. The inactivation of *S. aureus* is more effective and there is more light emission when the power dissipation in the plasma is higher. Also human skin with *S. aureus* is treated, the inactivation of bacteria is less effective. The inactivation of *S. aureus* is compared with the inactivation of three other staphylococci which are also found in neonates with sepsis and it is similar. Treatment of the skin did not show any clear difference in metabolic activity of the skin cells. The growth of the skin cells seems even to be stimulated for a more intense treatment. Histology shows local damage in the skin samples, the damage is very small and are therefore not causing a visible drop in the metabolic activity. The skin samples are not completely flat, a higher part of the skin will have a higher impact of discharges, which will cause this local damage.

The detrimental effects on skin are a cause of concerns and the investigation of a plasma source that does not use the neonatal skin as second electrode is recommended based on the outcome of this study. A lot of research needs

to be done to develop a safe and practical plasma source.

Contents

Chapter 1

Introduction

In the Netherlands, 160 to 210 thousand children are born every year [1]. Normally a child is born after 37-42 weeks of pregnancy. However, some children are born prematurely and viable, in a period of 22 till 37 weeks of the pregnancy [2]. In 2010 approximately 14.000 children were born too early, of whom one fifth before the 32th week of the pregnancy [3].

In this chapter the special care these premature born children are receiving to survive is outlined. The problem of catheter related-bloodstream infections in premature born children leading to sepsis is discussed. The use of a cold atmospheric plasma (CAP) source, which disinfects the skin around the catheter, may be a solution to decrease the number of cases with sepsis. The possible effective agents of such a CAP in the process of disinfection are discussed. In the end of the chapter the outline for the report is given.

1.1   The care of premature children

In order to enhance the survival of a premature newborn infant, it is placed in a special department of a hospital: the Neonatal Intensive Care Unit (NICU). Here the premature lies within a neonatal incubator. In figure 1.1 an example of such a incubator is shown. The air in the incubator is constantly filtered and germs are kept outside to limit the chance of infections. Besides that, the humidity and temperature are regulated in the incubator, in order to prevent cooling and great loss of water from skin and respiratory evaporation [5, 6, 7]. The humidity is between 40% to 85% and the temperature between 30 ° C and 37 ° C, depending on the age of the premature and for instance skin problems [8]. To limit the amount of stress for the newborns, the light should be dimmed, and circadian and noise in the incubator should be prevented as much as possible [9, 10, 11].

Figure 1.1: *An example of an incubator, a "Giraffe Incubator", for a good healing environment for a premature newborn. [4]*

Besides the environmental control of the incubator, the premature is monitored and helped with respiration and nutrition. During its time in the incubator the oxygenation, cardiac function, temperature, and brain activity of the premature are constantly monitored [12, 13]. Most prematures need help with respiration, since their lungs are not fully developed yet [14]. The prematures need special help with nutrition, since they can not yet suck or swallow [15]. Via a catheter the prematures are given nutrition, but also medication and water. The fluids with this nutrition have a high concentration and need therefore be supplemented in a large vein, to dilute the fluid and prevent irritations.

There are two types of catheters used for the supplementation of the nutrition. Firstly, the Umbilical Venous Catheter (UVC) shown on the left in figure 1.2. This catheter is connected with the umbilical cord. Such a catheter is placed maximum 1-3 days after the birth. After this time, the end of the umbilical is dried. As a consequence it is not possible anymore to insert a UVC. Another possible catheter is the Central Venous Cathether (CVC), which is shown on the right of figure 1.2. This catheter is inserted in a limb and the catheter tip ends in a large vein. Both catheters stay in the premature for 7 till 10 days and they are removed prematurely when there are complications, or when the infants tolerate feeding by the digestive system. One of these complications of venues catheters are catheter related-
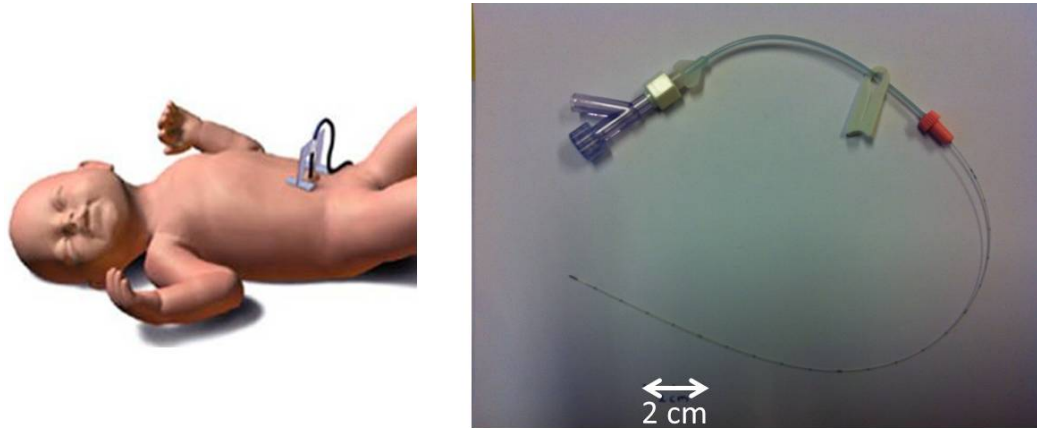
Figure 1.2: *On the left an infant with an Umbilical Venous Catheter (UVC) [16]. On the right a Central Venous Catheter (CVC) with stylet from VYGON*

bloodstream infections (CRBI) [17, 18, 19].

The skin is disinfected before the catheter is inserted under sterile conditions and a transparent dressing, a tegaderm is placed to cover the catheter. The tegaderm has two functions, holding the catheter on its place and protecting the wound. However, bacteria are not stopped by the tegaderm and grow underneath this transparent dressing, enter the bloodstream and cause a CRBI. The most common bacteria associated with CRBI are the coagulase[1]-negative staphylococci [20, 21, 22].

1.2 Coagulase-negative staphylococci

Staphylococci are gram-positive, which means that they have a single membrane around their cell which is covered with a thick peptidoglycan layer[2]. This plasma membrane encloses the cell, it defines its boundaries. The membrane is a very thin film of lipid and protein molecules, which are held together mainly by non-covalent interactions. The protein molecules in the membrane can act as sensor for external signals, like chemical signals, allowing the cell to change its behavior in response to changes in the environment. Some proteins in the membrane also transport specific molecules across the membrane. The cell membrane is not fixed: most of its molecules can move

---

[1]A protein produced by a bacteria that enables the conversion of fibrinogen to fibrin, this results in clotting of the blood.

[2]A polymer consisting sugars and amino acids. It gives the cell wall structural strength and counteracts the osmotic pressure from the cytoplasm in the cell.
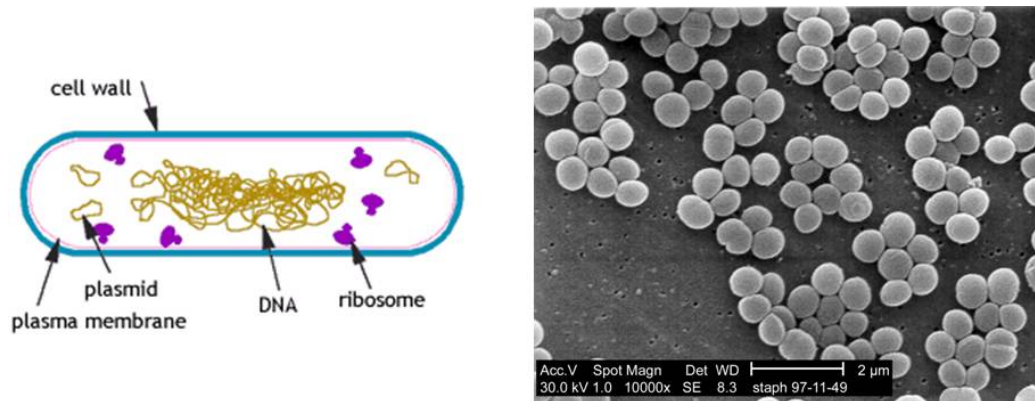
Figure 1.3: *On the left a generalized structure of bacteria [24] on the right a SEM showing a strain of Staphylococcus aureus bacteria [25].*

around in the plane of the membrane [23].

On the left of figure 1.3 the general structure of a bacterium cell is shown. Inside a bacterium, different organelles are responsible for the production of enzymes, converting energy or for the genetic code. On the right of figure 1.3 an image of staphylococcus aureus captured with a Scanning Electron Microscope (SEM) is shown.

There are approximately 20 staphylococci, important pathogens for the CRBI are the staphylococcus aureus, capitis, epidermidis and hominis. These bacteria normally live in harmony on the skin of humans, but can cause severe infections in humans [26, 27]. Sick premature neonates are biologically vulnerable for these bacteria since their immune system is immature [28, 14]. When the premature gets infected by these bacteria, neonatal sepsis can develop.

1.3 Neonatal sepsis

When bacteria cross the skin of the neonate as natural border, they can enter the blood stream so that neonatal sepsis can develop. A sepsis is characterized by a whole-body inflammatory state, common symptoms include high fevers, elevated heart rate and hyperventilation. Sepsis may lead to death, disabilities at a later age, a lot of stress for the premature and an inhibition of the growth [29]. Approximately 1 out of 10 premature born children in the Netherlands are tested positive for a bacterial infection which leads to sepsis [30] and around 10% of the prematures with sepsis do not survive the disease [29, 20]. The amount of cases with sepsis can be reduced by adjusting the quality in the NICU: nurses have to be consistent in washing their hands;

the time an umbilical catheter is placed should be limited; or the placing of the catheter or changing the infusion bag should be in a maximum sterile situation [28, 14]. However, an active way has to be found to inactivate the bacteria around the wound to eliminate the chance of sepsis to almost zero. The treatment with a plasma could be the answer for this active inactivation of the bacteria without affecting the skin itself.

1.4 Plasmas for disinfection

The use of plasma in a hospital for the sterilization of materials is not new. However, the use of an atmospheric plasma at room temperature to treat a patient directly in the hospital is new. The field of plasma science where a Cold Atmospheric Plasma (CAP) is used in the biology and medicine is titled: 'Plasma Medicine'. Multiple potential applications of plasmas in Plasma Medicine are known: treatment of burn wounds, treatment of ulcers, treatment of dental cavities, hand sterilization, tooth bleaching, or skin rejuvenation. In these applications the skin or tooth is disinfected and/or the proliferation of the skin is improved. Why microorganisms are killed and why the skin is stimulated to grow faster is not understood completely. The ideal plasma sources for specific treatments are not defined yet. A lot of research has to be performed to make sure the treatment is safe and to understand the processes playing a role in plasma medicine. [31, 32, 33, 34, 35, 36, 37, 38].

1.4.1 Possible Cold Atmospheric Plasma (CAP) sources to disinfect the neonatal skin

There are multiple sources developed for Plasma Medicine, which can be categorized in three categories [31, 39, 40, 41]. First, there are sources that create a plasma near the skin, an example of such a source is shown in figure 1.4 [42, 45]. Second, sources are developed that create a plasma which is transported to the skin with a gas flow, in figure 1.5 two configurations of such sources are shown [43, 46, 47, 48]. Finally, there are sources where the skin is one of the electrodes, in figure 1.6 an example of such a source is given [35, 42, 49, 44, 50]. In the latter a small current is going through the skin. For all three sources the plasmas can be produced by discharges in air, in noble gases or in any desired mixture in order to produce favorable atoms, ions and molecules for the biomedical applications.

When a plasma source is used to disinfect the skin around the catheter to prevent neonatal sepsis, the treatment should be absolutely safe, bacteria should be killed, but the skin should be unaffected. The skin of premature
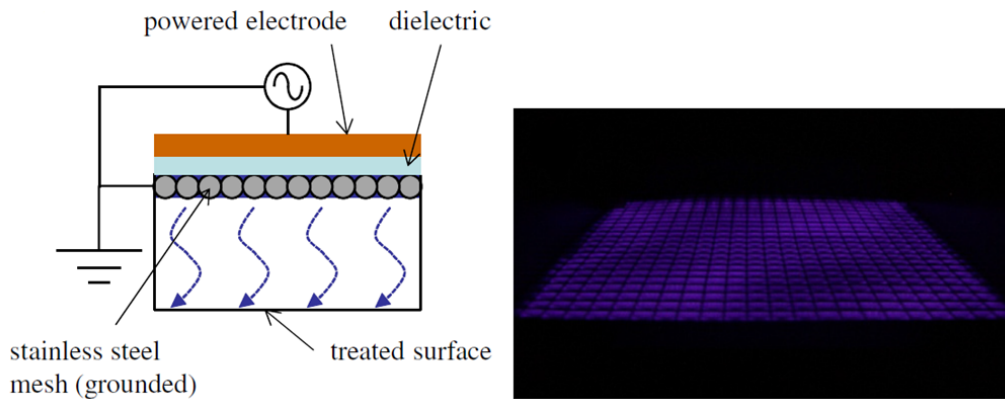
Figure 1.4: *On the left a schematic diagram of a surface microdischarge (SMD) and on the right a photograph of emission from a SMD taken from Sakiyama et al. [42].*
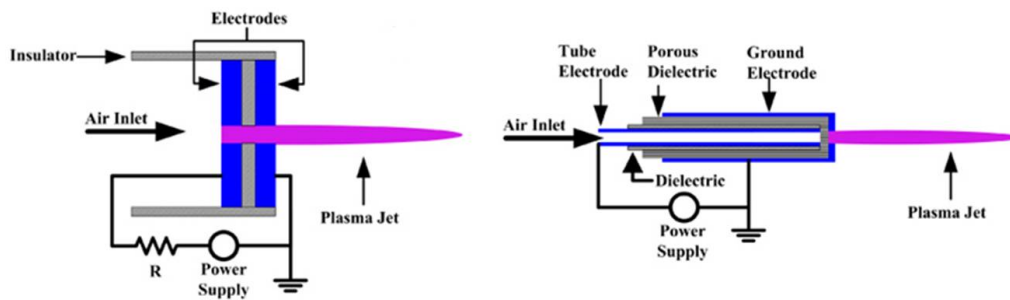
Figure 1.5: *The schematic diagram of two possible configuration for the formation of a plasma jet [43].*
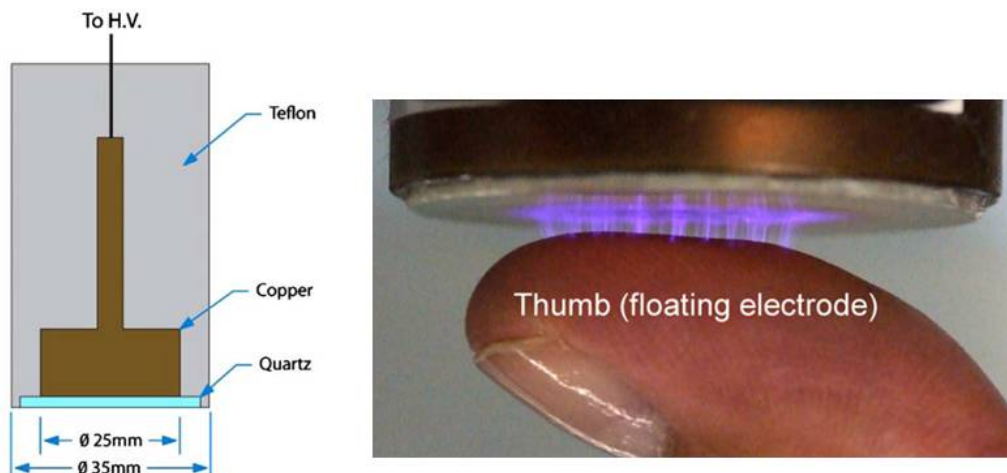
Figure 1.6: *On the left the treatment electrode of a Floating-Electrode Dielectric Barrier discharge (FE-DBD) and on the right a photo of the FE-DBD of Fridman et al. [35, 44] in contact with a thumb.*
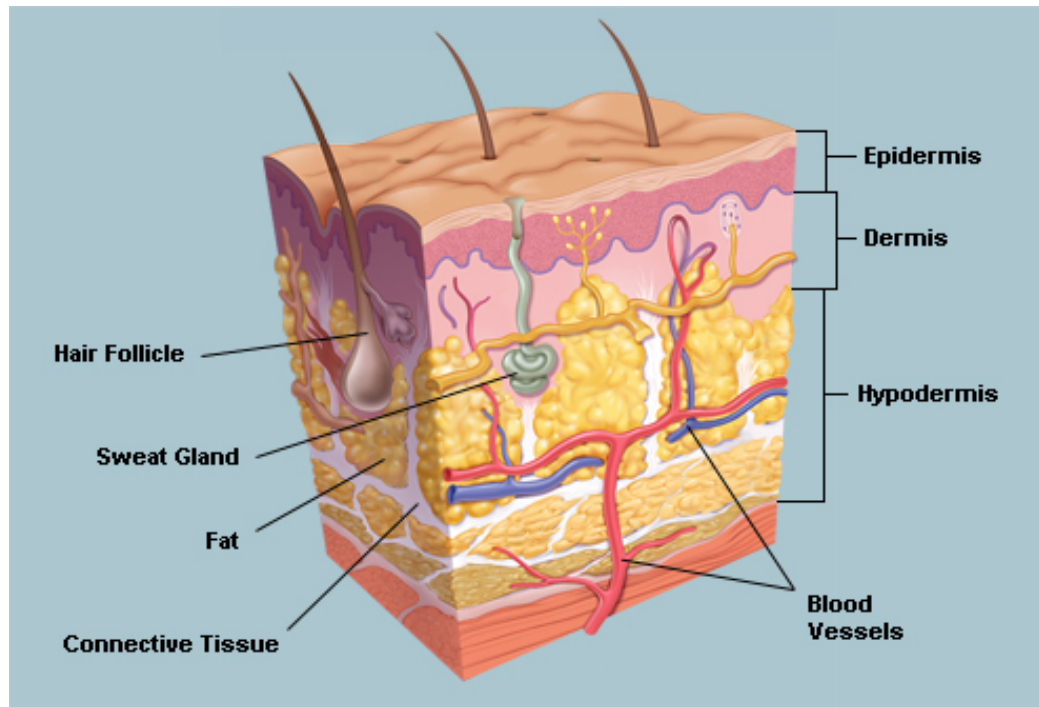
Figure 1.7: *The structure of skin [51].*

infants is different from the skin of an adult, in figure 1.7 the structure of skin is shown. The outermost layer of the epidermis, the stratum corneum, consists of dead cells and is only a few layers thick in the skin of premature infants, therefore it is very permeable. It has less collagen, less fat and fewer elastic fibers in the dermis than the skin of an adult [13, 14]. This skin as well as the bacteria will be exposed to the plasma, which has different possible bio effective agents.

1.4.2 The possible inactivation agents of the plasma

When there is a plasma, there is a complex mixture of mechanisms happening [52, 53]. It is not yet completely understood why which mechanism has, or which combination of mechanisms have, an effect or multiple effects. The impact of an mechanism or agent may differ per source, per application and per dose[3]. Four inactivation agents and their interaction may be responsible for the inactivation of bacteria: the heat, the UV-radiation, the electric field, and the reactive molecules [31, 34, 46, 41].

---

[3]The dose is the amount of time over which the plasma is applied.

1.4.2.1 Heat

When we have a plasma, energy is dissipated in the plasma. This energy will be for a part the kinetic energy of ions and molecules. So the plasma can heat up molecules, also molecules inside the organisms. When bacteria are heated up, proteins within the bacteria may denature and when vital tasks can not be carried out, the bacteria will die. An other reason why they die is due to the breaking of the non-covalent bindings in the membrane, the cell wall will open and the organisms will die. However, the human cells in skin have the same kind of proteins and a similar membrane and they will die as well from the heat [23, 54].

We all know that in order to kill bacteria in for instance the preparation of meat, a lot of heat should be transferred to the meat. A lot of heat is needed to have an effect and this heat would effect the cells in the skin as well. Therefore heat can not play a role in disinfection of the skin. Moreover, CAPs are at approximately at room temperature, so the transferred heat for this plasma sources will be very low [55].

1.4.2.2 UV-radiation

Since some of the electronic transitions in the plasma are larger than 3eV, photons with a wavelength in the (V)UV are emitted. The UV light is able to change the structure of the DNA within the cell, especially within a high energy range of 220 to 280 nm. For even shorter wavelengths, the propagation lengths or penetration depths are only enough to cause surface damage. UV is known to inactivate cells only if the dose is high enough. Most experiments with CAPs for biomedical applications do not result in the emission of any appreciable dose of UV radiation at the mentioned wavelength range. Therefore UV plays a minor role as a killing mechanism. [31, 34, 36]

1.4.2.3 Electric field

When a source is used, with the skin as the second electrode, the plasma is interacting with the skin. This leads to charging of the surface of the skin and the generation of currents and electric fields in the cells. When a plasma is created near the skin, without using the skin as second electrode, field lines may still cross the skin and lead to electric fields in the cells. The cells can be represented as a conducting medium surrounded by a lossy, dielectric envelope, the cell membrane. If an electric field of roughly 1 V is applied over this cell membrane (1 to 10 nm thick), the regime of electroporation is reached [56]. Here the cell membrane gets a higher permeability to move ions in and out of the cell to counteract the electric field. This higher permeability

Radical ROS	Non-radical ROS
Superoxide, O_2^-	Hydrogen peroxide, H_2O_2
Hydroxyl, OH	Ozone, O_3
Hydroperoxyl, HO_2	Peroxynitrite, $ONOO^-$
Carbonate, CO_3^-	Peroxynitrate, O_2NOO^-
Peroxyl, RO_2	Peroxynitrous acid, ONOOH
Alkoxyl, RO	Peroxomonocarbonate, $HOOCO_2^-$
Carbon dioxide radical, CO_2^-	Carbon monoxide, CO
Radical RNS	Non-radical RNS
Nitric oxide, NO	Nitrous acid, HNO_2
Nitrogen dioxide, NO_2	Nitrosyl cation, NO^+
Nitrate radical, NO_3	Nitroxyl anion, NO^-
	Dinitrogen trioxide, N_2O_3
	Dinitrogen tetroxide, N_2O_4
	Dinitrogen pentroxide, N_2O_5
	Alkyl peroxynitrites, ROONO
	Alkyl peroxynitrates, RO_2ONO

Table 1.1: *List of various radical and non-radical ROS and RNS [37].*

makes it easier to deliver molecules into the cell. When the applied electric field is applied for a too long time or with a too high amplitude, the process is irreversible, the cell membrane will not close again and the cells will die [57, 44].

1.4.2.4   Reactive molecules

An immense number of chemical reactions is occurring in a CAP. An example of this immense number of chemical reactions is given for surface microdischarges in humid air by Sakiyama et al. [42]. The chemical reactions in and around a CAP include excitation of molecules to higher energy states and to long lived metastable states. All these reactions lead to a high amount of different species, for instance reactive oxygen species (ROS) and reactive nitrogen species (RNS). In table 1.1 a list of ROS and RNS is given. Some of the species are radicals, they have an unpaired valence electron which makes them highly reactive.

In biology these reactive species (RS) play an important role, they are involved in the regulation of a large number of signalling pathways at multiple levels from receptors to nucleus [58]. They are involved in all processes,

like vascular contraction, blood coagulation, inflammation, immune system response, biosynthesis of growth factors, cell differentiation, cell migration and cell apoptosis. The cellular responses to different types of RS depend on their concentration and the type of cell. If we look for example to hydrogen peroxide (H_2O_2), this molecule will stimulate or inhibit cell proliferation or it will induce cell apoptosis [59]. An other known example is nitric oxide (NO), it will act as an anti-inflammatory agent for low concentrations. At high concentrations however, it will contribute to cell and tissue injury [60, 61]. The effect of RS also depends on the concentration of other present reactive species. The hydrogen peroxide-mediated apoptosis can be for instance inhibited or enhanced depending on the concentration of nitric oxide [62].

RS are playing an important role in Plasma Medicine, but this exact role is not completely understood yet. The complete understanding of the effect of the different concentrations and combinations of RS on the cell is important. The formation and the distribution of the RS by different kinds of CAPs has to be known. The mechanisms of the delivery of RS into the cell, by for instance the electroporation due to the electric field, should be researched. Also, the effect of RS on cells which are deeper into the skin, in lower layers of tissues, have to be understood. With this knowledge, it is easier to get a grip on the possible safe plasma applications.

1.5   Report Outline

The goal of our project is to investigate whether a Floating-Electrode Dielectric Barrier Discharge (FE-DBD) plasma source has potential to be used in the future to prevent neonatal sepsis. We use one specific plasma source for our project, it is a source where the skin is used as second electrode: the FE-DBD, of Fridman et al. [35] shown in figure 1.6. It has a relative large treating surface and is sufficient for the first tests in this field *[36, 33]*. First, the properties of this DBD are reported. Second, the effect of in vitro and ex vivo treatments with this DBD on bacteria and donor skin are shown. Finally, those two components of the project are compared. The report is organized in three parts corresponding to the above three topics.

The part on DBD diagnostics is subdivided in three chapters. In **chapter 2**, first the theory of microdischarges in the DBD and the chemistry involved is discussed. Further, the equivalent electric circuitry of the DBD is shown. With the electric circuitry, the correlation between different variables in the circuit are derived. Finally, the method to find the power dissipated in the DBD is outlined. The two versions of the setup, called in this work the old an the new setup, are shown in **chapter 3**. The methods to determine the

light emission and the dissipated power in the plasma of these two setups are discussed. In the end of the chapter, the FTIR setup is described. In the final chapter of this part, **chapter 4**, the results of the light emission measurements, the value for the dissipated energy per pulse for different settings and the results of measurements with the FTIR setup are given en discussed.

The part on interaction with bacteria and donor skin consists of two chapters. The experimental method for the in vitro and ex vivo experiments with the bacteria and skin are shown in **chapter 5** and the results and discussion of these experiments are given in **chapter 6**.

The final part contains the discussion, conclusion and outlook. In **chapter 7** the results of chapter 4 and 6 are compared and conclusions are drawn. In the last chapter, **chapter 8**, the outlook with some recommendations for future research in the context of using plasmas to prevent neonatal sepsis is given.

Part I

Plasma Diagnostics on the DBD

Chapter 2

The Dielectric Barrier Discharge

A gas discharge between two electrodes with one or multiple dielectrics placed between them is called a Dielectric Barrier Discharge (DBD). The dielectric materials in DBDs will block dc-current due to the capacitive coupling, so all DBDs are driven with alternating current or pulsed DC voltages. Besides this typical voltage form, the DBD has more typical operation conditions which are listed in table 2.1 . These operation conditions are for a DBD in air. A DBD is a non-thermal plasma, it has a low gas temperature and a significantly higher kinetic temperature of the electrons. Only under special conditions a diffuse mode can be generated in a DBD. At atmospheric pressure this mainly depends on the properties of the feeding gas [63]. In most circumstances, including in air at atmospheric pressure, the discharge always starts at many points of the surface and proceeds via the development of thin filaments, so called microdischarges. In section 2.1 the properties of these microdischarges are further discussed.

A wide range of geometrical configurations for DBDs are possible, in figure 2.1 typical arrangements are shown. In this report the left configuration of the planar DBD electrode arrangement is studied further. The electric circuit of this configuration and the corresponding power dissipated in the discharge of this DBD is discussed in section 2.2.

Electric field strength E of first breakdown	$\cong 150\,\mathrm{Td}$ ($p = 1\,\mathrm{bar}$, $T = 300\,\mathrm{K}$)
Voltage V_{pp}	3–20 kV
Repetition frequency f	50 Hz–10 kHz
Pressure p	1–3 bar
Gap distance g	0.2–5 mm
Dielectric material	glass, Al_2O_3, ferroelectrics, …
Thickness d	0.5–2 mm
Relative dielectric permittivity ε_r	5–10 (glass), …, 7000 (ferroelectrics)

Table 2.1: *Typical operation conditions of barrier discharges in air at atmospheric pressure [63].*
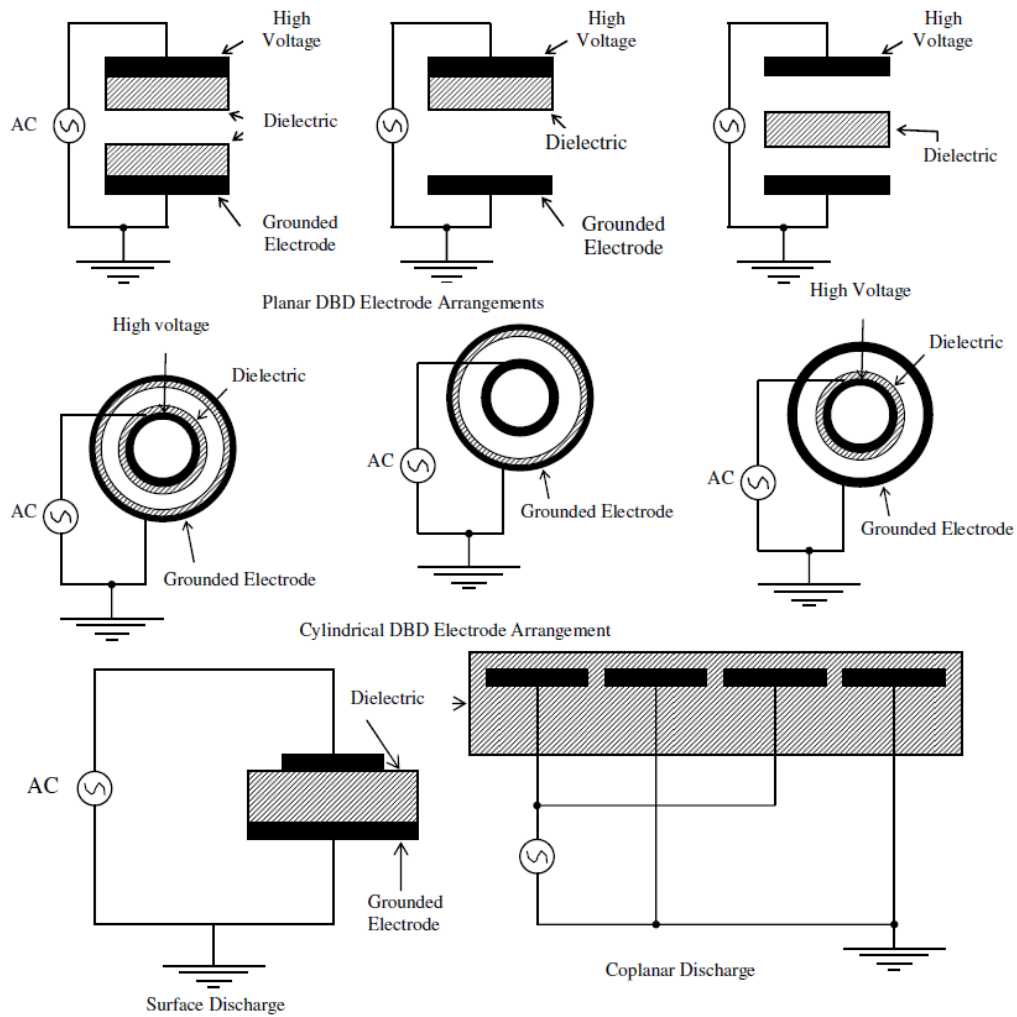
Figure 2.1: *Typical electrode and dielectric arrangements of DBD configurations [64].*

Duration:	a few nanoseconds	Total Charge:	$10^{-10} - 10^{-9}$C
Radius of filament:	about 0.1 mm	Density of electrons:	$10^{20} - 10^{21}$m^{-3}
Peak current:	0.1 A	Mean energy of electrons:	1-10 eV
Current density:	$10^6 - 10^7$A/m^2	Gas temperature:	around gap temp

Table 2.2: *Characteristic microdischarge properties for a 1 mm air gap at atmospheric pressure [65].*

2.1 Microdischarges

As mentioned in the introduction, the electric breakdown of a DBD is initiated in a large number of independent microfilaments. In table 2.2 the characteristic properties of one microdischarge channel in air at atmospheric pressure are summarized. In this section the physics behind one microdischarge is described, the processes and chemistry are discussed and a calculation for the ionization density in air is made.

2.1.1 The development of microdischarges

The development of microdischarges is discussed in this subsection [66, 67, 63]. The first electrons are present in the system due to external effects, like cosmic rays or previous discharges. In the presence of a high electric field the electrons are accelerated to a certain kinetic energy. If the kinetic energy is high enough, the electrons can ionize background gas, atoms or molecules, and create more electrons, which again can create more electrons. An electron avalanche is starting. A negative space charge is accumulated at the avalanche head. Typically, for atmospheric pressure barrier discharges it takes in the order of one microsecond before the local electric field reaches a certain critical level and a breakdown starts. An extremely fast streamer propagates under the influence of the external electric field and the self-generated field in typically 1-2 ns between the two electrodes. At the streamer head, extremely high electric fields occur and at the inside a thin conductive channel with high electron densities is formed. On its way, pairs of ions and electrons are produced by free electrons in the high field region, which sustain the extension of the plasma channel. When the streamer arrives at the dielectric surface the microdischarge channel spreads into a surface discharge covering a region much larger than the original channel diameter. This part is called the footprint of the discharge. The charge built up on the dielectric will reduce the field at the location of a microdischarge within a few ns after breakdown, and terminates the current flow. In this way the dielectric barrier limits the amount of transferred charge and energy deposited in a

microdischarge channel (i.e. heating of the surroundings). Due to the charge accumulation at the footprints, there is a so called memory effect, subsequent filaments will form at different locations between the electrodes.

When the sign of the voltage is alternated, a breakdown in the opposite direction can occur. Due to the charge accumulation on the surface and charge in the gas gap, the critical local electric field for breakdown is reached with a lower external applied field. The effect of the charge accumulation can still be present in the order of hours. The electrons do not leave the surface and are trapped, leading to static electricity. The charge in the gas gap may have an effect up to 10 seconds, see subsection 2.1.3.

The characteristic microdischarge properties in table 2.2 do not depend on the external driving circuit for a wide range of operating frequencies and voltage shapes. They are determined by the gas properties, the pressure and the electrode configuration. Raising the power density for a given configuration, pressure and gas means generating more microdischarges per unit of time and/or microdischarges per unit of surface area [63, 68].

2.1.2 Processes in a dielectric barrier discharge

The time constants of the relevant processes in DBD's cover many orders of magnitude. In figure 2.2 some relevant processes and their time constants are shown. As mentioned in the previous subsection, the production of high-energy electrons is realized within a few nanoseconds. Excitation and dissociation by electron collisions are again extremely fast processes, followed by free radical reactions that occur at an intermediate time scale, typically 1 to 100 µs. These reactions will happen before any substantial species transport can take place by convection or diffusion. The production of active chemical particles is efficient because no energy is lost to the heating of the surroundings. The heavy particle temperature will not be much higher than room temperature, and far below the electron temperature. For medical applications this cold non-thermal plasma is therefore favorable.

2.1.3 The ion density

In section 2.1.1 it is already mentioned that not only charge accumulation on the surface, but also ions and electrons present in the gas gap can facilitate an easier breakdown. Of course, due to background ionization, there are always some electrons in the gas gap. The natural background ionization levels by radioactivity and cosmic rays are normally around $10^3 - 10^4 \mathrm{cm}^{-3}$[69]. However, after a discharge more charge is present. If the discharge is in air, most of the charges are produces by the ionization of oxygen and nitrogen:
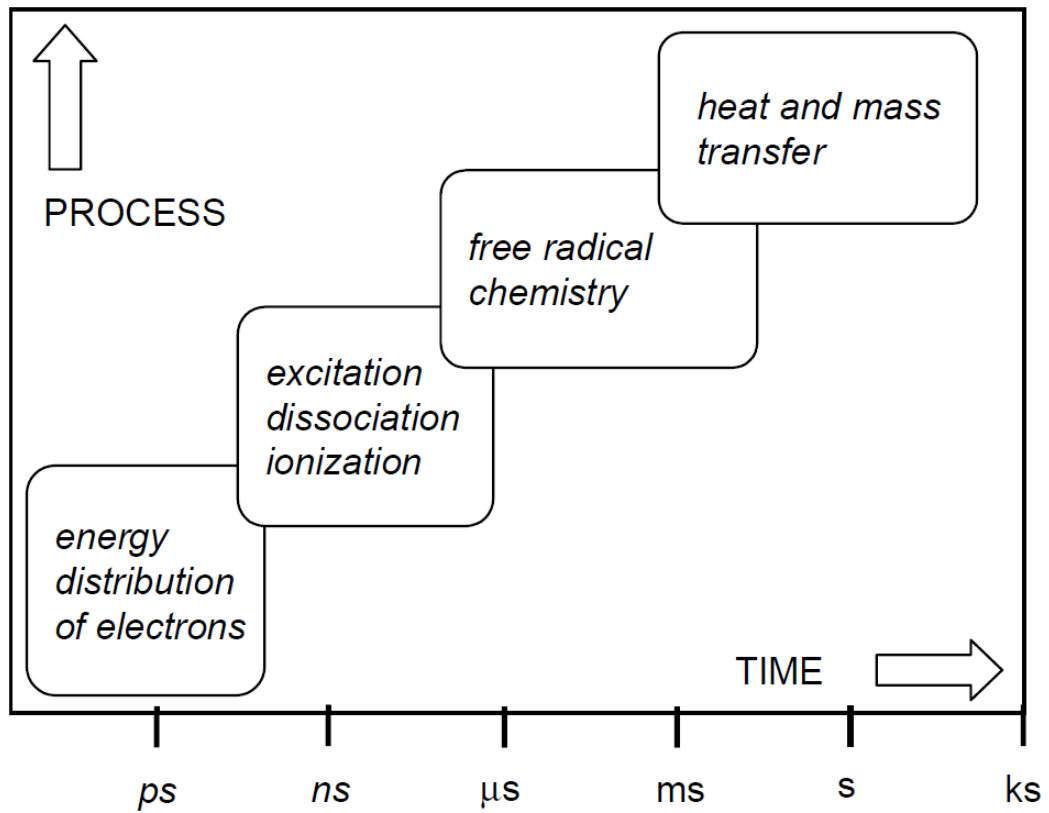
Figure 2.2: *Time scale of some relevant processes of the filamentary barrier discharge. [63]*

$$O_2 + e \rightarrow O_2^+ + e + e \,, \tag{2.1}$$

$$N_2 + e \rightarrow N_2^+ + e + e \,, \tag{2.2}$$

with an ionization energy of 12.07 eV and 15.58 eV, respectively. The present number of ions (or electrons) in a gas can be quantified by the number of ions per volume: the ion density n. The ion density in the microfilament will mainly decrease after the discharge as function of time due to dissociative recombination and due to diffusion of the ions. The ion density for homogeneous recombination where spatial inhomogeneity, and the drift of charged particles are neglected can be described by the following differential equation:

$$\frac{\partial n}{\partial t} = D_{ion} \cdot \nabla^2 n - k_{rec} \cdot n^2 \,, \tag{2.3}$$

with k_{rec} the effective recombination rate and $D_{ion} \approx 5 \cdot 10^{-2} \mathrm{cm^2 \cdot s^{-1}}$ the diffusion coefficient under standard conditions in air [66]. However, due to the interaction between the ions and electrons a ambipolar diffusion coefficient is needed, which is given by

$$D_a = D_{ion}(1 + \frac{T_e}{T_i}) \,, \tag{2.4}$$

where T_e is the electron temperature and T_i the temperature of the ions. On a time scale a few times longer than the discharge, the electron temperature will be approximately equal to the ion temperature. The diffusion coefficient in equation 2.3 can be replaced by the ambipolar diffusion coefficient, $D_a = 2D_{ion}$.

At some time point the ion density in the volume of a microdischarge will be equal to the background ionization. For this time point the previous discharge will only have effect by charge accumulation on the dielectric surface and no longer by electrons in the gas gap. The ion density can roughly be determined as function of time for the dissociative recombination and diffusion with the steps discussed in the next two sub subsections [66].

2.1.3.1 Dissociative recombination

The ionization density will decrease with the dissociative recombination rate of positive with negative ions. The two- and three-body ion-ion recombination which dominate and determine the dissociative recombination rate in dry air are

$$O_2^- + O_4^+ \rightarrow O_2 + O_2 + O_2 \quad k_1 = 10^{-7} \text{cm}^3 \text{s}^{-1}, \tag{2.5}$$

$$O_2^- + O_4^+ + M \rightarrow O_2 + O_2 + O_2 + M \quad k_2 = 2 \cdot 10^{-25} \text{cm}^6 \text{s}^{-1}, \tag{2.6}$$
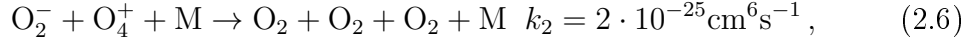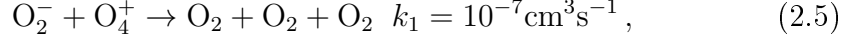
where M is either a neutral oxygen or a neutral nitrogen molecule. These two reactions are dominant, since the formation of O_2^- and O_4^+ are very fast. In air the negative ion O_2^- will be formed by the attachment of electrons to the electronegative oxygen. This three-body attachment reaction is given as

$$O_2 + e + M \rightarrow O_2^- + M, \tag{2.7}$$
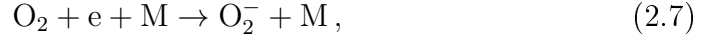
where M can represent oxygen, nitrogen or water molecules. Electrons are quickly attached, the attachment time is about 5 ns in air at standard temperature and pressure for an electron temperature of 1 eV [66, 70]. The O_4^+ ion is formed quickly after the discharge according to the following reaction path [71]

$$N_2^+ + N_2 + M \rightarrow N_4^+ + M, \tag{2.8}$$

$$N_4^+ + O_2 \rightarrow 2N_2 + O_2^+, \tag{2.9}$$

$$O_2^+ + O_2 + M \rightarrow O_4^+ + M. \tag{2.10}$$
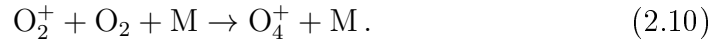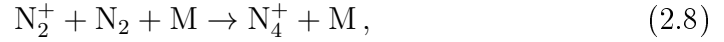
The effective recombination rate can be estimated by combining the rates in equation 2.5 and 2.6 as follows

$$k_{rec} \approx k_1 + k_2 \cdot [M] = 5 \cdot 10^{-6} \text{cm}^3 \text{s}^{-1}$$

where the neutral particle density is $[M] \approx 2.5 \cdot 10^{19} \text{cm}^{-3}$ for atmospheric air at room temperature. For humid air, more dissociative recombinations are possible and clusters will be formed with water and the oxygen ions. The radius of the molecules increase, therefore the recombination rate of equation 2.5 and 2.6 may be higher, but this change is relatively small [72, 73]. The ionization density for homogeneous recombination, when neglecting the diffusion, is given by solving equation 2.3:

$$n(t) = \left[\frac{1}{n_0} + t \cdot k_{rec}\right]^{-1} \tag{2.11}$$

with n_0 the initial ion density at $t = 0$.

2.1.3.2   Diffusion of ions

In the previous section a value for the ion density as function of time is given for dissociative recombination. However, after the discharge, ions formed in the discharge will diffuse. When the dissociative recombination is not taken into account and only the diffusion radial direction is included, the differential equation 2.3 is given by

$$\frac{\partial n}{\partial t} = D_{ion} \frac{1}{r} \frac{\partial}{\partial r} \left(r \frac{\partial n}{\partial r} \right) , \qquad (2.12)$$

where r is the radial distance from the center of the microfilament. In the first-order approximation for equation 2.12, when we assume a homogeneous distribution of the ions over the whole radius of the filament at time $t = 0$ is given by

$$n(t) \approx \frac{n_0}{\frac{t \cdot D_{ion}}{R^2} + 1} , \qquad (2.13)$$

where R is the radius of the filament. In table 2.2 the typical radius of a filament is given to be about 0.1 mm.

In figure 2.3 the decay of the ion density in dry air in the volume of a cylindrical filament with a radius of 0.1 mm, with an initial ion density of 10^{15}cm^{-3} ($n_e = n_i$ and table 2.2) and with an ambipolar diffusion coefficient under standard conditions in air of $D_{ion} \approx 0.1 \cdot 10^{-2} \text{cm}^2 \cdot \text{s}^{-1}$ is shown. In blue the decay for only dissociative recombination is given according to equation 2.11 and in red the decay of the ion density by diffusion is shown. It is clear that under the conditions in air and $n_e = 10^{15} \text{cm}^{-3}$, the decay due to dissociative recombination is dominant in this time scales. Further the ion density after 10 ms is still higher than the background ionization of $10^3 - 10^4 \text{cm}^{-3}$ and an effect on a subsequent discharge within 10 ms can not be neglected in dry air.

2.1.4   Energy transitions within a molecule

In addition to all the reactions between the molecules and the ionization of molecules, excitations from one electro energy state to a higher one and transitions between vibrational and rotational states may occur within the molecule. The vibrational states of a molecule are determined by the amount of atoms, the bond strengths, and the symmetry within a molecule. In parallel with the transition of one vibrational state to another, multiple rotational transitions, or changes in angular momentum, are possible. At one defined energy, a certain transition in vibrational and rotational state is possible,
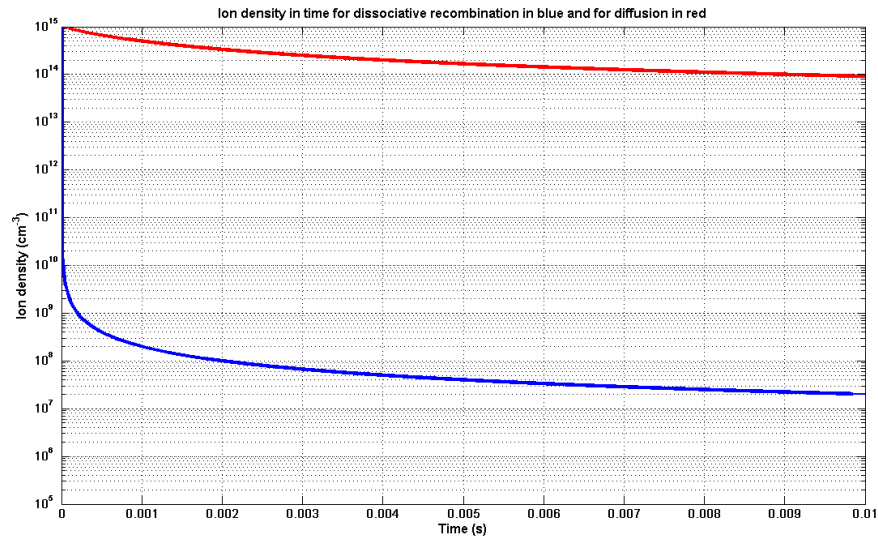
Figure 2.3: *The ionization density in dry air as function of time for only dissociative recombination in blue (equation 2.11) and for only diffusion of ions (equation 2.13) in red. The constant values are the initial ionization $n_0 = 10^{15}$ cm^{-3}, the radius of the filament $R = 0.01$ cm and the ambipolar diffusion of ions in air $D_{ion} \approx 0.1$ cm$^2 \cdot s^{-1}$.*
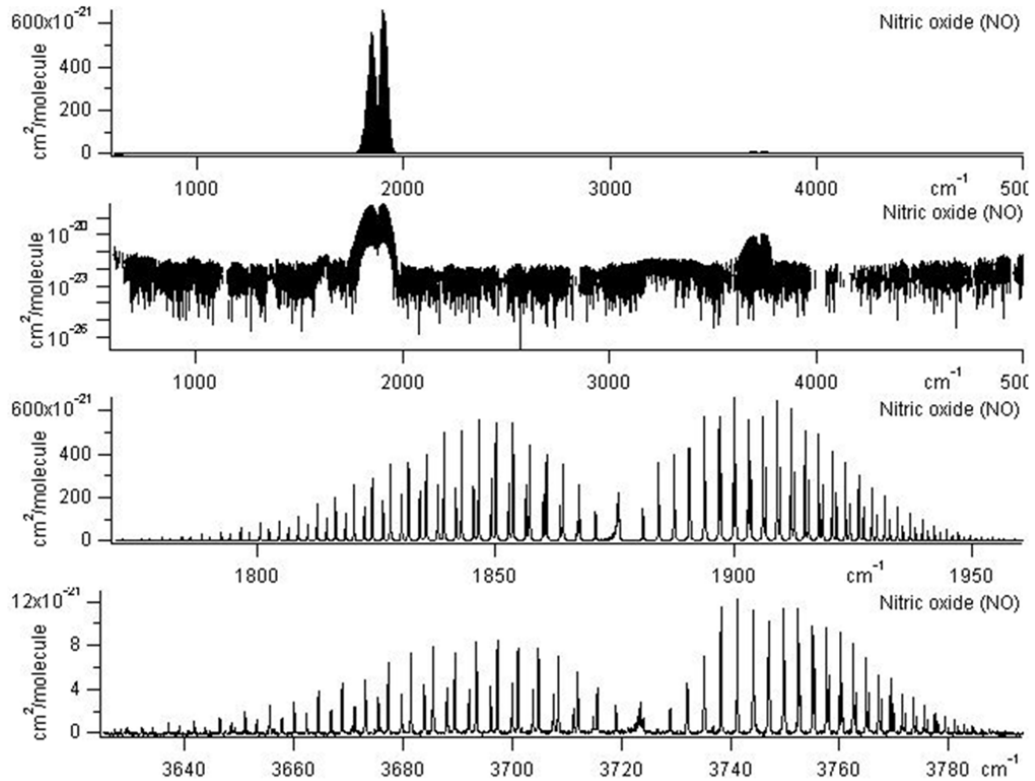
Figure 2.4: *The spectrum of Nitric Oxide [74].*
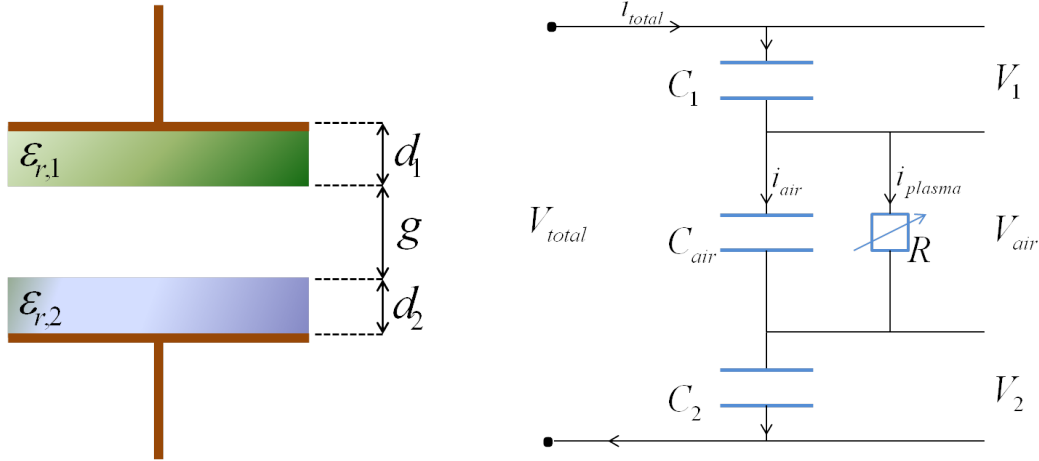
Figure 2.5: *On the left the two-sided BD configuration for a certain gap distance g, with two different dielectric surfaces on both sides with a certain thickness respectively with a dielectric permittivity $\varepsilon_{r,1}$ and $\varepsilon_{r,2}$ and thickness d_1 and d_2. On the right the equivalent circuit for the configuration, when there is no discharge the resistance will be infinitely large. During a discharge the resistance will be time dependent.*

only photons with a certain wavelength are absorbed or emitted by a certain molecule. In figure 2.4 an emission spectrum of Nitric Oxide is shown as example. Two transitions in vibrational states in the infrared (1876 cm^{-1} and around 3726 cm^{-1}) are visible in the figure. The transition between two vibrational states with the same rotational quantum number is called the Q-branch[1]. The R-branch of the spectrum is the side of the higher frequency side of the spectrum, here energy of the rotational transition is added. The other side, towards a lower frequency, is called the P-branch. Depending on the temperature more transitions between rotational states are possible for one transition in vibrational state [75].

2.2 Schematic electric circuit

In figure 2.5 the two sided DBD configuration is shown. The gap distance is indicated with g, and the relative dielectric permittivity of air is approximately equal to the vacuum permittivity ε_0. For this configuration there are

---

[1]This transition is not always possible due to the quantum mechanical selection rules.

Material	$\sigma(\mathrm{S/m})$	ε_r
Quartz	-	4.5
Water	$5.5 \cdot 10^{-6}$	4-88
Polyvinylchloride (PVC)	-	3
Glass	-	3.7-10
Skin (dry)	0.13	4

Table 2.3: *The relative permittivity for different dielectric materials at a low frequency and the electric conductivity for deionized water and the skin. When ions are added to the water or the skin is more humid, the conductivity will rise . [76, 77, 78]*

two dielectric surfaces, both can have a different distance, d_1 and d_2, and a different relative permittivity, ε_{r1} and ε_{r2}. In table 2.3 a few relevant values for the relative permittivity are shown. In the right of figure 2.5 the equivalent electric circuit of the two sided DBD configuration is shown. The value of the resistance is different for a situation with and without plasma. When there is no discharge, the resistance in the plasma is infinitely large, since there is no plasma. When, however, we do have a discharge, the resistance through this discharge is time dependent. Besides the resistance, there are three capacitance in the system, one of the air gap and two of the dielectric surfaces. A capacitance C of a parallel plate capacitor is given by

$$C = \varepsilon_0 \varepsilon_r \frac{A}{b}\,, \tag{2.14}$$

with A the surface of the plates of the capacitor and b the distance between the two plates. Equation 2.14 is only valid when the width of the plates is much greater than their separation, so $A \gg b$. For the three capacitors in series in figure 2.5 the total capacitance is in theory given by

$$\frac{1}{C_{total}} = \frac{1}{C_1} + \frac{1}{C_2} + \frac{1}{C_{air}} = \frac{d_1}{A\varepsilon_0\varepsilon_{r,1}} + \frac{d_2}{A\varepsilon_0\varepsilon_{r,2}} + \frac{g}{A\varepsilon_0}\,. \tag{2.15}$$

If there is no discharge, the stored charge per time moment over every capacitor is equal and related to the voltage over each capacitor by

$$V(t) = \frac{Q(t)}{C}\,. \tag{2.16}$$

The voltage over the air gap, V_{air}, is given with equation 2.16 by

$$V_{air}(t) = \frac{Q(t)}{C_{air}} = \frac{V_{total}(t)C_{total}}{C_{air}} = \frac{V_{total}(t)}{\frac{d_1}{\varepsilon_{r,1}g} + \frac{d_2}{\varepsilon_{r,2}g} + 1}\,. \tag{2.17}$$

If thickness of a dielectric, d_1 or d_2, is increased or a material with a lower dielectric permittivity, ε_{r1} or ε_{r2}, is chosen, a higher voltage over the total circuit, $V_{total}(t)$, is needed to achieve the same voltage over the gas in the gap. The voltage over the gas gap should be the same as the value of the breakdown voltage, in order to have a discharge. Besides the thickness and the dielectric permittivity, the gas gap g has an effect on the total voltage needed to have a breakdown. The breakdown voltage itself depends on the distance of the gap g. In order to understand the effect of changing g, an expression for the breakdown voltage is needed. The breakdown voltage for gas spaces bounded by two dielectrics have practically the same breakdown voltage as if it were between metal electrodes [65] and is given for a diffuse DBD[2] by

$$V_{breakdown} = \frac{apg}{ln(pg) + b} \,,\tag{2.18}$$

where p is the pressure, g is the gap distance and $a = 4.36 \cdot 10^7 V/(\text{atm} \cdot \text{m})$ and $b = 12.8$ for air at atmospheric pressure [80]. The dependence of the width of the gas gap g is given by combining equations 2.17 and 2.18. For a larger distance g a higher voltage on the system is needed to reach the breakdown voltage in air at atmospheric pressure.

It must be noted that as discussed in section 2.1.1, the required breakdown voltage over the gas is always lower after the first discharge in the DBD, due to charge accumulation on the dielectric surfaces and an increased background ionization. The first breakdown voltage is given by equation 2.18, the voltage needed to enhance breakdown after the charge accumulation is lower. The above mentioned relation between the variables, g, d and ε_r and the voltage of the system $V_{total}(t)$ are still valid when incorporating the charge accumulation and background ionization.

2.2.1 Average power dissipated in the discharge

From the electric circuit in figure 2.5, the energy $E(T)$ dissipated in one whole period T can be determined and is given by

$$E(T) = \int_0^T i_{plasma}(t) V_{air}(t) dt \,.\tag{2.19}$$

This equation can be rewritten, as shown in appendix A, as

---

[2]For streamer breakdown, the Paschen law is not valid, the Meek's criterion is valid.[79]

$$E(T) = \int_0^T V(t)i(t)dt \,. \tag{2.20}$$

The plasma current and voltage over the air gap are not needed, an integration over the total current and voltage over the system will do. This is in agreement with the consideration of the equivalent circuit: only energy losses in the discharge are included; other losses are disregarded. The electrical energy delivered into the system over one period T is therefore equal to the energy dissipated in the discharge. The average power dissipated in the discharge is given by

$$P = E(T)/T \,. \tag{2.21}$$

Instead of using the integral in equation A.11, a well known method to determine the dissipated power in a dielectric barrier discharge is by using Q-V plots. The theory behind these Q-V plots is given in the following section.

2.2.1.1 Determination of the average power dissipated in the discharge with a Q-V plot

In the theory of ozonizers by i.e. Manley [81], the power dissipated in a dielectric barrier discharge can be derived directly from plots of the dielectric surface charge Q with respect to the applied voltage V_{total}. In figure 2.6 such a Q-V plot, or Lissajous figure, is shown. This parallelogram is obtained when a dielectric barrier discharge is driven by a sinusoidal voltage.

The slope of the four sides of the parallelogram in figure 2.6 can be explained as follows. During the AB side of the parallelogram, there is no discharge and therefore no charge transfer occurs through the gas gap. At point B, the voltage is high enough to generate a plasma. During the BC side, there are discharges and charge is transferred. The ending of the discharge coincides with the maximum of the applied voltage at point C, due to charge accumulation on the surface. During the rising of the voltage in side BC, the local electric field due to the charge accumulation is rising as well. When the voltage is dropping again, the local electric field due to the charge accumulation is too high and the total electric field is too low for a breakdown. The voltage keeps dropping for side CD and no charge is transferred. At point D the applied electric field together with the accumulated charge is sufficient for a breakdown in the opposite direction. So, from point D charge is transferred until the cycle reaches again the minimum of the voltage at point A.
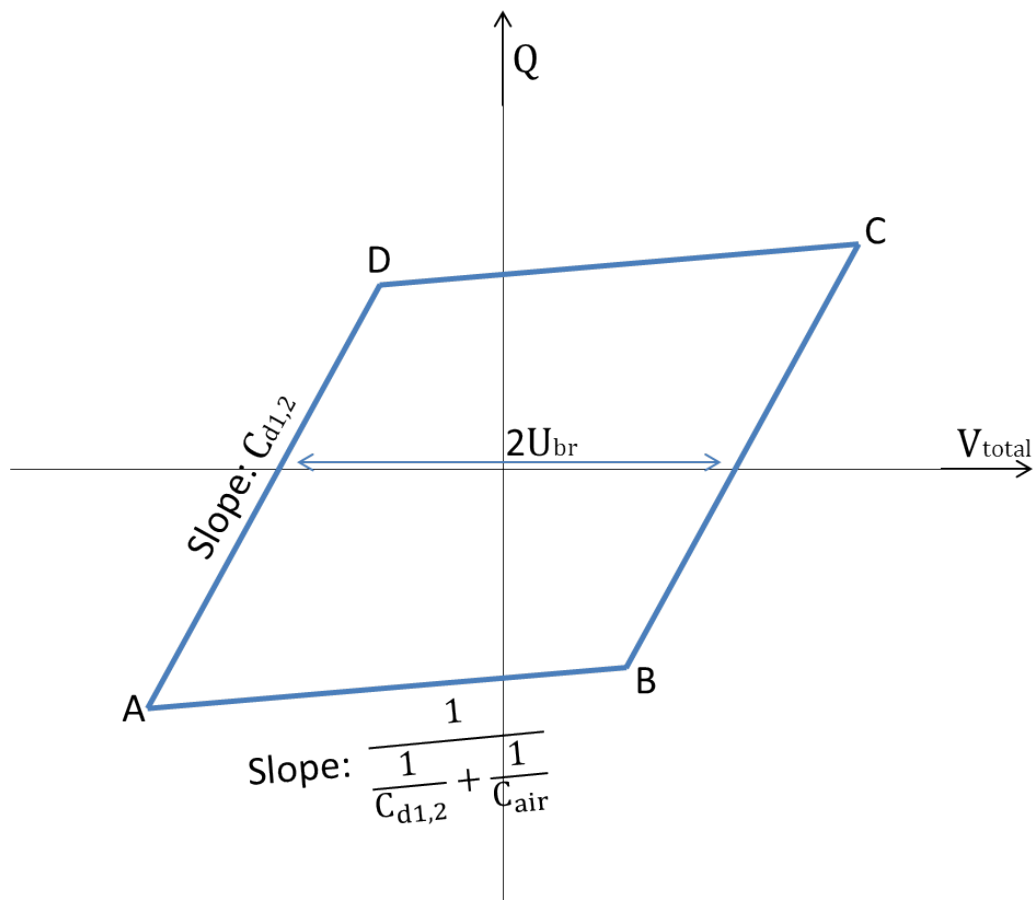
Figure 2.6: *Schematic presentation of Q-V plot from classical electrical theory of sinusoidal voltage driven ozonizers, where U_{br} is the breakdown voltage.*

During the cycle, the energy stored in the capacitor is equal to $E = \frac{1}{2}QV_C$, where V_c is the voltage over the capacitor. If the energy stored in the capacitors was the only energy in the system, the Q-V plot would be a straight line. However, energy is dissipated in the plasma. The area of the Q-V plot is equal to the energy dissipated in the plasma during one cycle of the voltage.

From figure 2.6 the area of the Q-V plot can be obtained by

$$E(T) = 4U_{br}C_{d1.2}\left(V_{total} - U_{br}\frac{C_{d1,2} + C_{air}}{C_{d1,2}}\right).\qquad(2.22)$$

By dividing this energy by the period T (equation 2.21), the averaged power dissipated in the discharge is obtained.

Chapter 3

Experimental setup and techniques

In the previous chapter the principles of the DBD and the discharge are discussed. In this chapter the characteristics of the setup of the DBD used in the project are discussed, including the electric circuitry of the power generator. Two power generators are used in the project and both are discussed in this chapter.

Further different measurement techniques for determining the power dissipation in the plasma and the light intensity are shown. In the final section of this chapter the setup and the measurements for FTIR spectroscopy with the DBD are discussed.

3.1 The Dielectric Barrier Discharge Plasma Generator

In this section the DBD used in the experiments is discussed. In this research, two power generators are used to drive the DBD. The first one is the *DBD Plasma Generator with Digital Control, Model PG100-3D*, the device is from Drexel university, from the Plasma Power, LLC company. The electrode is generously made available by Prof. Fridman [33]. The second one is made with the transformer coils with ferrite core from the first plasma generator, after the first one broke. First the electric circuitry of the new power generator is discussed. With this circuitry the principles of the power generator can be understood. The old power generator works on the same basic principle, but the exact electric circuitry is not known. The difference with the new power generator and the properties of the old power generator are discussed. In the following part, the setup outside the power generator
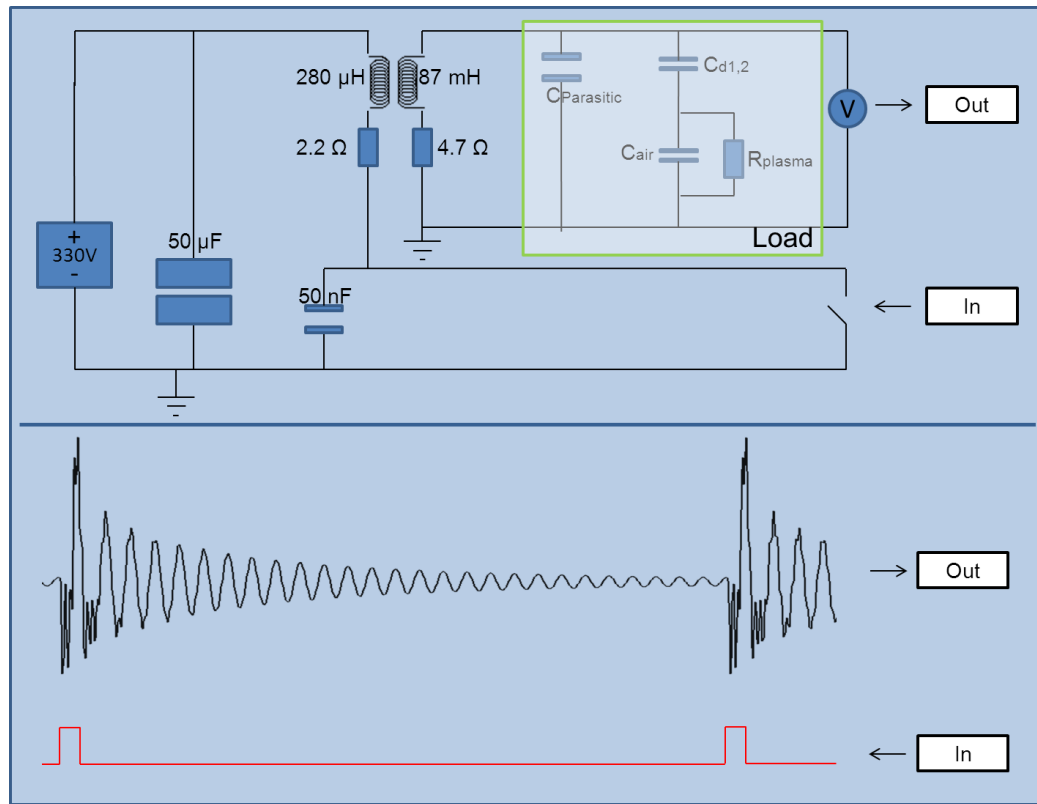
Figure 3.1: *The schematic of the power generator. When the switch is open, the capacitors get charged. The switch is controlled by a pulse generator, the pulse signal is shown in red. During a pulse the switch is closed and the large capacitor slowly discharges through the coil at the primary side. When the switch opens the current changes abruptly and the coil counteracts this change. The coil and the small capacitor start to resonate and in the secondary coil this voltage is converted to a high voltage signal, the high voltage signal is measured and shown in black. This voltage signal is fed to the DBD.*

is shown. Finally, the effect of heating up the core of the transformer is discussed.

3.1.1   The electric circuitry of the new power generator

In this part of the report the electric circuitry of the new power generator, shown schematically in figure 3.1 , is discussed. The power generator is driven by a power supply which delivers 330V to the circuit and a current up to 450 mA, from *Delta Electronika, DC power supplies*. When the switch is open, the capacitor of 50 μF gets charged. The switch (1700 Volt IGBT) is

driven by a pulse generator[1], with a adjustable pulse width, pulse frequency and duty cycle[2], the pulse signal is shown in red at the bottom of figure 3.1. During a pulse the switch is closed and the large capacitor discharges slowly through the primary coil and the switch. At the moment the switch opens again, the current through the primary coil wants to change abruptly. For a longer pulse width, the current built up in the primary coil is larger and this leads to a larger change in current through the coil. The magnetic fields created in the primary coil to counteract the change in current leads to high voltage at the secondary side of the circuit, since the inductance or the number of windings N of the secondary coil is many times higher than the inductance of the primary coil ($V = N\frac{d\Phi}{dt}$ where Φ is the magnetic flux, due to the primary coil, through one turn of the secondary coil). The two coils will transform the voltage to a high voltage signal which is fed to the load.

In figure 3.1 a measured high voltage signal which is fed to load is shown in black. To understand the shape of this voltage signal better, the electric circuitry is simulated with *LTspice IV*. The voltage signal has two resonance frequencies. Both the lower resonance frequency and the higher resonance frequency are determined by all the capacities in series with the primary and secondary coil. The higher the capacitance, the lower the resonance frequency, since the resonance frequency ω_0 of a capacitor C in series with a coil L is given by

$$\omega_0 = \frac{1}{\sqrt{CL}}\,.\tag{3.1}$$

Both the higher and lower resonance frequencies have a damping rate. The damping depends partly on the value of the resistors in the system and on the configuration of this resistors, the coils and capacitors. The damping factor of a series RLC circuit is given by

$$\alpha = \frac{R}{2L}\,,\tag{3.2}$$

and the damping factor of a parallel RLC circuit is as follows

$$\alpha = \frac{1}{2RC}\,,\tag{3.3}$$

For the load, both equations are not valid, since the resistance of the plasma is in series with the coil, but is parallel to the capacitors. When

---

[1] A TUeDACs box which is controlled with Pulse Delay Generator software, both are designed by Gerard Harkema.

[2] The duty cycle is defined as the percentage of one second the pulse generator is generating pulses. In the top diagram of figure 3.3 an example for 50% duty cycle is given.
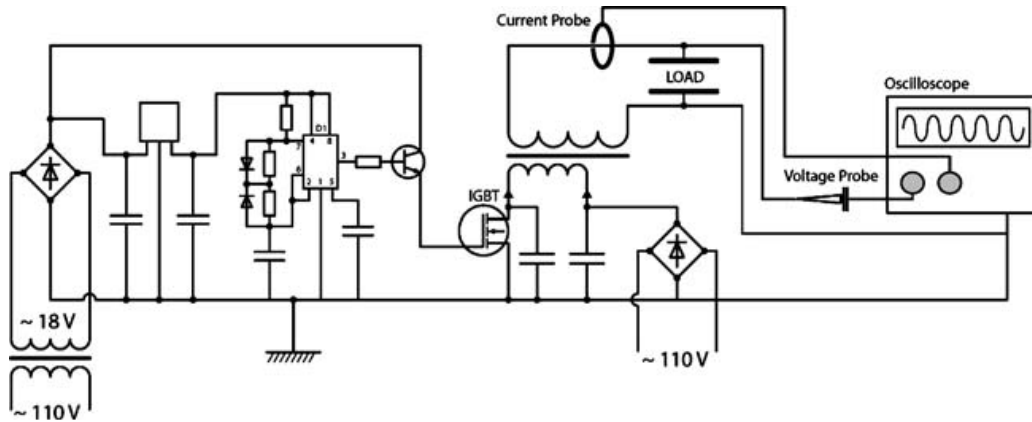
Figure 3.2: *The block diagram of the power generator and load from Drexel University, Fridman et al. [33].*

the resistance in the plasma is higher, the damping will be lower. When the total capacitance of the air gap and dielectric materials will rise, the damping rate will be higher as well. The parasitic capacities in the load will be constant and will therefore not change the damping rate. The values of the inductance and resistances in the power generator will also stay constant during all measurements.

3.1.2   The original power generator

A block diagram of the power generator and setup is available and shown in figure 3.2 . The exact electric circuit of the original power generator is not known. The transistor shown in figure 3.1 is from the original power generator and is re-used in the new power generator. The principles of the electric circuitry of the original power generator will be the same as the electric circuitry described in the previous subsection. However, the power supply and pulse generator are integrated in the power generator and there may be some feedback coupling which is not present in the new power generator. The resonance frequency of the original power generator is around 39kHz. Besides this 39kHz, the power generator generates a high level of the electromagnetic RF energy in a broadband spectrum. Depending on the load, the DBD generates pulses of a DC high voltage between 10 and 30 kV.

In the original power generator the duty cycle, pulse width and pulse frequency can be adjusted as well.

Firstly, the duty cycle can be changed, from 1% till 100%. This determines the percentage of every second the box is generating voltage pulses. In the top of figure 3.3 a schematic view of the voltage pulses generated by

Figure 3.3: *From top till bottom. First on a 1 second time scale a schematic view of the voltage pulse for a duty cycle of 50%. Second a schematic view of a pulse frequency of the DBD of 2000Hz is shown on a time scale of 2 ms. In this schematic, the pulse width is between 1 and 10 μs. At the bottom figure, the pulse generated in the power generator is translated in the electric circuitry to a decreasing sinusoidal voltage signal.*

the power generator with a duty cycle of 50% is shown. So for a duty cycle of 50%, the control box generates during 500 ms pulses per 1000 ms.

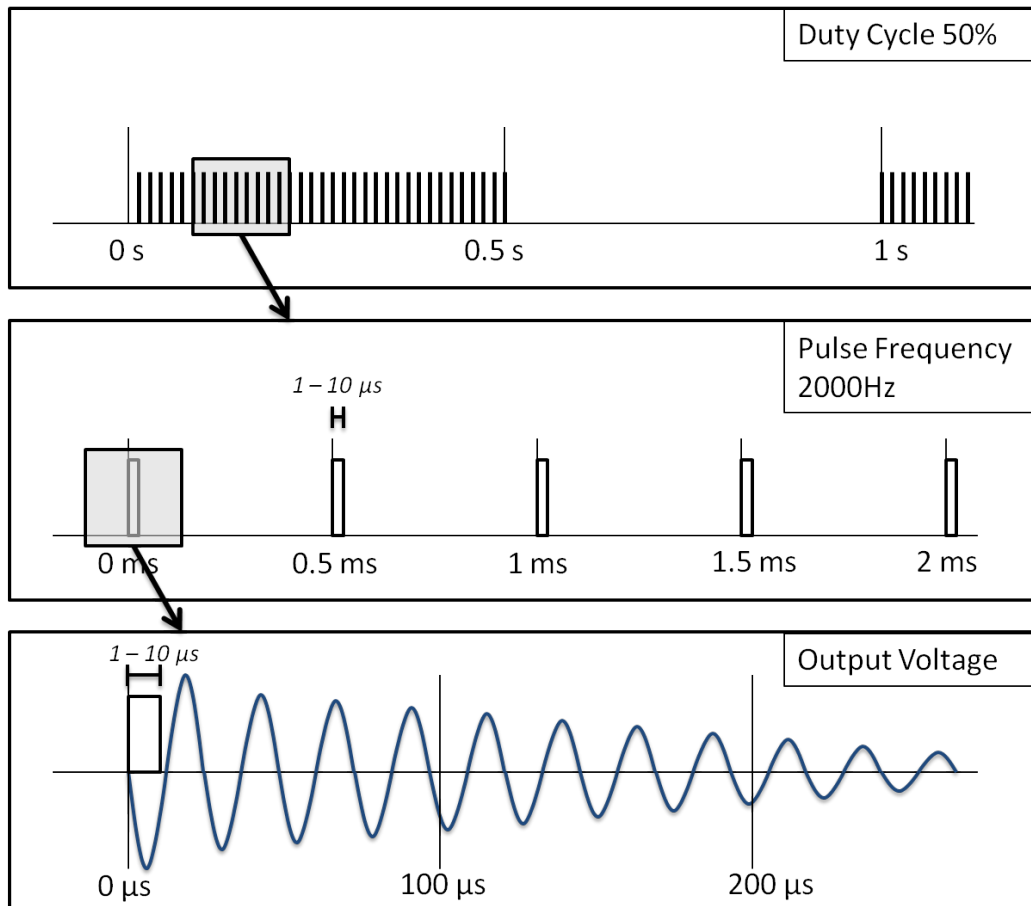The second adjustable parameter is the pulse frequency. The box can be set on 10 different frequencies: 50 Hz, 100 Hz, 251.1 Hz, 502.3 Hz, 1026.7 Hz, 1543.2 Hz, 2155.2 Hz, 2702.7 Hz, 3086.4 Hz and 3610.1 Hz. In this report these frequencies are referred to as 50 Hz, 100 Hz, 250 Hz, 500 Hz, 1000 Hz, 1500 Hz, 2000 Hz, 2500 Hz, 3000 Hz and 3500 Hz. In figure 3.3 the center diagram is a schematic view of the output voltage of the control box of the DBD for a pulse frequency of 2000 Hz. For a pulse frequency of 2000 Hz the time between two pulses is 0.5 ms. In this center diagram the width of a single pulse is indicated, this is the third parameter on the control box, which can be set to 1, 2, 3, 4, 5, 6, 7, 8, 9 or 10 μs. The standard settings during the experiments are a pulse frequency of 1500Hz, a the duty cycle of 100%, and a pulse width 10 μs.

3.1.3   The setup of the DBD

In figure 3.4 the setup and the electrode of the DBD are shown. In the previous section the two different control boxes of the DBD are already discussed. These boxes are connected with two similar types of loads[3]. A banana plug connects the load with the box. A wire of approximately 1 meter long runs to a copper electrode. Both the wire and the electrode (except for the operation side) are enclosed by insulating material to limit the chance of discharges on other locations. On the "operating" side of the electrode a 0.5 mm thin plate of quartz is attached as dielectric. This quartz substrate is placed parallel above the to be treated flat substrate, which has an equal or larger surface area than the electrode with the quartz, which is round with a diameter of 2 cm or 2,3 cm. During the project the substrates used are of different materials: metals, PVC, glass, pig and human skin, and culture plates. Due to the different electric properties of these materials, the plasma formed can be different.

The distance between the quartz and the specific substrate is variable too. This distance determines for a part the total capacity in the system, which again can have an influence on the filament formation. Underneath the substrate a metal is placed and connected to the ground on the control box. A mount is holding the electrode with the dielectric quartz in position above the substrate and the grounded metal. The standard setting for the distance between the quartz and the substrate is 1mm and the standard

---

[3]The two different loads used for this research are both made at Drexel university, Advanced plasma solutions. A second load was needed, due to a crack in the dielectric material covering the metal of the first load.
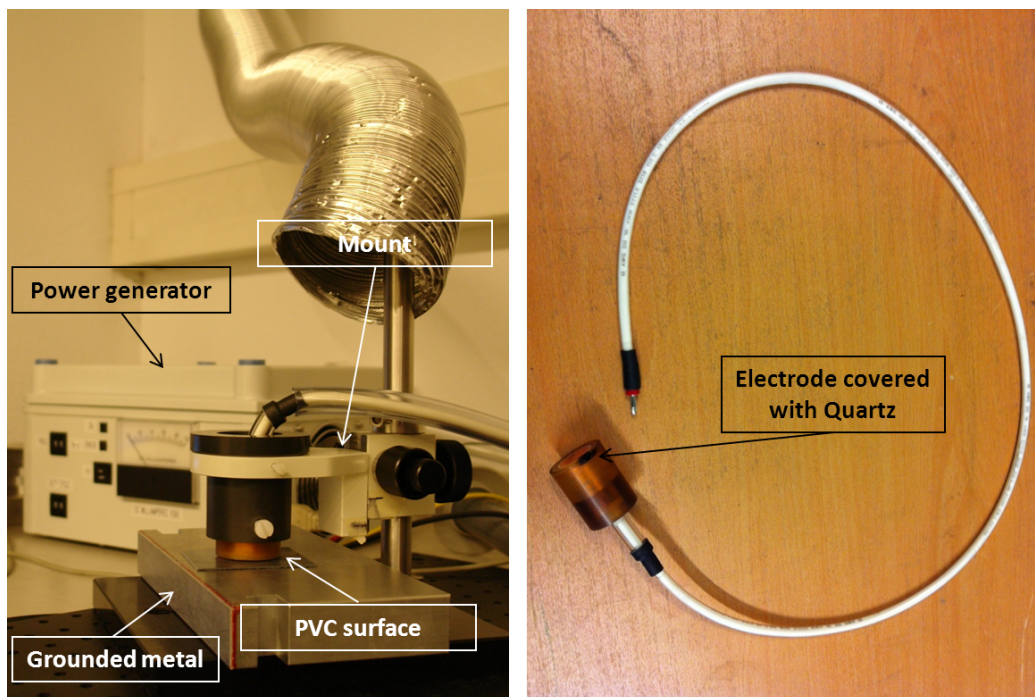
Figure 3.4: *On the left the electrode ($\oslash 2$ cm) covered by quartz, held by the mount, with a distance of approximately 1 mm from a PVC substrate. The PVC substrate is placed on a grounded metal. On the back the old power generator is shown. In the right photo the electrode ($\oslash 2$ cm) and wire with banana plug are captured.*

substrate used is Polyvinyl chloride (PVC) with a thickness of 1 mm. The impact of the three different settings of the pulse generator (the duty cycle, frequency and pulse width), the distance between quartz and the substrate and different types of material are researched.

3.1.3.1 Two different setups

As mentioned in the previous section, there were two similar loads used for the experiments. There are three differences between the first and second load:

1. a diameter of 2 and 2,3 cm of the electrode,

2. a wire of 1.1 and 0.8 meter[4],

3. and an extra insulation wire around the cable and no extra insulation wire.

The first load is used in combination with the old power generator and this combination is called in this report the old setup. The new power generator in combination with the second load is called the new setup throughout this report. The three points mentioned above as well as the different electric circuitry of the power generators will have an influence on the plasma formation.

3.1.4 Heating up of the core of the transformer

Due to power dissipation in the core of the transformer, the value of the inductance given in figure 3.1 is fluctuating, which leads to a different discharge in the DBD. A slight shift in the temperature of the ferrite core of the transformer induces a certain change in the permeability of the core, which on its turn leads to a slight shift in the inductance of the coils [82]. The value of this inductance determines the resonance frequency of the voltage signal. The down-ringing voltage signal of the previous pulse is still present when the new pulse is generated. Therefore, when the resonance frequency is changed, the starting position of the new pulse on the sinusoidal damping voltage signal of the previous pulse is different. When the new pulse starts on the maximum voltage value of the previous pulse, this will result in a different new pulse than for the case the new pulse starts on the minimum voltage value of the previous pulse. The voltage fed over the DBD, the height

---

[4]For measurements with the ICCD camera and the new setup, this length was 1.3 meter.

of the voltage peaks, is different and therefore the formation of discharges will change.

The change in discharge formation is larger for higher pulse frequencies. For a pulse frequency below 1000 Hz, the previous pulse is damped away. The start voltage for these pulse frequencies will always be zero. For a pulse frequency of 1000 Hz or higher the previous pulse is present, the amplitude of the previous pulse will be higher for a higher pulse frequency. When the amplitude is higher, the starting position of the new pulse can fluctuate over a higher voltage range. The voltage fed to the DBD can change more for higher pulse frequency than for a lower pulse frequency.

The power dissipated in the core depends on the settings of the DBD. If we look for instance at the frequency of the generated pulses, more power is needed to generate the higher amount of pulses per second, so the core of the transformer will heat up more. Therefore the shift in resonance frequency is higher for a higher pulse frequency or a longer pulse width.

When doing a measurement, the memory effect of the previous measurement should be kept in mind. So when the previous measurement was with a higher power, the core of the transformer has already a certain temperature above the room temperature. A measurement directly after the previous measurement will therefore give a distorted result. In the new setup, in order to minimize the memory effect, two steps are taken. Firstly, the experiments are performed from settings with low to higher power. So from low to high pulse width or pulse frequency. Secondly, the setup is on for a long time before a measurement is performed, to reach the temperature equilibrium in the core of the transformer.

3.2   Determine the power dissipation of the plasma

In this section the methods and setup to determine the power dissipation are discussed. In the theory, section 2.2.1, already two different methods to determine the power dissipated in the plasma are described:

1. Taking the integral for the total voltage times the total current over one whole period T , $P = \frac{\int_0^T V_{total}(t) i_{total}(t) dt}{T}$.

2. Taking the area of the Q-V plot.

The second and common way is only feasible for a sinusoidally driven DBD. For a pulsed DBD, no Lissajous figure will be obtained. Therefore the first method has to be applied for the setup used in this research. The total

current in this equation, I_{total}, can be measured directly or can be obtained by differentiating the measured charge $Q(t)$.

So in order to determine the power dissipated in the plasma the voltage over the total system $V_{total}(t)$ is measured and the total current I_{total} or the charge $Q(t)$ are determined. In figure 3.5 the setup for measuring the total voltage signal and current or charge signal is shown. For the total voltage signal a 1:2213 V[5] *Tektronix* voltage probe with a capacity of 3pF is connected parallel to the load, it is connected directly to the power generator and the ground. A Rogovski coil is used to measure the total current, I_{total}, through the wire between discharge and ground. In order do determine the charge, $Q(t)$, a large capacitor of 0.47 μF is connected between the discharge and the ground[6]. With such a high value of the capacitance, the connection of the capacitor will have no influence on the system. By measuring the voltage over this capacitor with a 10 V *Agilent* voltage probe the charge can be calculated according to equation 2.16. Both the voltage probes and the Rogovski coil are connected to an oscilloscope, the *Agilent InfiniiVision 7000B DSO7034A Oscilloscope [83]*, with a sampling speed of 4GSa/s and a bandwidth of 350 MHz. The signal on the scope is averaged 1024 times and the scope triggers on the edge of the first positive peak of the total voltage signal.

Before the energy dissipated in the plasma for the pulsed dielectric barrier discharge is determined, the validity of the first method is tested. A sinusoidal power generator, the *PVM/DDR Plasma Driver* [84], is connected to the load. The power dissipated in the plasma is calculated with the first method, for the total current measured directly and for the total current determined by the charge differentiated to the time. These two values for the dissipated power are compared to the value for the dissipated power obtained with the area of the Q-V plot, the second and common method.

The measurements with the sinusoidal power generator are performed for different settings. Changes were made firstly in the setup and secondly in the generation of the sinusoidal voltage signal. The setup was changed in three ways:

1. A distance between the quartz and the PVC sheet of 1 mm,

2. a distance between the quartz and the PVC sheet of 2 mm,

---

[5]The calibration of the voltage probe is performed with a Northstar PVM-1 voltage probe.

[6]The position of the Rogovski coil and capacitor have an influence on the amplitude of the measured value. The further from the power generator the lower the amplitudes will be, this is due to high frequency signal reflections in the wires.
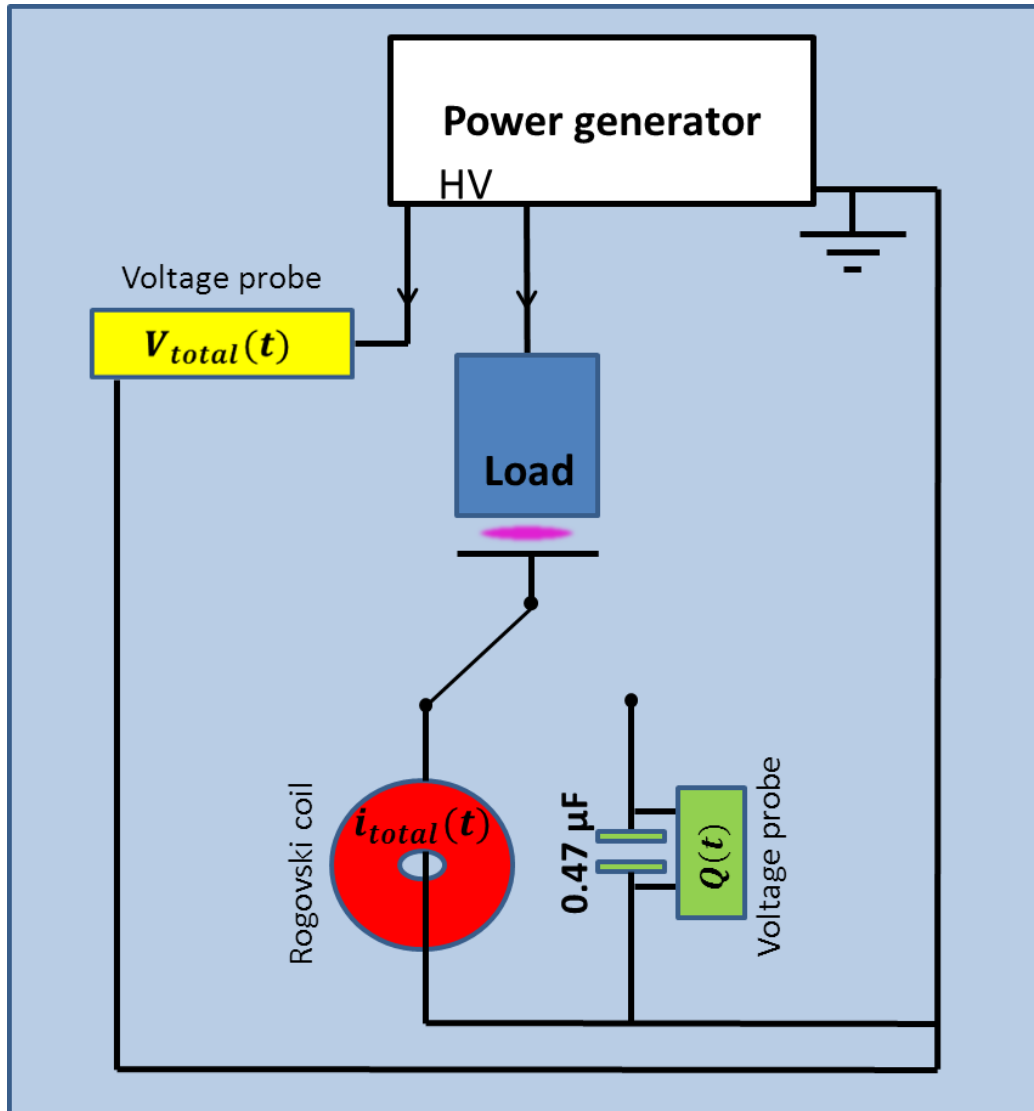
Figure 3.5: *In the top of the figure we have the power generator which is connected to the load. A voltage probe is connected parallel to the load in order to measure the total voltage $V_{total}(t)$. Between the second electrode and the ground either a Rogovski coil or a capacitor, with capacity $C = 0.47$ μF, is connected. The first one is connected to determine the total current I_{total} and the second is connected, to use the voltage probe over the capacitor to calculate the charge $Q(t)$, where $Q(t) = V(t) \cdot C$.*

3. and a distance between the quartz and a metal surface of 1 mm.

For all those three different settings, measurements are performed for random different frequencies and amplitudes of the sinusoidal voltage signal.

The energy dissipated in the plasma for the pulsed power generator is measured for different settings as well. For every specific settings, three individual measurements are made. The three values of the power dissipation belonging to these three measurements are averaged and a standard deviation is determined.

3.3   Measurements on the relative light intensity of the plasma

The relative light intensity measurements of the plasma are performed with two different devices: first a spectrometer is used, and second an intensified charge-coupled device (ICCD) camera, is used. Both the devices and the experiments with these devices are discussed in this section.

3.3.1   Use of the Avantes spectrometer

The spectrometer used in this project is an Avantes spectrometer, the *AvaSpec-ULS2048-USB2 Fiber Optic Spectrometer* [85]. The hardware of the Avantes spectrometer is connected with an USB to a desktop, here the settings of the spectrometer can be controlled with the software of the Avantes spectrometer. In the software the integration time and the amount of averages for one scan can be set. One scan is taken over the wavelength range from 200 to 1100 nm. The resolution belonging to this scan range is around 1 nm.

The setup for the measurements with the Avantes spectrometer is shown in figure 3.6 . The light in the center of the plasma of the DBD is captured by a lens with a focal length of 5 cm, which images the light on an optical fiber. The plasma is not constant in time, due to the fluctuations in the position of the filaments between substrate and DBD. In order to exclude the time variation, the time of one measurement has to be long enough. The integration time combined with the amount of averages for every measurement is 5 minutes. Before measurements with this setup are performed on the plasma, a dark scan of the surrounding light is taken, which is subtracted from the scans of the plasma.

The relative light intensity for the different settings of the old setup is determined with the Avantes spectrometer. The value of the relative light intensity is obtained by the integration of a spectrum over the wavelength
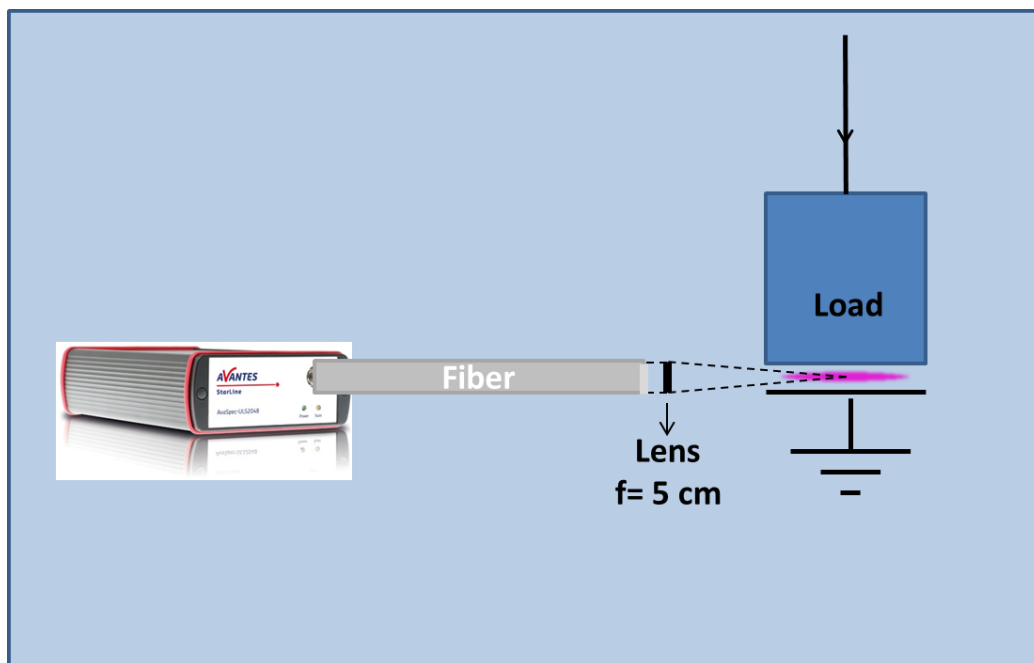
Figure 3.6: *The setup for measurements with the Avantes spectrometer. The fiber of the Avantes spectrometer is focused with a lens, focal length of 5 cm, in the center of the discharge.*

range of 200 to 1000 nm. Spectra are measured for different duty cycles, frequencies, pulse widths and finally distances. Within every setting, we made the measurement three times. In order to exclude gradual changes of the surrounding, the measurements of every set are performed in a random order.

3.3.2   Images with the ICCD camera

The camera used for the experiments is the *4 picos ICCD camera of Stanford Computer Optics, Inc* [86]. Relevant settings of this ICCD camera are the delay time, the gate time, the amount of frames per image, and the micro channel plate (MCP) gain voltage. The delay time and gate time of the ICCD camera depend on the measurement. The amount of frames per image is 100, so for every image, 100 independent frames are added together. One frame has a standard integration time of 20ms. The gain voltage can be set from 0 to 1000V. When one photon hits the photon cathode, the photo electron is accelerated towards the MCP. The height of the gain voltage determines the rate of electron multiplication in the MCP. A low original photon signal can be amplified by several orders of magnitude with the gain voltage [87]. During measurements this gain should be low enough, so there is no saturation of the signal.

In figure 3.7 the setup with the ICCD camera is shown. The ICCD camera is added to the old and new setups which are described in subsection 3.1.3. Images with the ICCD camera are made of the intersection with the center of the plasma, in figure 3.7 this intersection is shown in green. Every point of the intersection is imaged with an lens in front of the camera and the lens of the ICCD camera. Before images of the plasma are made, a dark image is captured and subtracted from the images made of the plasma. For the measurements with this setup, the ICCD is triggering on the total voltage signal V_{total}. As described in the previous section, the imaged plasma is not constant in time. Therefore no time resolved images of the plasma can be made of the DBD, since the microfilaments are formed at different positions in time.

However, two other kinds of images are made for this project. First, images are made as function of time during a voltage pulse. From this a time depended light intensity profile can be made. Second, images are made for a whole pulse. The relative light intensity produced in one pulse can be compared for different settings. Both types of measurements are described in detail in the following part.

3.3.2.1   Time dependent relative light intensity

In figure 3.8 an example of a time dependent light intensity measurement with the ICCD camera is shown. In the graph on the bottom of figure 3.8 the voltage signal of a pulse is shown in blue and the current signal of a pulse is shown in red. The green bar indicates the time point in the pulse, on which the image shown on the top of the figure, is recorded. The delay time of the ICCD camera determines this time point. For the measurements, this delay time is shifted with steps of 1 μs, where the gate time is also 1 μs. With this shift in the delay time, images can be made for a large time range in a specific pulse. For every measurement, the first image is made approximately 3 μs before the start of a pulse. In the example of figure 3.8, the first image would be made with a delay time of 633 μs. The delay time of the last image depends on the measurement and is set after a time point in the pulse where no plasma is formed anymore. The difference in delay time between the first and the last image of a measurement is in the range of 85 and 170 μs.

Due to a delay time of 1 μs, no individual filaments are visible. Due to the high density of filaments in this time range, the plasma looks diffuse in figure 3.8. Although a delay time of 1 μs is too long to capture individual microfilaments, the resolution of 1 μs is short enough to see how the light emission is related to the voltage signal.

The images made by the camera are used to determine the relative light intensity for different settings on different time points. All images are integrated over the x- and y-direction to get a value for the relative light intensity of the plasma per time point. This intensity can be plotted in the same figure as the voltage signal of the pulse. The relative light intensity per time point experiments are performed for different pulse frequencies, pulse widths, distances and finally different materials for the old, but also the new setup. The gain voltage in the old setup is 670V and is 710V for the new setup.

3.3.2.2   Light intensity per pulse

The measurements for the relative light intensity for one whole voltage pulse are performed for the old and the new setup. For both setups the measurements are performed for all 10 pulse frequencies and all 10 pulse widths mentioned in subsection 3.1.2. For every measurement, 20 images are made[7], which can be integrated and averaged in order to determine the light intensity per pulse. From the 20 images a standard deviation is determined as

---

[7]These images are made in two batches of 10 images. For one batch, all 10 images are made in direct succession of each other.
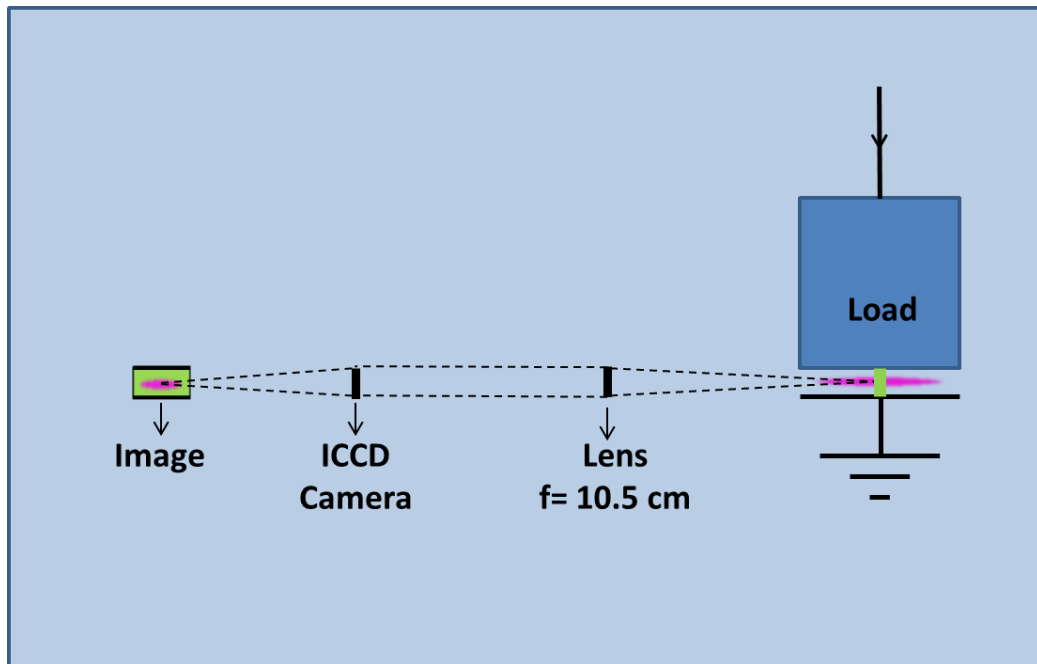
Figure 3.7: *The old or new setup in combination with the ICCD camera. The intersection with the center of the plasma (green) is imaged with an external lens (f=10.5 cm) and the internal lens of the camera.*

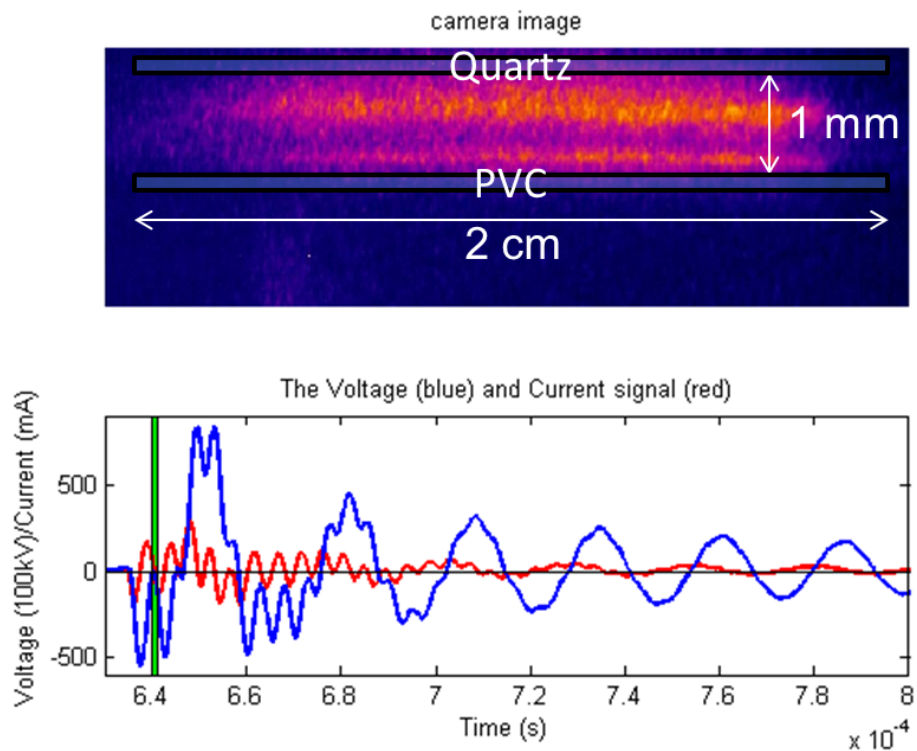**Figure 3.8:** *The image of the camera (top) and the current en voltage signal (bottom) for a frequency of 1500Hz, a pulse width of 10 μs, a distance of 1mm between the DBD and PVC, at the time moment in the pulse indicated by the green bar.*

well.

The delay time and gate time of the ICCD camera are set, so all light emission during one whole voltage pulse is captured. The images have a gate time of 250 μs, since no plasma (light) is formed in the pulse after 250 μs. The delay time of an image is set approximately 3 μs before the start of the pulse.

The method for the old setup is different than for the new setup. The voltage gain for the measurements with the old setup is 580V for different frequencies and 630V for the different pulse widths. In the new setup the value for the voltage gain is respectively 600V and 640V. For the old setup the the memory effect of the heating of the transistor is not taken into account yet. The value of the frequency or of the pulse width is changed randomly between the 10 values during the experiment. The values are changed randomly during the experiment, to exclude effects of changes in the lab. In the new setup the value for the frequency as well as the value of the pulse width is changed from a low to high power.

3.4 Fourier Transform Infrared Spectroscopy

Fourier Transform Infrared (FTIR) spectroscopy is a technique to get more insight in the chemistry within the DBD. With FTIR spectroscopy an infrared spectrum of absorption of a gas can be obtained. The particles in the gas absorb light and excite between specific vibrational and rotational states (subsection 2.1.4). By comparing the known vibrational and rotational spectra for different molecules with the obtained absorption spectrum, the gas composition can be determined.

In this research the Fourier Transform Infrared (FTIR) spectroscopy measurements are performed with a Bruker spectrometer, the VERTEX 80v [88]. A schematic of the spectrometer is shown in figure 3.9 . The light of a broadband infrared light source (a MIR lamp) is directed into a Michelson interferometer, where one of the mirrors (Mirror 2) is moving parallel to the light beam. While the mirror is moving with a fixed speed, the retardation between the two light beams in the interferometer is changing. For different distances between the mirrors, the light will interfere constructively or destructively with each other depending on the wavelength. So every specific distance between the mirrors, leads to a specific spectrum of the outcoming beam. This outcoming beam is focused in the sample compartment shown in figure 3.10. The discharge area of the DBD connected with the new power generator is positioned in this focus and light will be absorbed here. The volume between the inner and outer ZnSe windows is flushed with nitrogen,
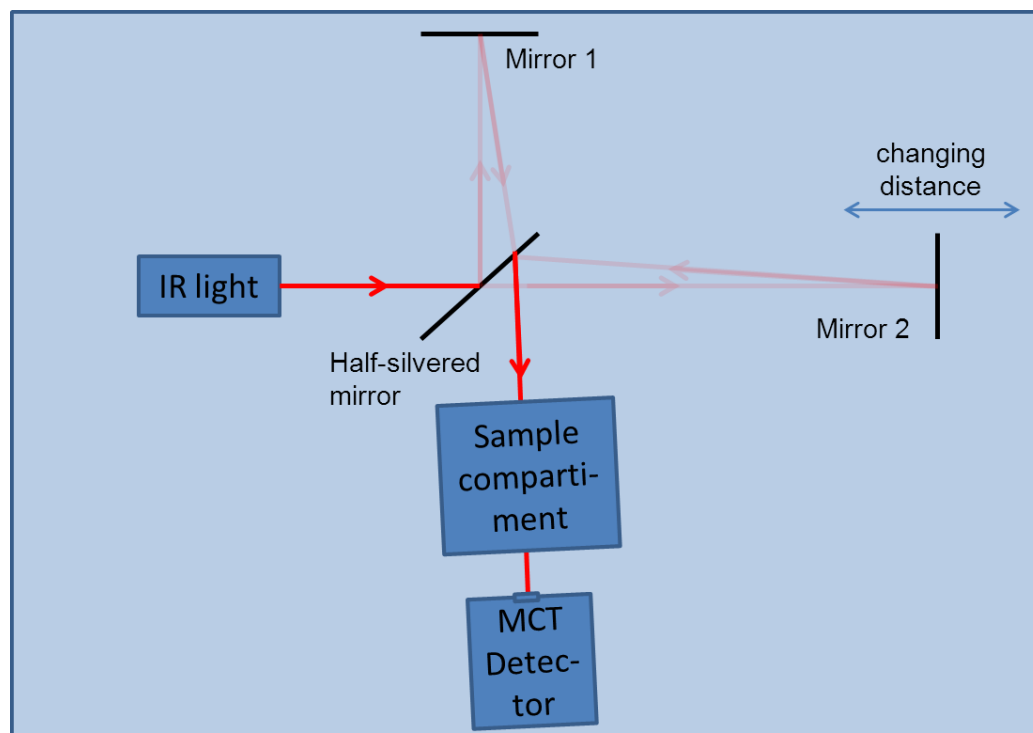
Figure 3.9: *A schematic of the light path in a FTIR spectrometer. The light of the infrared source is shone into the Michelson interferometer. Due to the moving mirror 2, the spectrum shone into the sample compartment is changing. In the sample compartment, light at certain wavelengths is partly absorbed. The absorption spectrum is detected by a Mercury cadmium telluride (MCT) detector.*
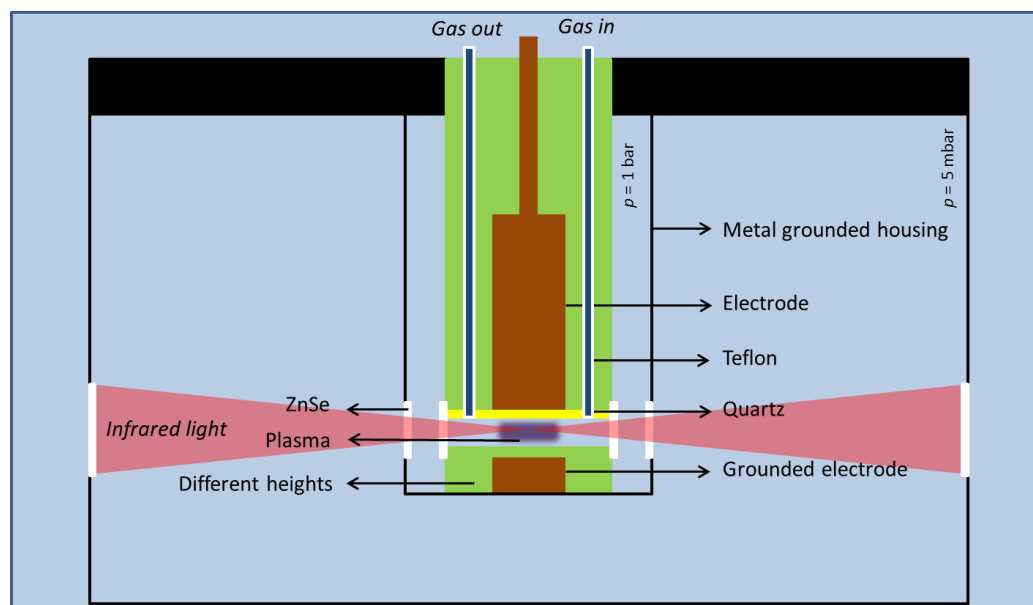
Figure 3.10: *The schematic of the used sample compartment in the FTIR, the IR light beam passes through the discharge area of the DBD and light is absorbed. The volume between the inner and outer Zinc Selenium (ZnSe) windows is flushed with nitrogen, to reduce the absorption of light in this part of the setup. Outside the ZnSe windows, the compartment is in vacuum. The metal housing around the DBD, shields the FTIR spectrometer from the EM fields originating from the DBD.*

to limit the absorption in this part of the sample compartment. Due to the vacuum outside the ZnSe windows, the absorption in this part of the sample compartment is low as well. The light coming out of the sample compartment is detected by a Mercury Cadmium Tellurium (MCT) detector. The detector detects the intensity of the light beam for every individual retardation, or distance, between the beam paths in the Michelson interferometer. The intensity as function of the retardation is called an interferogram. This interferogram is Fourier transformed to the absorption spectrum[8].

3.4.1   The absorption spectra

In this research the FTIR spectrometer is used for two different measurements. In the first measurement, the discharge area of the DBD is filled with gas: Argon (Ar) with 203 ppm Nitric Oxide (NO). For the second measurement the DBD is switched on.

3.4.1.1   The absorption spectrum of Nitric Oxide

The measurements on NO are performed to find the right settings of the FTIR spectrometer and see whether the absorption path length is long enough. Two settings of the FTIR are the resolution and the averages. The resolution has to be small enough to see the shape of the individual vibrational bands, by comparing the height of the bands with calibration measurements, the densities of molecules can be determined [90]. The height of the band scales linearly with the density. The amount of averages has to be high enough to smooth out the noise. A better resolution and more averages lead to a longer measurement time. The absorption path in the FTIR is only 4 cm, only in this 4 cm particles can absorb light.

   Before the discharge volume with a height of 4 mm is filled with the NO gas, the volume is flushed with nitrogen. During this flush, a reference absorption spectrum is obtained. The absorption spectrum of NO is subtracted from the reference absorption spectrum, to obtain a spectrum with only the absorption peaks.

3.4.1.2   The absorption peaks for a discharge

The absorption spectrum is obtained while the DBD is switched on. The new power generator is set on a pulse frequency of 500 Hz, a pulse width of

---

[8]Before the transformation, the interferogram is multiplied with a Blackman-Harris window, to bring the interferogram smoothly down to zero at the edges of the sampled region. This apodization prevents side lobes in the calculated spectrum. [89]

10 μs and a duty cycle of 100%, where approximate 0.5 W is dissipated in the discharge. The distance between the quartz and the Teflon is set on 3 mm. At this gap width, there is still a discharge and more light can pass through the cell. For the cell, flushed with dry air, the absorption spectrum is measured as well. This spectrum is subtracted from the spectrum obtained with the plasma on to obtain a spectrum with absorption peaks.

Chapter 4

Results and Discussion on Plasma diagnostics

In this chapter the results of the measurements described in chapter 3 are shown. First, the link between the voltage signal, the light emission and the plasma current is discussed by a measurement with the old setup. Second, the voltage signal and the light intensity for different settings are shown for first the old and then the new setup. Next, the results for the power dissipation calculations are shown. First the validity of the method is tested and then the method is applied for different settings of the new setup. In the end of the chapter the results of the measurement with the FTIR setup are analyzed.

4.1   The relation between the light emission and the electric signal

In this section a result is given for the voltage signal, light emission and plasma current in the old setup for a pulse frequency of the DBD of 1500 Hz, a pulse width of 10µs and with a gap distance between the quartz and the PVC substrate of 1mm.

4.1.1   The relation between the light emission and voltage signal

The light emission in relation with the voltage signal is discussed in this part. In figure 4.1 the voltage signal in blue and the light intensity as function of time in green are plotted in the same figure. The behavior is in agreement
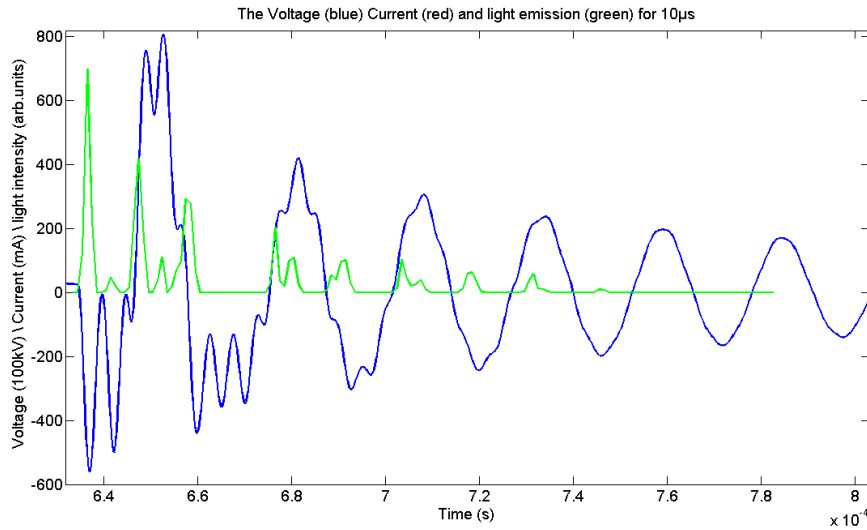
Figure 4.1: *The light intensity compared to the electric signal, for a 1500Hz frequency, a pulse width of 10 µs and a distance to the PVC of 1 mm.*

with the theory of the development of microdischarges (2.1.1). The first emission of light happens on the negative voltage slope. Electrons on the quartz of the DBD are moved to the PVC substrate by microfilaments, leaving the quartz with less electrons and the PVC with an abundance of electrons, which reduces the external applied field. For the second negative voltage peak, again a plasma is formed. This time the light emission is relatively low, due to the remaining charge on the PVC which reduces the applied electric field, and the few number of electrons that didn't leave the quartz at the first breakdown. There is also a positive effect of the first negative voltage peak, the background ionization will be relatively high for the second negative voltage peak, which makes it easier to have a discharge. When the voltage has a positive peak, the charge accumulation on the PVC has an enhancing effect on the discharge and electrons move back to the quartz and interact with molecules and atoms and form a plasma between the two dielectric surfaces. Also, here there is a second light emission peak for the second positive voltage peak with a lower light intensity. This second voltage peak is higher than the first one, therefor it is possible to have a net high enough electric field for a breakdown. Even though there is remaining charge on the PVC substrate. Also for succeeding positive voltage pulses the second peak is higher than the first, therefore a second light emission peak is possible. For the negative voltage peaks the second peak is lower, and here no second emission peak is shown. the net electric fields are not high enough for a breakdown in the gap. The intensity of the plasma decreases in

time, since the damping of the voltage signal. Due to the lower voltage, the time the electric field in the gap is is high enough for electric breakdowns is shorter. At some point in time, the minimum kinetic energy of the electrons to exciting molecules and atoms for an electron avalanche is not reached.

4.1.2 The correlation of the plasma current and light emission

Instead of comparing the light emission to the total applied voltage signal, the light emission can be compared with the plasma current. The plasma current is given by $i_{plasma}(t) = i_{total}(t) - i_{air}(t)$, where $i_{total}(t)$ is the total current in the load and i_{air} is the displacement current. The total current $i_{total}(t)$ is measured in a single shot with a Rogowski coil. In order to determine the displacement current i_{air}, the measured voltage signal is used, according to $i_{air}(t) = C_{totalsystem} \frac{dV_{total}(t)}{dt}$ (equation 2.16). This $i_{air}(t)$ is fitted with the current signal $i_{total}(t)$, for the time range between 720 and 820 μs. In this time range, no light emission is measured, so there is no plasma current and $i_{air}(t) = i_{total}(t)$. This fit gives the total capacity of the system $C_{totalsystem} \approx$ 14pF [1] and is shown in the top of figure 4.2 . Now, if this displacement current is subtracted from the total current measured with the Rogowski coil, the plasma current is determined.

On the bottom plot in figure 4.2 the plasma current is shown in blue. When looking to figure 4.2 there is a correlation between the light emission and the plasma current. However, for the later light emission peaks there are no visible plasma current peaks. This may be due to two reasons. First, the signal to noise ratio is low, since the measurement was only single shot. The current signal can not be averaged since the exact position of the current peaks changes per shot and the current peaks would be averaged out as well. Second, the bandwidth of the oscilloscope is too small: the duration of one plasma current peak is in the ns range, but the bandwidth of the oscilloscope is 350 MHz. So not all peaks are detected by the oscilloscope.

Every single plasma current peak is measured as an oscillation, this can be due to the network, the presence of inductance, or an artifact in the measurement technique. For the latter, reflections in the cable of the Rogowski coil can cause these oscillations. To prevent or minimize this oscillation a fast-current probe could be used [91].

---

[1]This capacity also includes all the parasitic capacities in the system.

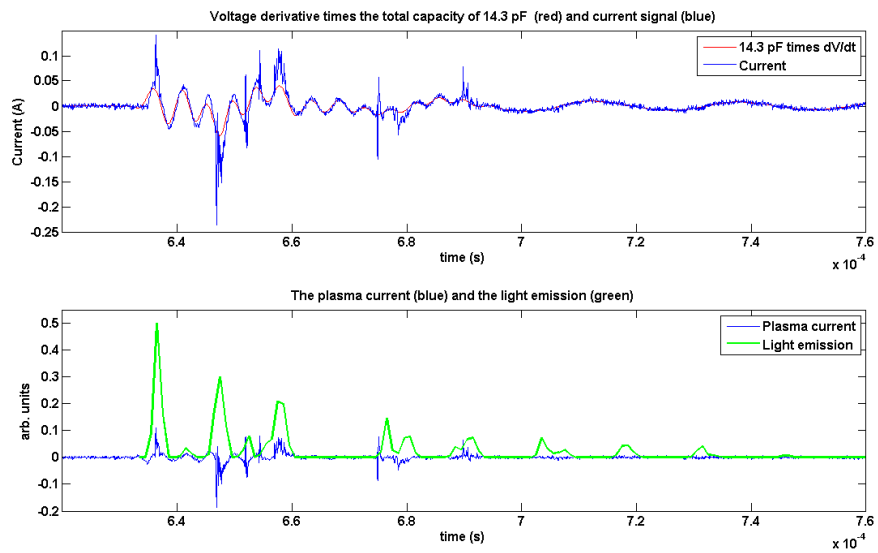**Figure 4.2:** *In the top figure the single shot current signal in blue and the derived voltage signal times the factor 14,3 pF in red. In the bottom figure the blue minus the red line in the top figure in blue and the light emission of the plasma in time in green. Both the voltage signal and the single shot current signal are smooth with the Savitzky-Golay filtering*
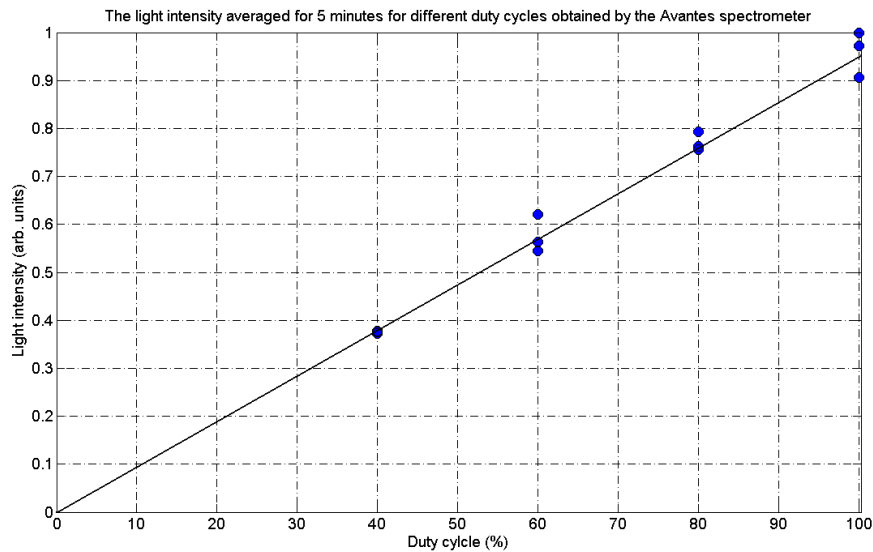
Figure 4.3: *Three data points for the normalized light intensity shown for a duty cycle of 40%, 60%, 80% and 100%. For a frequency of 1500Hz, a pulse width of 10 µs and a distance of 1 mm. The data is obtained with an integration time of 500 ms and 600 averages.*

4.2 The behavior of the DBD for different settings

A way to get insight into the effect of different settings, like the pulse width or gap distance of the DBD, is by investigating the light emission and the voltage signal. In this part the voltage signal and the effect on light intensity are recorded for the old setup for different duty cycles, pulse frequencies, pulse widths, gap distances and materials. This is possible by measuring the time depended light intensity in a pulse of the DBD (section 3.3.2.1) and/or by recording the light intensity of a whole pulse and/or by measuring the light intensity averaged in 5 minutes (section 3.3.2.2 and 3.3.1)

4.2.1 The relation between the duty cycle and the light intensity

For the effect of the duty cycle we only used the Avantes spectrometer (section 3.3.1). In figure 4.3 the relation between the duty cycle and the light intensity is shown. As expected, this behavior is linear and through the origin. If the DBD is creating a plasma for 40% of the time the intensity will be twice as low
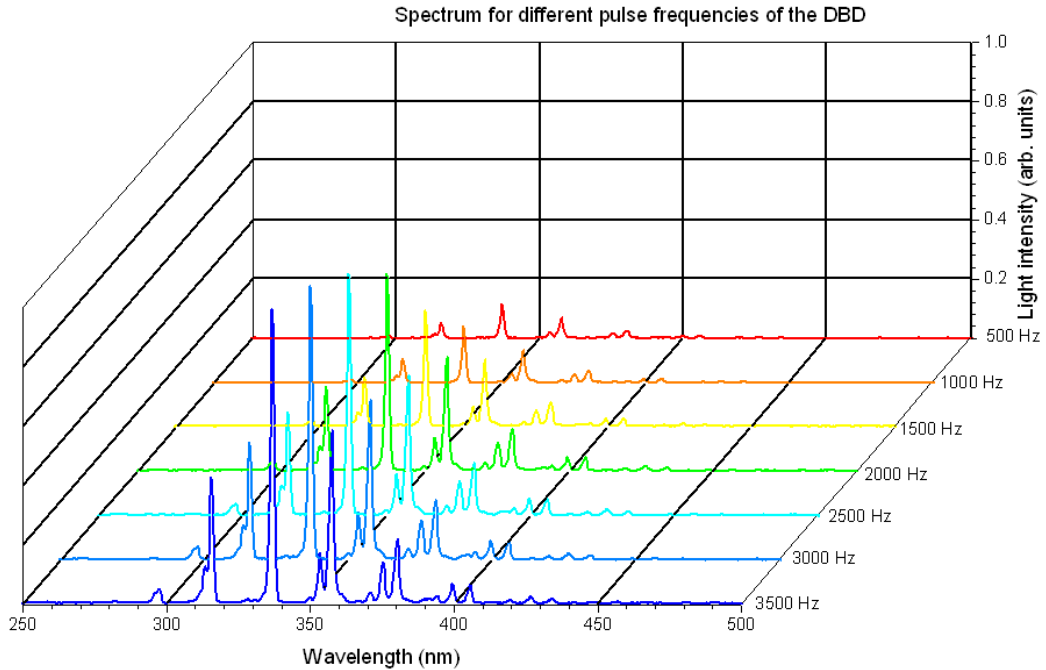
Figure 4.4: *Relative light intensity per given wavelength for different pulse frequencies of the old setup.*

as for the plasma creating by the DBD 80% of the time. The duty cycle has no effect on the voltage waveform or the electric circuitry. For a duty cycle of 10% and the standard settings, there are approximately 150 successive pulses during every second the the DBD is on. Within every pulse a lot of individual microfilaments are formed. It is difficult to form the first filaments, these filaments form charges and particles which make the formation of later filaments easier. In an operation with 150 pulses, the effect of the difficult forming of the first few filament is negligible. The relation between light intensity and duty cycle will still be linear for a duty cycle of 10%.

4.2.2 The behavior of the light intensity and voltage signal as function of the pulse frequency

In figure 4.4 the results of scans with the Avantes spectrometer in the wavelength range from 200 to 1100 are shown for different pulse frequencies in the old setup of the DBD. The ratio between the peaks in a spectrum does not change for different pulse frequencies, or in other words, only the amount of microfilaments formed changes, not the properties of these microfilaments. This is as expected as discusses at the end of subsection 2.1.1.

The voltage signal and light intensity signal for pulse frequencies of 250Hz, 1500Hz and 3500Hz for the old setup are shown in figure 4.5. It seems that the light intensity is lower for a lower frequency, however this is due to the lower amount of pulses during the 20 ms integration time of the ICCD camera. For a frequency of 3500 Hz, the shutter opens 70 times during the integration time, but for a frequency of 500 Hz, this is only 10 times. The position of the light peaks does not change for different frequencies.

In figure 4.6 the light intensity captured with the ICCD camera is shown as function of time for different pulse frequencies of the old setup. This behavior is not completely linear as expected. First, products formed by the microfilaments in the previous pulse are present in a higher concentration, when the second pulse is generated with a shorter delay. With these products present, the formation of new microfilaments will be easier. In section 2.1.3 the decrease of ions in the gap are estimated. The presence of ions in the gap will have an enhancing effect on new breakdowns. Second, if the voltage of the previous pulse is present when the new pulse starts, this will lead to a higher or lower maximum voltage as shown in red in figure 4.6 and overall higher or lower voltage peaks. These higher or lower voltage peaks lead to more or fewer discharges, respectively, and therefore to a higher or lower light intensity for higher pulse frequencies. For instance, at a frequency of 1500 Hz, the light intensity as well as the maximum voltage have a small dip in figure 4.6.

Finally, for frequencies higher than 2500Hz, an other effect seems to be present as well. The intern power supply can not deliver enough power to fully charge the large capacitor in the time between two pulses, see subsection 3.1.1 and figure 3.1. This leads to lower voltage peaks as shown with the red data. Fewer microfilaments will be formed, which leads to a smaller amount of current peaks, as shown in appendix B. The current peaks in a single shot current signal are directly correlated with the amount of microfilaments in the gap.

Two reasons, related to the heating of the transformer discussed in section 3.1.4, explain why the error bars are larger for a higher frequency. First, for the highest frequencies, most of the power is dissipated in the system. Therefore a higher temperature raise can be expected for the higher frequencies and a longer time to reach equilibrium. If measurements are performed before this equilibrium is reached, results may differ. Second, the time between two pulses is shorter for a higher frequency. The damping of the voltage signal is less at the time the new pulse is generated. The difference between the amplitude of the maximum and the minimum voltage signal in the previous pulse is larger and therefore the effect when shifting the starting point of the new pulse will be more drastic.
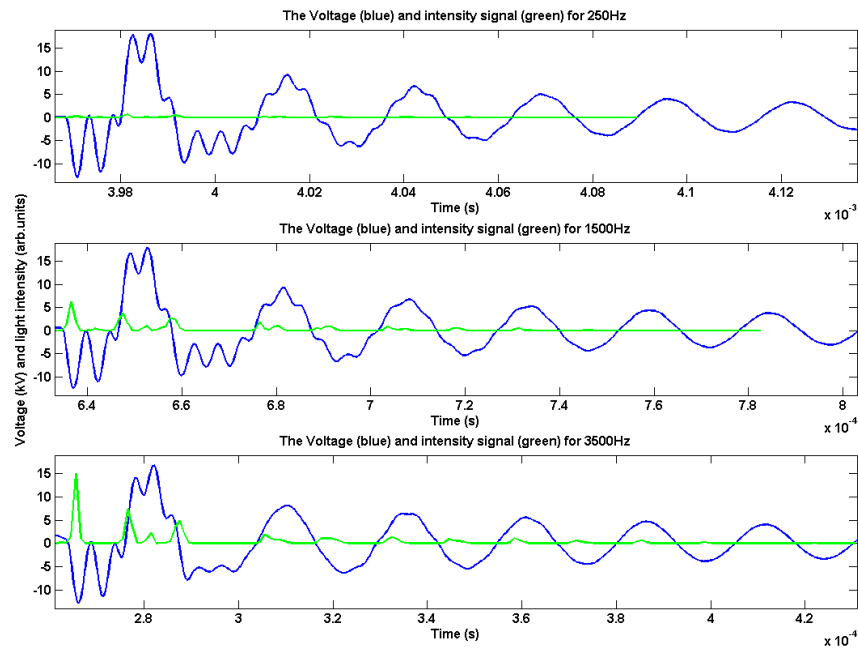
Figure 4.5: *The light intensity in arbitrary units in green and the voltage signal in blue in respect to the time for a frequency of 250Hz, 1500Hz en 3500Hz.*
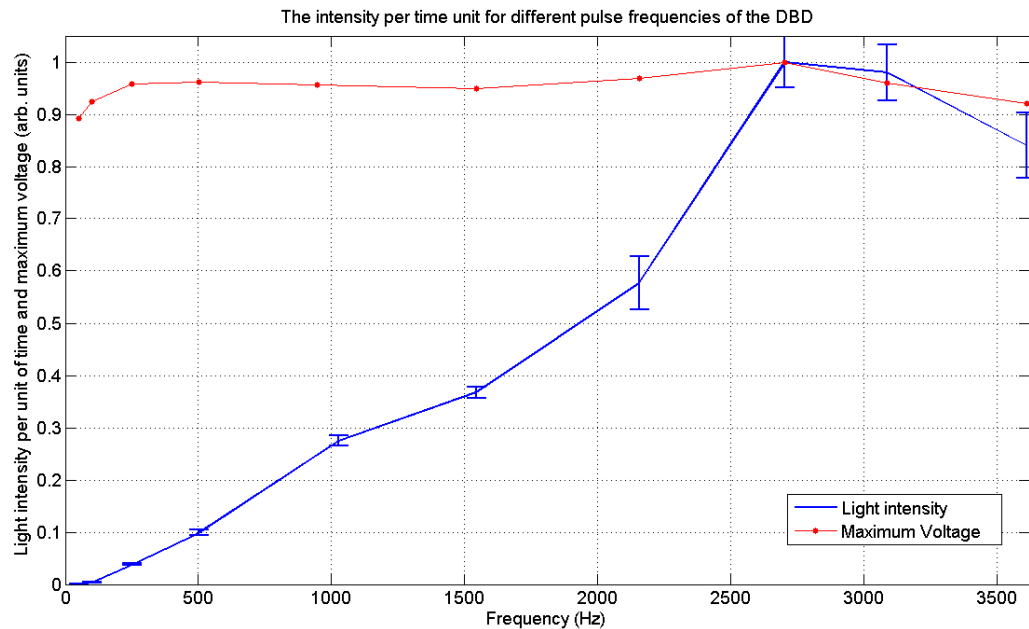

Figure 4.6: *The normalized light intensity recorded with the ICCD camera for different pulse frequencies and a duty cycle of 100%, a pulse width of 10 μs and a distance of 1 mm to the PVC substrate.*

4.2.3 The influence of the pulse width of the DBD

When the pulse width is smaller, the time the large capacitor is discharging over the primary coil is shorter. The current built up in the primary coil during this time is smaller. So, when the switch is opened, the current which the coil wants to preserve is lower and therefore the magnetic flux through the the secondary coil is lower. This leads to the lower maximum value in the voltage signal for a smaller pulse width and therefore a lower light emission. In the right graph of figure4.7 the light intensity and voltage signal are shown as function of time for a pulse width of 10 µs and a pulse width of 2 µs and indeed, the amplitude of the voltage and light emission are lower for a pulse width of 2 µs.

The results for the measurements with the fiber and with the ICCD camera, for the light intensity per time unit as function of the pulse width are shown in figure 4.8. The results are the same. The lower light emission and amplitude of the voltage for a smaller pulse width is also visible. The nonlinearity of the light emission and maximum voltage is due to the heating of the transistor. When the pulse width is broader, the transistor is heated more. So the position on which the new pulse starts on the resonating voltage of the previous pulse shifts. For a pulse width of 4 and 9 µs this position is probably a bad start position.

The jump from 1 to 2 µs is due to the small and irregular amount of discharges at a pulse width of 1 µs. At this pulse width not every voltage pulse generates discharges. The maximum voltage at this pulse width is not always high enough to have a breakdown, the maximum voltage is in the range of the breakdown voltage.

4.2.4 Influence of the gap distance on the light emission of the plasma and the voltage signal

In figure 4.9 the light emission and voltage signal are shown for a gap distance of 1mm and 2mm. In figure 4.10 we see the light intensity the fiber pics up from the plasma. For both the light emission taken by the camera and the fiber, the optical path is changed. Therefore the comparison of results quantitatively should be done with great care. In figure 4.10 the relatively low light intensity at 1 mm is due to the masking of the view of the fiber. However we can say something about the plasma itself for the other distances. The intensity is dropping, but the masking of the view of the fiber is smaller. The rate of the drop can not be determined, but for a larger distance we have less light intensity. The light emission signal in figure 4.9 has this drop in light intensity as well. For a gap distance of 1 mm, there is light emission for

Figure 4.7: *The intensity in arbitrary units in green and the voltage signal in blue in respect to the time for a pulse width of 10 and 2μs.*
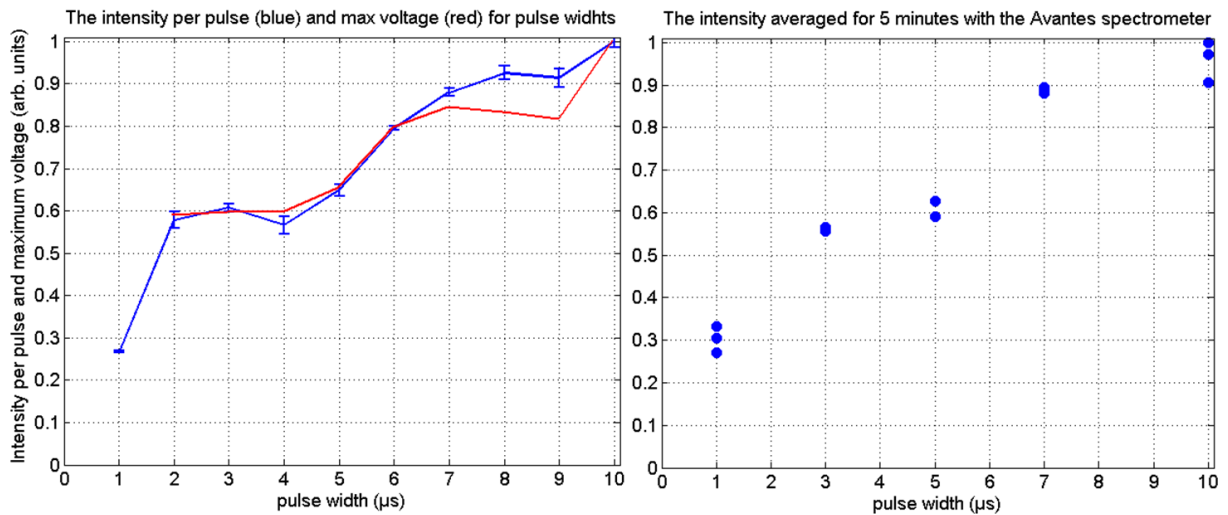
Figure 4.8: *The normalized light intensity shown for different pulse widths for a frequency of 1500Hz, a duty cycle of 100% and a distance of 1 mm. In the left graph the maximum voltage is shown in red. The data in the graph on the right is made with an integration time of 500 ms and 600 averages.*

Figure 4.9: *The intensity in arbitrary units in green and the voltage signal in blue in respect to the time for a distance of 1mm and 2mm.*
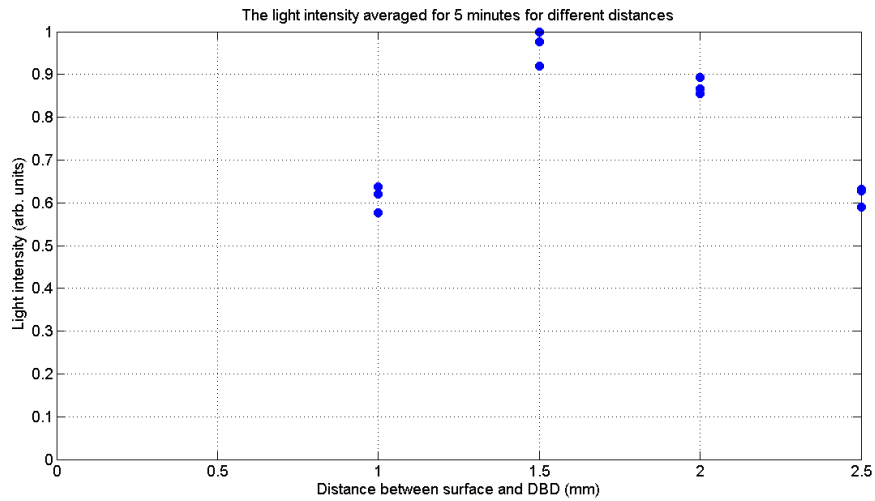
Figure 4.10: *The normalized light intensity shown for different distances between the DBD and the perplex plate for a frequency of 1500Hz, a duty cycle of 100% and a pulse width of 10 µs. The data is made with an integration time of 500 ms and 600 averages.*
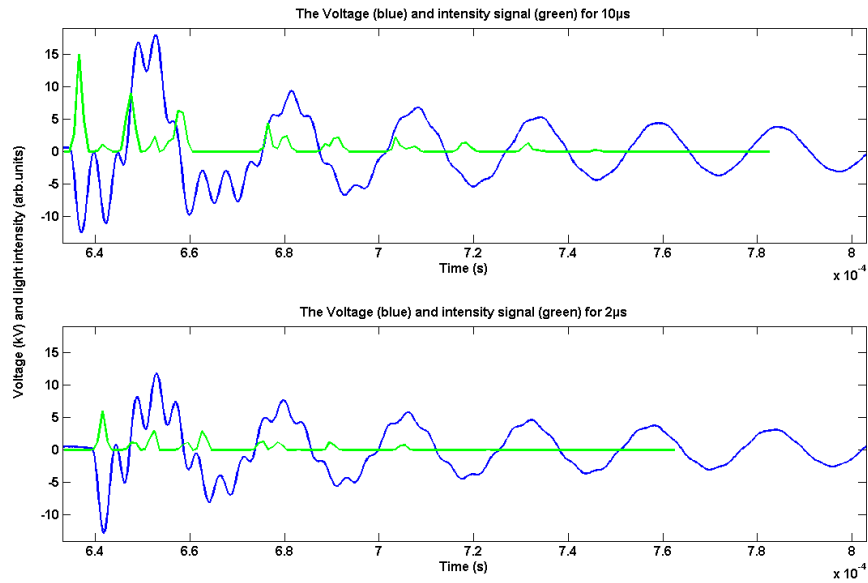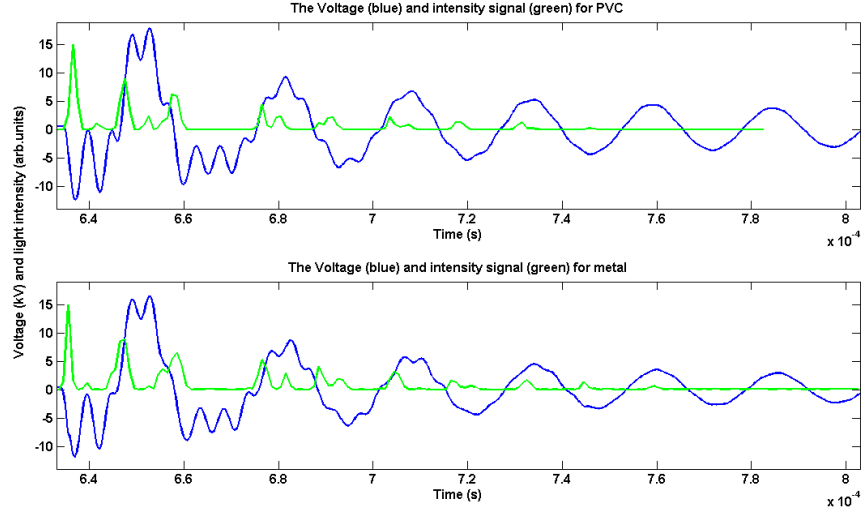
Figure 4.11: *The intensity in arbitrary units in green and the voltage signal in blue in respect to the time for a PVC and metal surface.*

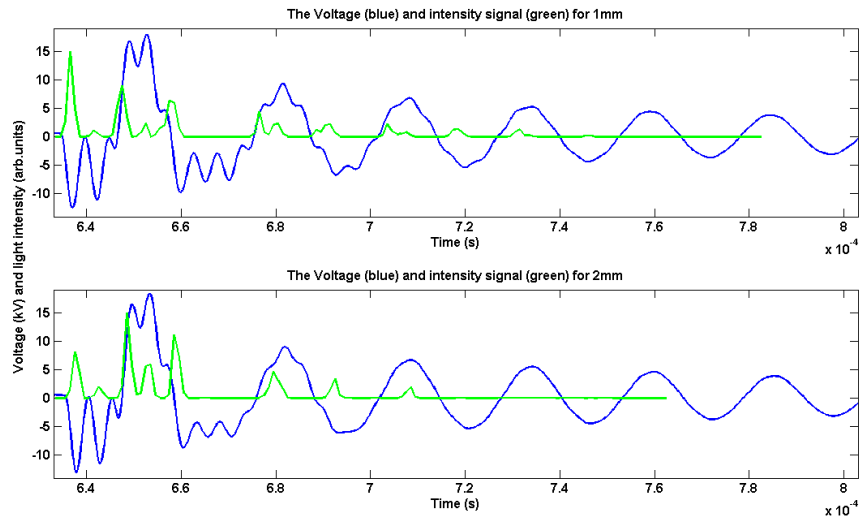voltage peaks at a later time in the pulse than for a gap distance of 2 mm. This drop in intensity can be explained by the same mechanism in equation 2.17 and 2.18: for a larger gap distance g, the voltage of the system should be higher in order to reach the breakdown voltage.

In figure 4.9 the higher resonance frequency is damping at a higher rate for a gap distance of 2 mm. The larger gap leads to a higher capacity and this leads to the higher damping rate as shown in section 3.1.1.

4.2.5   Influence of a conductive or dielectric material

The light intensity and the electric signal for PVC and metal in the old setup are shown as function of time in figure 4.11 . Due to changes in the optical path by removing the PVC sheet the results are not comparable in a quantitative way. However the light intensity in time of the two settings can be discussed, as well as their voltage signals. It seems that discharges are possible in the setup without the PVC for a longer time after the first voltage peak. If, in equation 2.17 the value for the factor $\frac{d_2}{\varepsilon_{r,2}g}$ is set to zero (or a substrate is chosen with a smaller capacity), the voltage over the air gap, V_{air} reaches the value for the breakdown voltage for a lower voltage over the system. This lower voltage needed for a breakdown also explains the slide shift of the light intensity peaks to the left, for the system with no second dielectric.
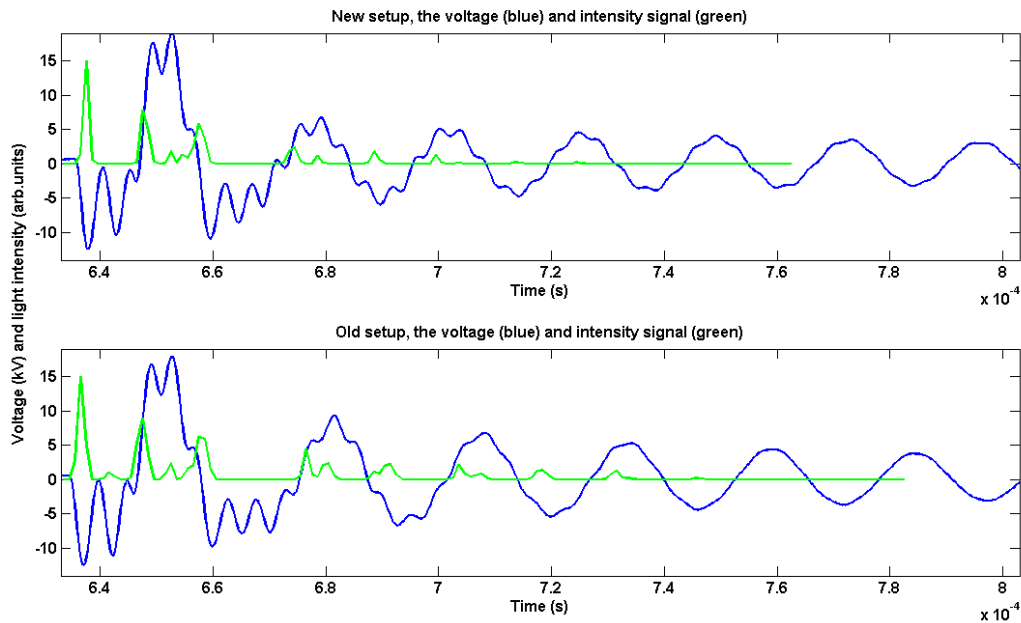
Figure 4.12: *The light intensity compared to the electric signal, for a pulse frequency of 1500Hz, a pulse width of 10 μs and a distance to the PVC of 1 mm. At the top for the new setup and on the bottom for the old setup.*

When comparing the damping of the two voltage signals, the damping for the metal surface is higher. Since the capacity of the system is higher for only the metal surface, this higher damping rate is expected.

4.3   The relation between the light emission and the voltage signal for the new setup

The new setup, with a similar power generator and load, may have a different influence on the formation of the plasma and the voltage signal than the old setup. In this section the measurements with the old setup in section 4.2 are repeated in order to compare both old and new setup with each other, for the four different settings. Before this comparison is made for each setting, first an example of the relation between the light emission and voltage signal for old and new setup are shown in figure 4.12 . Here the same plot is shown as in figure 4.1 at the bottom and a plot for the new setup is shown at the top, for both the settings are a pulse frequency of 1500 Hz, a pulse width of 10μs and a distance between quartz and PVC of 1mm.

First the voltage signals of both setups are compared, the blue lines in figure 4.12. For the new setup the frequency is a little higher than the 39kHz of the old setup. This is due to the interaction of the coils and capacitors in the new electric circuit: the product of the capacity and inductance is smaller[2]. Further the damping of the voltage is faster for the new setup due to the the difference in resistance and capacity of the new and old load. The relation between the voltage signal and the light emission is not changed, on the high or low enough rising voltages a breakdown occurs. Since the optical path is changed between the two measurements and also the voltage gain is different, the light emission measurements can only be compared qualitatively. However, it can be stated that for the new setup the subsequent peaks are relatively lower in intensity. So for the new setup, there is light emission for fewer peaks in the pulse. This corresponds with the faster damping of the voltage signal, at an earlier point in the pulse the voltage may not be high enough to generate an electric breakdown.

4.3.1 The influence of the pulse frequency for the new setup

For different pulse frequencies, the light intensity as function of time and the light emission for one whole pulse have been measured, see section 3.3.2. In figure 4.13 the time dependent voltages signals for 250 Hz, 1500 Hz and 3500 Hz are shown in blue.

The maximum voltage, the light intensity per pulse and the light intensity per unit time for different frequencies are plotted in figure 4.14. The light emission per pulse as well as the maximum voltage are increasing for frequencies above the 500 Hz. The increase in the light emission is due to available chemical species formed by the previous pulse and the starting position of the voltage pulse on the resonating voltage signal of the previous pulse. This leads to an increase in the amplitude of the voltage and a higher number of discharges.

In figure 4.14 there is no drop in the light intensity at the highest frequencies as in the old setup, since now the power supply can deliver enough power to the large capacitor to charge it completely before the switch closes again. Like already explained for the old setup, the error bars for higher pulse frequencies are again larger.

---

[2]Since the resonance frequency, ω_0, depends on the capacity C and inductance L as $\omega_0 = \frac{1}{\sqrt{LC}}$.
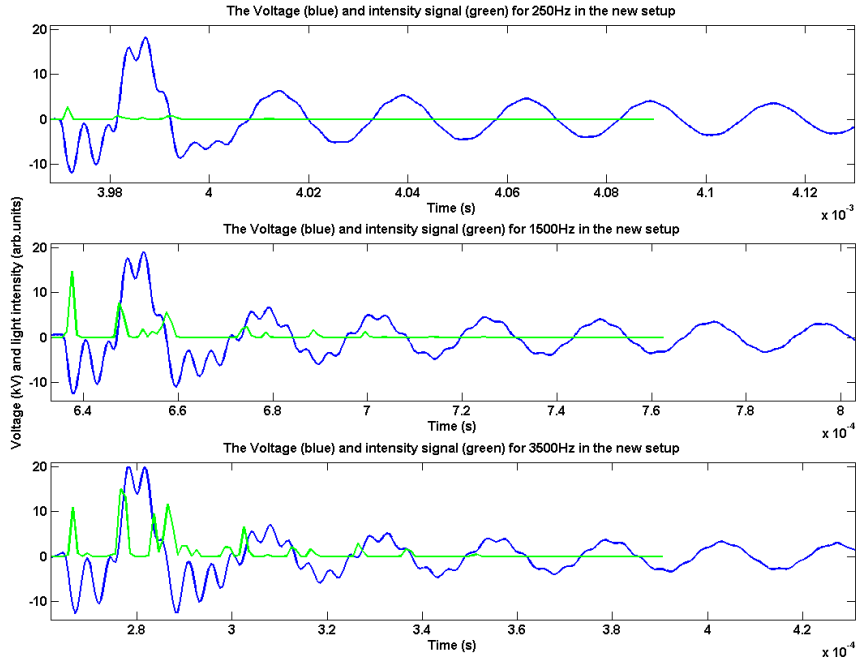
Figure 4.13: *The intensity in arbitrary units in green and the voltage signal in blue as function of the time for the new setup for a frequency of 250Hz, 1500Hz and 3500Hz.*
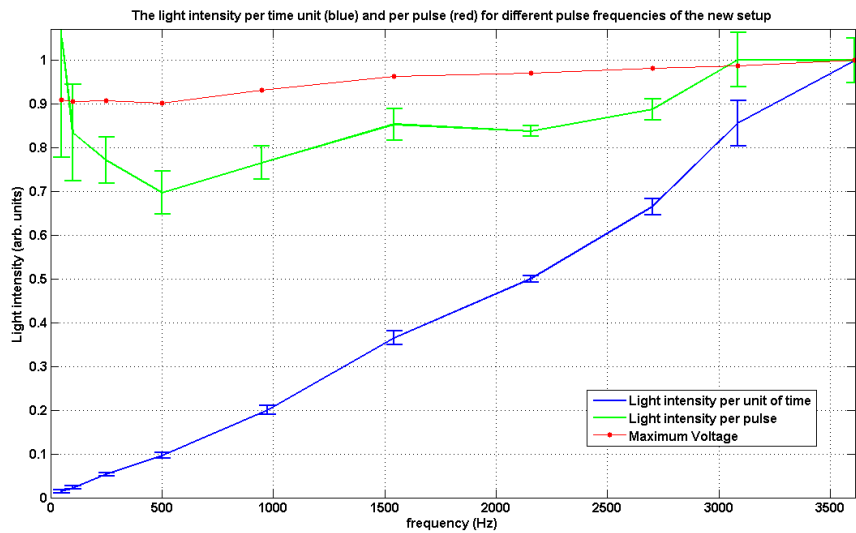
Figure 4.14: *The normalized light intensity per time unit in blue and the normalized light intensity per pulse in red shown for different pulse frequencies and a duty cycle of 100%, a pulse width of 10 μs and a distance of 1 mm to the PVC substrate.*

Figure 4.15: *On top the light intensity in arbitrary units in green and the voltage signal in blue in respect to the time for a pulse width of 10 and 2µs. On the bottom of the figure the normalized light intensity shown for different pulse widths in blue and the normalized maximum voltage in red. Both measurements are for a frequency of 1500Hz, a duty cycle of 100% and a distance of 1 mm.*

4.3.2   The light emission and voltage signal for different pulse widths of the new setup

In figure 4.15 the voltage signal and the light emission as function of time are shown in the top and on the bottom the normalized light emission per

pulse is shown. On the bottom of the figure also the normalized maximum voltage is shown in red. Besides the time the coil has to charge before the switch opens again, the starting point on the voltage signal of the previous pulse has an influence on this maximum voltage. The correlation with the normalized light intensity is not one-to-one, but the dip in maximal voltage and the light emission are at the same point, for the pulse widths of 4 and 9 µs: the same pulse widths as for the old setup.

In the new setup, for a pulse width of 1 μs, at every voltage pulse discharges are formed. This is due to another geometry of the load or a different control of the plasma.

4.3.3 The influence of the gap distance and material

The last two variables to measure with the new setup are the gap distance and the difference in dielectric material. First, the distance between the quartz surface and the PVC is changed, and second a PVC substrate or only the grounded metal is used. In figure 4.16 the voltage signal and the light emission are shown for a distance 1 and 2 mm and for a plasma between quartz and PVC and a plasma between quartz and metal. For both the top and bottom figure no quantitatively comparison can be made, due to a change in the optical path. For the top plot in figure 4.16 no difference is visible with the measurement with the old setup in figure 4.9. However, in figure 4.11 and on the bottom of figure 4.16 a difference can be discerned. The same drop in voltage for the setup without PVC is shown, but this drop is even higher in the new setup. This is again due to the difference in capacity of the new and old load en the relative change in total capacity when the PVC is removed.

4.4 The power dissipation in the plasma

In this section the method described in section 3.2 is performed to determine the power dissipation in the plasma. First the validity of the method is proven and then the power dissipation is determined for different settings of the new setup.

4.4.1 The power dissipation for a sinusoidally driven DBD

In figure 4.17 an example of a Q-V plot for the sinusoidally driven DBD is shown. The edges of the Q-V plot are rounded off due to energy losses in

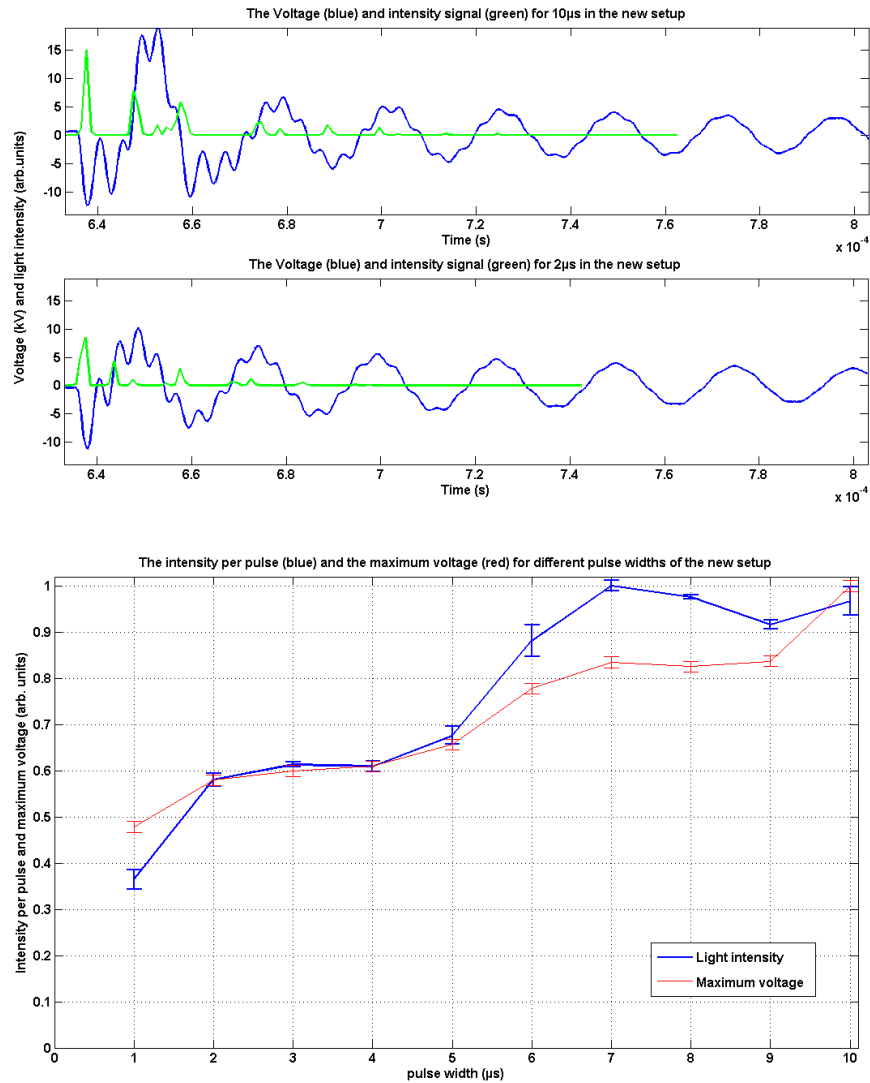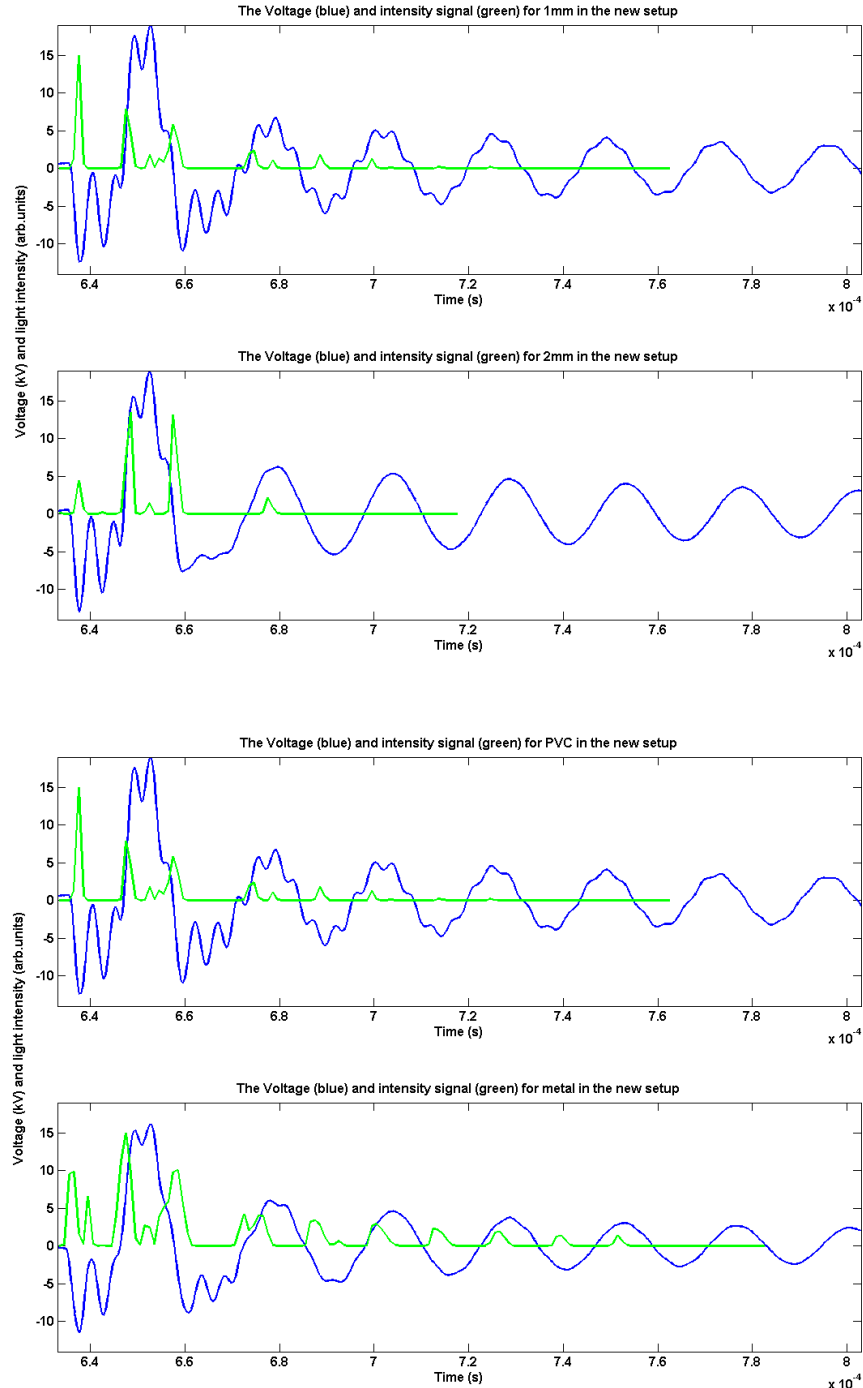**Figure 4.16:** *The intensity in arbitrary units in green and the voltage signal in blue in respect to the time for a distance of 1mm and 2mm in the top of the figure. On the bottom the light emission in arbitrary units in green and the voltage signal in blue in respect to the time for a PVC and metal surface underneath the electrode covered with quartz.*

resistances in the setup, which are not there in the ideal case described in section 2.2.1.1. The value for the power dissipation in the plasma can be calculated by determining the surface of such a Q-V plot, and this value can be compared with the integral given by

$$P = \frac{\int_0^T V_{total}(t) i_{total}(t) dt}{T} \, . \tag{4.1}$$

The total current $i_{total}(t)$ is measured directly with a Rogowski coil and is derived from the charge. In figure 4.18 both the current signal measured directly and the current derived from the charge are plotted in the same graph. The signals are very different from each other. The bandwidth of the scope is not good enough to sample every independent plasma current peak when the current is measured directly with the Rogowski coil. Furthermore, the current signal is averaged 1024 times, but the plasma current peaks are not always on exactly the same position. The measured averaged total current is therefore distorted and cannot be used to obtain the power. For solving the integral in equation 4.1, the charge is used.

In figure 4.19 the power dissipated in the plasma calculated for several settings is shown. In black, the value for the power dissipation is calculated with the Q-V plot. The error in this value is determined by the fluctuations within every period of the voltage and with the systematic error in the system[3]. The black and the colored values for the power dissipation in the plasma with a gap distance of 1 mm are in agreement for all the settings. The value for the power dissipation, for the measurement where the distance between the PVC substrate and quartz substrate is 2 mm, is not in agreement. But, in general, both methods give the correct value for the power dissipated in the plasma.

4.4.2 The energy per pulse dissipated in the plasma for the new setup

For different settings in the new setup, the energy dissipated in the plasma is determined. This energy can be used to calculate the power dissipated in the plasma, depending on the number of pulses per second.

In figure 4.20 the energy dissipated in the plasma and the energy dissipated in the plasma per volume[4] for different gap distances between the

---

[3]The script used for these calculations is written by Cornelissen, L.E. and Schepers, L.P.T..

[4]For the energy dissipated in the plasma per volume it is assumed that the energy is distributed homogeneous in the volume, but in reality more energy will be at the two
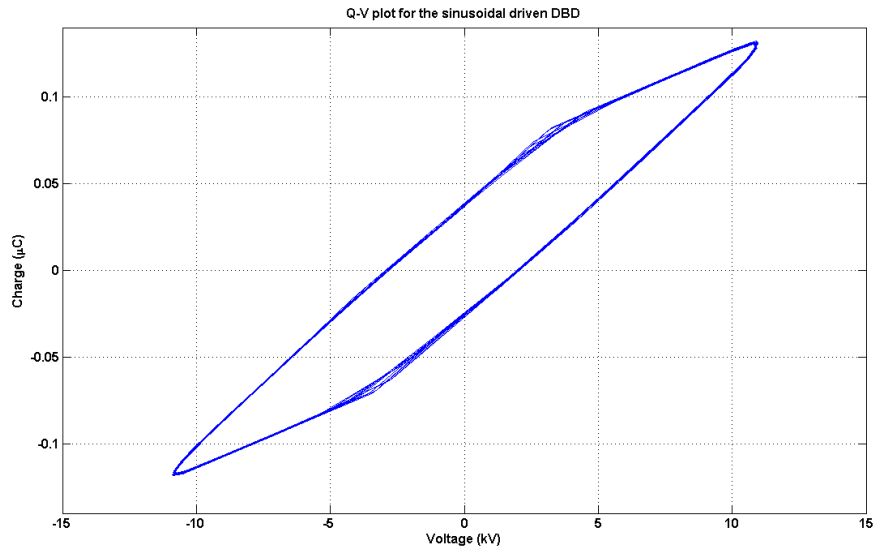
Figure 4.17: *The Q-V plot for the measurement made with a frequency of 22.2 kHz and a distance between the quartz and PVC surface of 1 mm.*
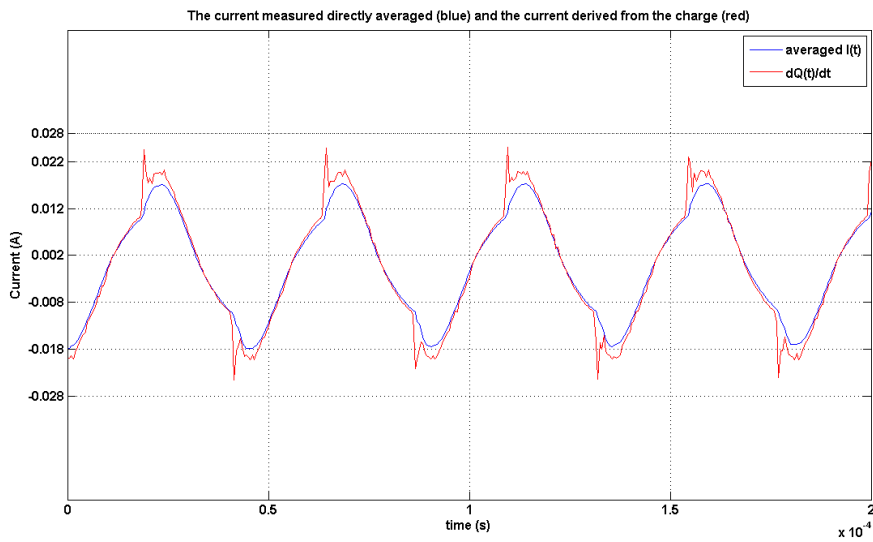
Figure 4.18: *The averaged current signal in blue and the current signal derived from the measured charge in red. The measurement is made for a frequency of 22.2 kHz and a distance between the quartz and PVC substrate of 1 mm.*

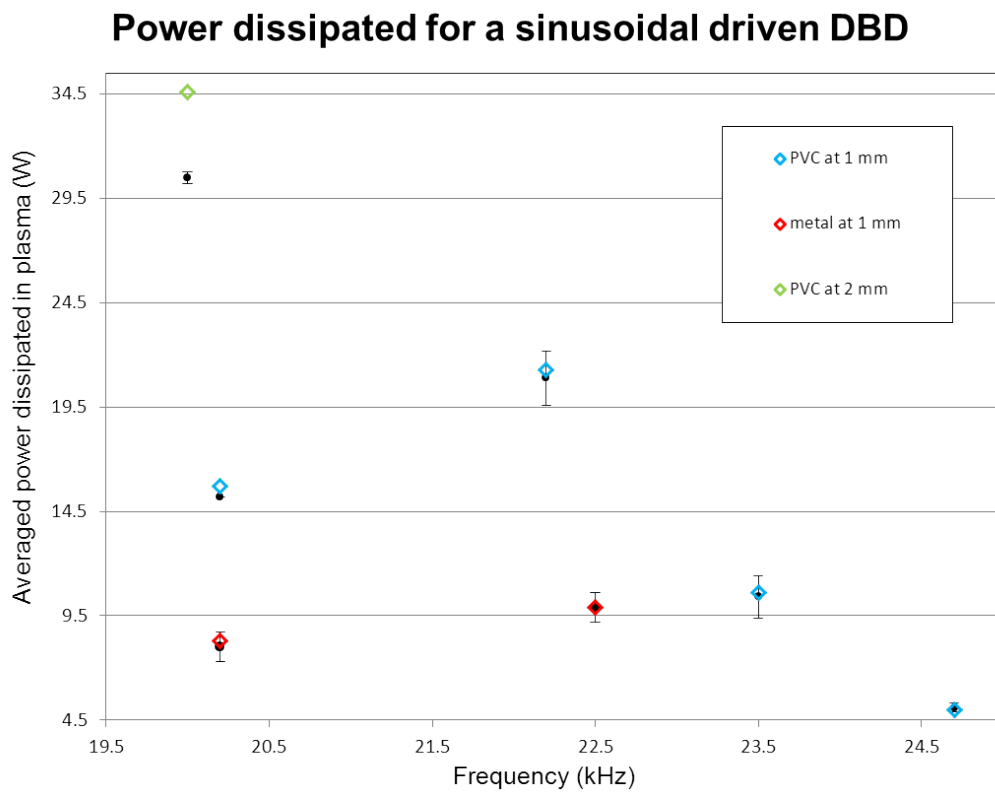**Figure 4.19:** *The power dissipated in the plasma for different settings and frequencies. In black the power dissipated calculated with the Q-V plot and in color the same power dissipated calculated by integrating the voltage times the derivative of the charge.*

quartz and a substrate of PVC with a thin piece of cover glass on top is shown. Overall the energy dissipated per pulse is less for a larger gap distance, since the breakdown voltage is larger for a larger gap distance. This behavior was also visible in the light intensity measurements in subsection 4.2.4. For a gap distance of 4 mm only a few times a discharge is occurring, for a gap distance of 4.5 mm no discharges are present in the gap. The distance at which no discharge is occurring anymore depends partly on the length of the wire of the load. In this experiment the length of the wire was only 0.8 meter, for a longer wire this distance will be smaller than 4 mm. For a longer wire, the current which reaches the load is lower due to signal reflections in the wire and the voltage over the gap is smaller due to more resistance in the wire. The energy dissipated in the plasma is non-zero even though there is no plasma in the gap for a gap distance of 4 and 4.5 mm in figure 4.20. Approximately 1 mJ is dissipated in other parts of the system, in resistive elements.

The energy dissipated in the plasma for different pulse frequencies is shown in figure 4.21 , the 1 mJ offset found in figure 4.20 is also present in this figure. The behavior of the energy per pulse is equal to the behavior of the light emission per unit time in figure 4.14.

The energy dissipated in the plasma in one pulse for different pulse widths is plotted in figure 4.22 . The offset will depend on the pulse width and will be smaller for a shorter pulse width. The energy dissipated per pulse is measured for only a metal as counter electrode and for three different substrates: PVC, PVC with a thin piece of cover glass on top, and donor skin. The latter two are used for experiment on biologic material in part II. In table 2.3 the relative permittivity of the three different substrates are given.

The behavior of the energy dissipation as function of pulse width is equal to the behavior of the light emission as function of the pulse width. The difference in ratio between a pulse width of 1μs and 4μs can be due to the differences in the used load. Only for the donor skin the value for the power dissipation at a pulse width of 1μs is lower than the value for the power dissipation at a pulse width of 4μs. For the measurements with skin, there were no discharges for every voltage pulse at a pulse width of 1μs.

The differences in the values for the power dissipation for the different settings are due to changes in the total dielectric capacity of the system. For a higher capacity of the two dielectric materials, the voltage over the air gap reaches the breakdown voltage for a lower total voltage (equation 2.17), which leads to a higher number of discharges for the same voltage pulse fed

---

surfaces of the DBD than in the bulk.

Energy per pulse for different gap distances
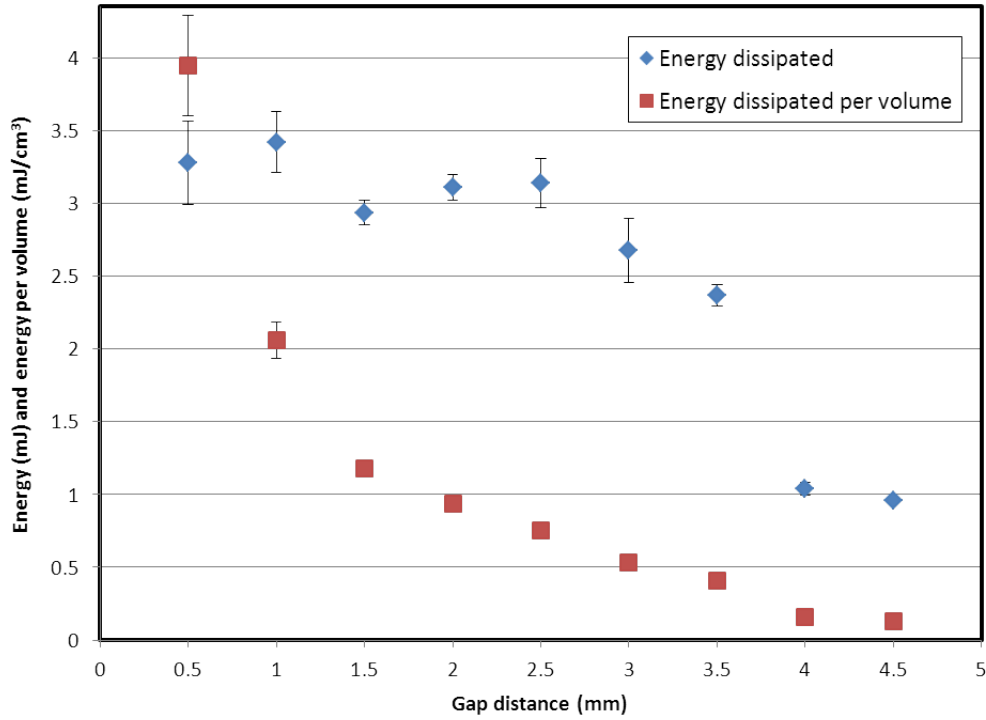
Figure 4.20: *The energy per pulse for different gap distances for a pulse frequency of 1500 Hz, a pulse width of 10 μs and, a substrate of PVC with a thin piece of cover glass on top.*

Energy per pulse for different pulse frequencies
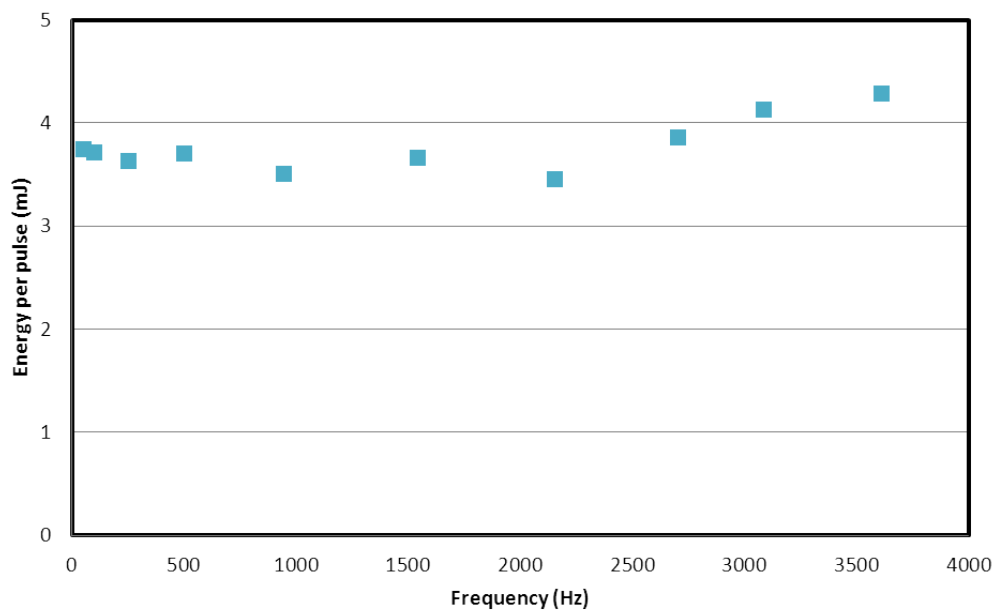
Figure 4.21: *The energy dissipated in the plasma for one pulse, for a pulse frequency of 500, 1500, 2500 and 3500 Hz. For a gap distance of 1 mm, a PVC substrate and a pulse width of 10 μs.*
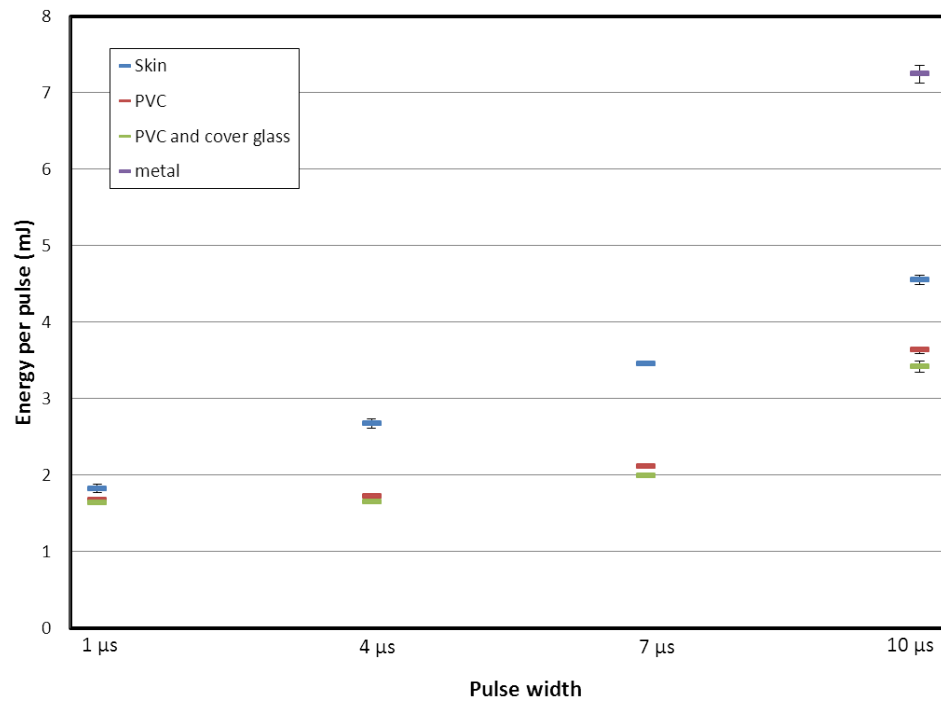
Figure 4.22: *The energy dissipated in the plasma per pulse for different pulse widths, for different materials as second dielectric and no second dielectric. The measurements are done for a fixed gap distance of 1 mm and a pulse frequency of 500 Hz.*

over the DBD. Since skin has a higher dielectric constant than PVC, the total dielectric capacity is larger for a system with skin than for a system with PVC, this is in line with the results in figure 4.22. When a thin piece of glass is placed on top of the PVC, an additional capacitor is added to the system. The total dielectric capacity of the system will therefore be smaller and a drop in the energy dissipation is expected. This effect is also visible in the graph. For a system without substrate, a system with only a metal as counter electrode, the total dielectric capacity is also higher and this results in the higher energy dissipation in the plasma.

4.5 Absorption spectra

The absorption spectra are obtained by the FTIR spectrometer described in chapter 3. First the absorption spectrum for Nitric Oxide is made and second for a DBD discharge.

4.5.1 The absorption spectrum of Nitric Oxide

In figure 4.23 the absorption spectrum of NO is shown for a resolution of 0.1 cm^{-1}and for 128 averages. The individual peaks are clearly visible and the signal to noise ratio is 6. The signal to noise ratio is not larger due to two reasons, first the overall light intensity is low. The small gap distance and the four ZnSe windows limit the amount of light which reaches the detector. Second, the optical path is small and the absorbance is small. In the volume approximately $2.5 \cdot 10^{15}$ NO molecules[5] can absorb the light. In the path length there are even less NO molecules that can absorb light.

4.5.2 The spectrum for a discharge

No difference between the spectra for a discharge and no discharge are visible with this FTIR setup. Apparently the densities of species generated in the plasma, such as N_2O, HNO_3, O_3 and N_2O_4, are too low to detect in this small path length. With the result of the previous section a maximum possible concentration of NO in the plasma can be determined. This maximum concentration is determined with a signal to noise ratio of 1, the NO concentration should be 6 times that small in this case than in the case of section 4.5.1. The maximum concentration of NO is therefore 35 ppm. To detect smaller concentrations a multipass cell could be used to increase the path length up to tens of meters [42, 90].

---

[5]Derived with the ideal gas law.
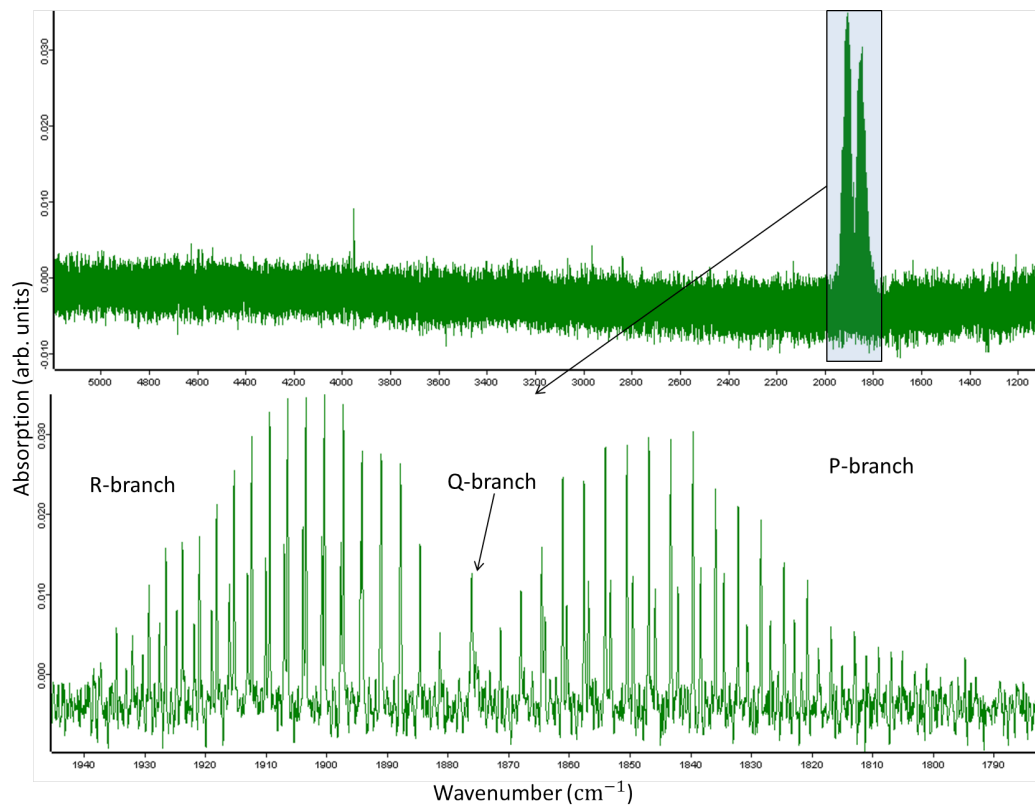
Figure 4.23: *The absorption peaks of NO. At the bottom a zoomed spectrum for the transition to the first vibrational state.*

Part II

Plasma interaction with Bacteria and Skin

Chapter 5

Experimental procedures of bacteria and skin[1]

Experiments on the inactivation of bacteria and on donor skin are performed. First, treatments on *Staphylococcus aureus* are discussed. Second, the experiments on other bacteria are shown. Then, the scheme for treating bacteria which are on donor skin and evaluating their inactivation is described. At the end of this chapter, the experimental method to determine the effect of an ex vivo treatment on skin is given.

5.1 Treatment on *Staphylococcus aureus*

In this batch of experiments we treat *S. aureus*, isolated from a burn patient, with the old and new setup. For the old setup, experiments are done for different pulse frequencies, pulse widths and gap distances. For the new setup experiments are performed for different pulse widths only.

The experiments are done on *S. aureus* since it is one of the most common bacteria associated with CRBI as mentioned in chapter 1. Bacteria are routinely cultured on LB agar[2]. One colony is suspended in 5 ml LB and is cultured overnight at a temperature of 37 ° C. At this stage the growth of the bacteria is stationair and no longer exponential. In figure 5.1 the different growth phases of bacteria are shown.

---

[1]In cooperation with "Vereniging Samenwerkende Brandwondencentra" in Beverwijk, Bouke Boekema PhD.

[2]The culture substrate LB agar is prepared in bottles with 300 ml purified water, 7.5 gram Luria Broth (LB) and 4.5 gram Agar. By placing the bottles in an autoclave, the contents is sterilized at high pressure and temperature. When the contents is cooled, the agar acts as gelatine and the culture substrate gets fixed.
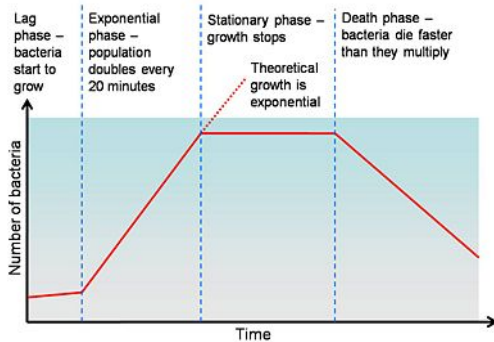
Figure 5.1: *The different growth phases of bacteria cultures. The time (usually) in hours and the number of bacteria on a logarithmic scale[92].*

Before quantitative measurements for different settings are performed, a practical treatment time for the experiments has to be found. A treatment time where not all bacteria are inactivated, to be able to discriminate between treatments. In order to find this treatment time, culture plates of 15x15 cm are treated with a fixed duty cycle of 50%, pulse frequency of 1500 Hz, gap distance of 1 mm and pulse width of 10 μs or equally a dissipated power in the plasma of approximately 2.8 W[3]. The culture plates are Petri dishes filled with 40ml LB agar. Before the culture plates are treated with a plasma, bacteria are spread out on the substrate: 200 μl of $1 \cdot 10^9$ Colony-forming units (CFU) per 1 ml Phosphate Buffered Saline (PBS). On one culture plate, 5 different treatments can be performed. In figure 5.2 different treatment times on such a square culture plate are shown. For a treatment time of 5 seconds, there is a smaller active radius and more CFU are present in the area as large as the electrode, than for a treatment time of 10, 15 and 20 seconds. For the following up experiments approximately the effective treatment time of 5 seconds is used. The duty cycle is reduced by 5 times, to 10% and the treatment time is increased by 6 times, to 30 seconds. This increase in time is implemented to reduce the relative uncertainty in time between switching the plasma on and off.

5.1.1 The method for finding quantitative values after treatment

Multiple steps are taken to get quantitative inactivation values for plasma treatments:

---

[3]This value is determined by a measurement with the new setup and may therefore deviate little from the actual value.
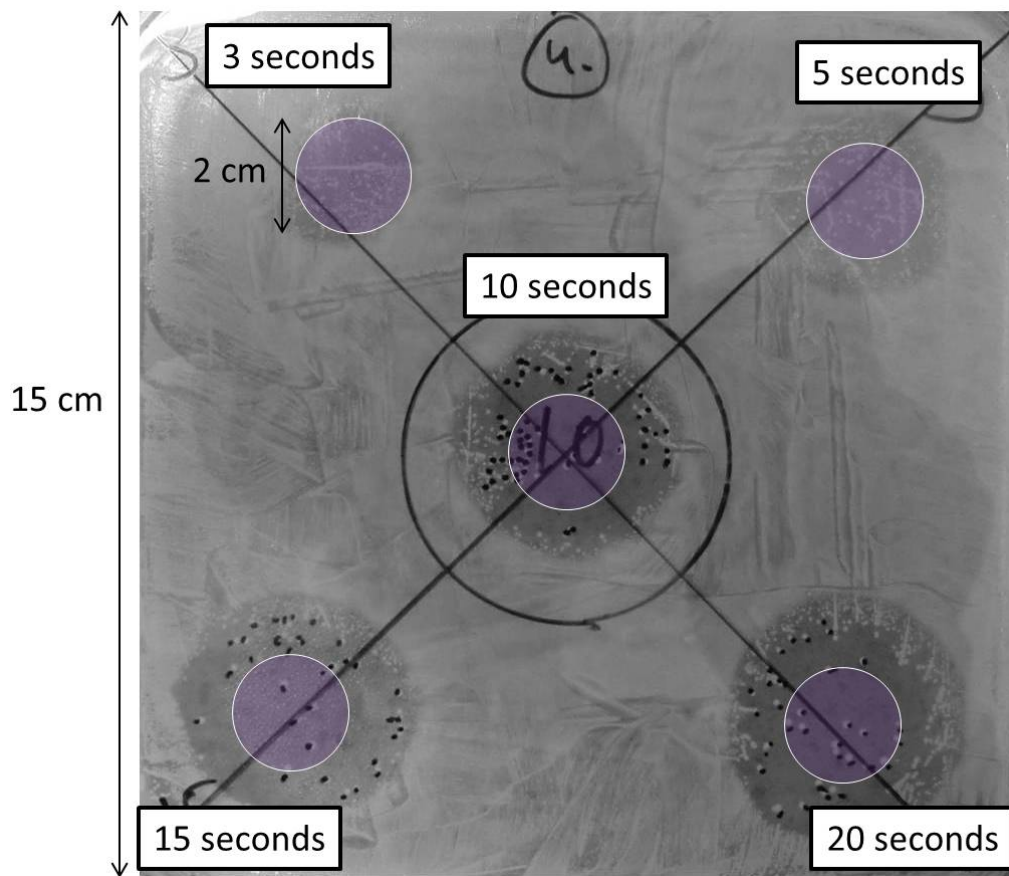
Figure 5.2: *The treatment of a square culture plate for a treatment time of 3, 5 10, 20 and 30 seconds, the position of the DBD is indicated in purple. The treatment was with a duty cycle of 50%, a pulse width of 10µs a pulse frequency of 1500Hz and with a distance between the culture plates and the DBD of approximately 1mm.*

1. 50 µl of a suspension of $2 \cdot 10^7$ CFU *S. aureus* per 1 ml pure water is put in 4 to 5 small drops on sterilized 22x26 mm cover glasses, with a thickness of 0,17 mm.

2. The glasses are placed in a hood to dry. The time at which the glasses are drying has to be no longer than 20 minutes, otherwise all the bacteria will dry out completely and die.

3. After the drops are dried, the different cover glasses are treated by placing them on a 1mm thick sheet of PVC and placing this under the DBD. This PVC sheet is the same used in the experiments in chapter 4, the thin cover glass will have only small electric effects. The change is power dissipated in the plasma was small, as shown in section 4.4.2 figure 4.22.

4. After the treatment, 1 ml of the buffer solution PBS is added to the glasses. The glasses and PBS are put in an ultrasonic bath for 5 minutes. This to dislodge bacteria from the glass and mix them with the buffer solution.

5. For every treatment, different dilutions are made from the 1 ml PBS (up to 10^{-3}). For every dilution, twice 100 µl is spread out over two LB agar plates. To verify the CFU/ml, the initial bacterial suspension was also diluted and spread on agar plates.

6. The treated Petri dishes are placed in an incubator which is at a temperature of 37 ° C. The Petri dishes stay here overnight, to culture the colonies. It is possible to count the colonies and calculate the amount of CFU in the diluted 1 ml PBS. In figure 5.3 an example of counting CFU on a culture plate is shown.

In figure 5.4 the scheme for the measurements done with *S. aureus* on glass with the old setup is shown. For every set of measurements (orange), 15 cover glasses are prepared: 5 different treatments (blue) are done in triplicate. These measurements are performed twice (purple). For the new setup only a pulse width measurement is performed, for 1, 4, 7 and 10µs. With a pulse frequency of 500 Hz and a gap distance of 1 mm. The lower pulse frequency is chosen to exclude the effect of the heating of the transformer coil.

5.1.1.1 Processing the data

In the previous section it is reported that every set of measurements is performed twice. Within every set, three measurements are done for every setting, including three measurements for the untreated glasses. This gives six
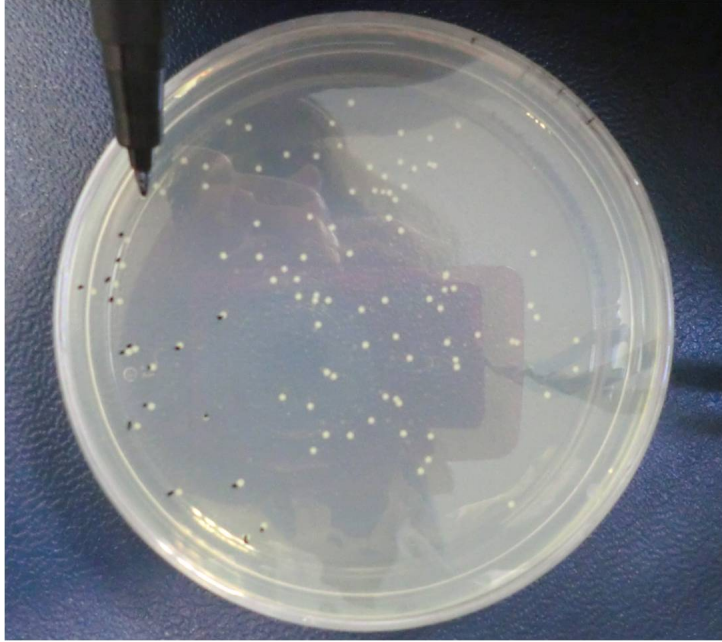
Figure 5.3: *Example of counting the 105 colonies which grew overnight on this culture plate.*

individual measurements in total for every setting. The colonies on the culture plates are counted and the amount of CFU in the original 1 ml PBS per measurement can be derived from these numbers.

For the results not only the CFU are of interest. The log reduction is usually used when discussing the rate of bacteria kill. For a log reduction of 1, the number of bacteria is reduced with 90%, and for instance for a log reduction of 2 this number is reduced with 99%. In order to find the log reduction, the average log of the number of CFUs for the three treatments of one setting is subtracted from the log value of CFU for the three untreated glasses. Since per setting, two times three independent treatments are performed, the two values for the log reduction are averaged again for an overall average. For the latter, a normal distribution is assumed and the standard deviation is calculated for the six individual measurements per setting, this gives the error in the overall averaged log reduction per setting.

These results of the old setup are qualitatively checked by redoing all the treatments for different pulse widths, pulse frequencies and gap distances on 15x15 cm culture plates. Again, 200 µl of 10^9 CFU per 1 ml PBS is spread out on these culture plates, before they are treated with the old setup.
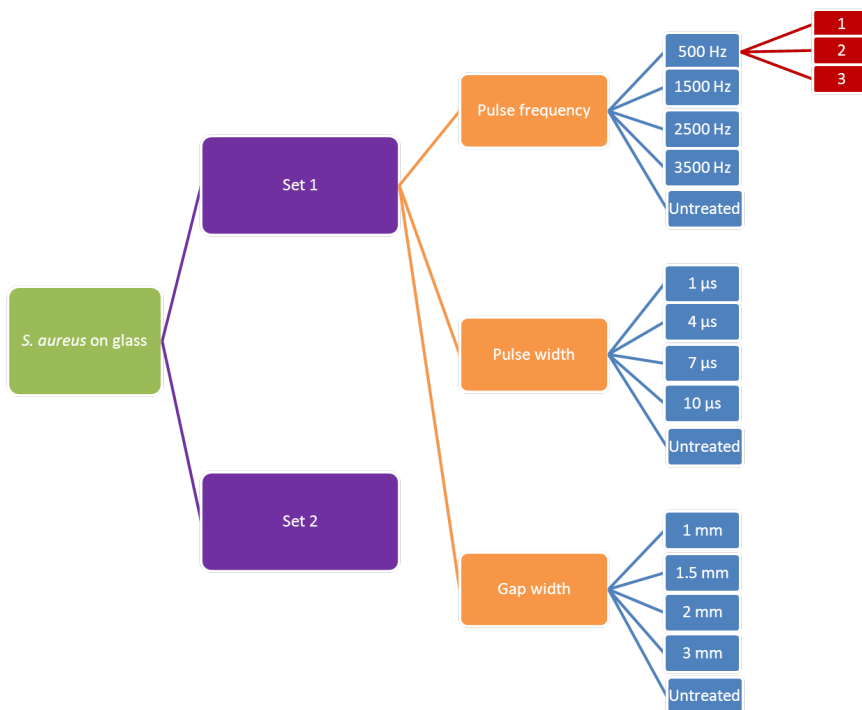
Figure 5.4: *The scheme of measurements with the old setup for S. aureus on cover glass, where every measurement is done in triplicate (red).*
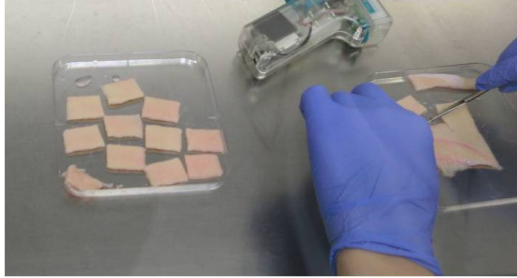
Figure 5.5: *Cutting human skin in the same size as the cover glass used in previous experiments.*

5.2 The effect of treatment on other Staphylococci

Besides the *S. aureus*, other bacteria are found in the blood of infected newborns. These are *Staphylococcus epidermis*, *Staphylococcus capitis* and *Staphylococcus hominis*. The bacteria used in the experiments are isolated from burn wound patients. The bacteria are in the stationary growth phase by culturing them similar to the *S. aureus* overnight in a culture medium. In order to compare the effect of the plasma on these different bacteria with the effect on the *S. aureus* we spread 200 µl of 10^9 CFU per 1 ml PBS on 15 by 15 cm culture plates. For every type of bacteria two culture plates are used, which gives a total of 8 culture plates. Every culture plate is treated with the old setup and four times, with treatment times of 5, 10, 20 and 30 seconds and a fixed duty cycle of 10%. The height is fixed on approximately 1mm, the pulse width is 10µs and the pulse frequency is 1500 Hz.

5.3 Treatment of donor skin with the new setup

It is important to get insight at bacterial inactivation on the skin and the effect of the DBD treatment on the skin itself. Therefore experiments with donor skin are performed in this research. The skin used in this experiments is from one donor. The skin is cut into pieces approximately the same size as the cover glasses (22x26 mm) as can be seen in figure 5.5. Prior the treatment, the skin pieces are placed on a culture substrate of LB agar. This culture substrate is chosen because of its resemblance in water density and therefore electric properties of the layers underneath the skin. Moreover, the culture plate prevents the skin to contract. All the treatments with donor skin are done with a gap distance fixed at approximately 1 mm and a pulse frequency of the new setup of 500 Hz.
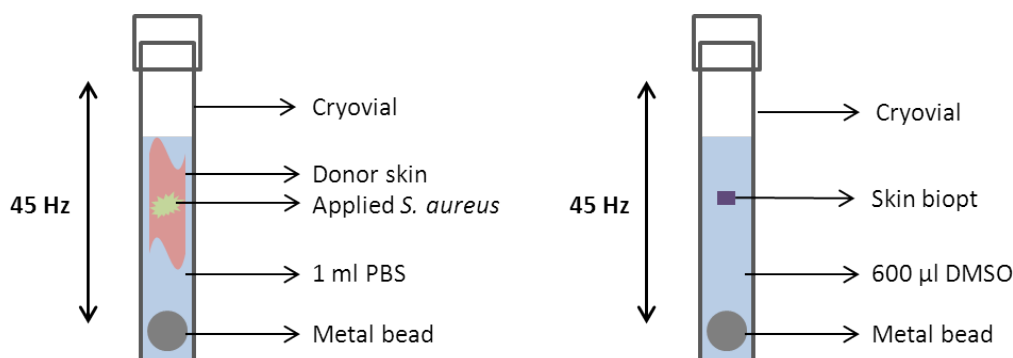
Figure 5.6: *On the left a cryovial for the experiment on the bacterial inactivation on skin, on the right the preparation of a cryovial for the analysis of skin damage. The metal bead moves quickly up and down in the cryovial, with a frequency of 45 Hz, in the TissueLyser LT.*

5.3.1 Bacterial inactivation on skin

For different pulse widths, skin pieces contaminated with bacteria are treated. In total 10 pieces of skin are cut and drops of 50 µl $2 \cdot 10^7$ CFU *S. aureus* per 1 ml pure water are put on the skin pieces. After the drops are evaporated, 8 pieces are treated with the new setup for a pulse width of 1, 4, 7 or 10 µs[4] and 2 pieces are untreated. The 10 skin samples are placed in cryovials containing 1 ml PBS and a metal bead of 7 mm in diameter. To dislodge bacteria from skin, the cryovials are placed in a TissueLyser LT [93] for 10 minutes at a frequency of 45 Hz, in the left of figure 5.6 the cryovial is shown. The suspension in the cryovials is diluted and for different dilutions twice 100 µl is spread out on the culture plates. The original amount of CFU on the skin after treatment and a log reduction for different treatments can be determined.

5.3.2 Analysis of skin damage

It is important that only the bacteria get inactivated by a treatment and the treatment has no effect on the skin. The effect of the plasma on the skin is investigated by a MTT assay and by histology.

For the MTT assay 9 skin pieces are cut, one piece is untreated and the other 8 are treated with the new setup for a pulse width of 1, 4, 7 and 10 µs. From every treated piece, 5 skin biopsy punch samples of the skin are taken. From the untreated piece of skin, 7 samples are taken. This number

---

[4]The values for the energy dissipated per pulse for these different pulse width are given in subsection 4.4.2.

of biopsy punches is took, because samples have different thicknesses and different locations underneath the electrode. By having a larger number of samples, the result is more reliable.

The skin samples are put in 2 ml medium containing 2mg/ml MTT[5] dye and in the incubator at 37°C for 2 hours. During this time, enzymes from the cells in the epidermis reduce the dye to a crystal formazan, which is insoluble and purple. Every sample is put separately in a cryovial with a metal bead (7 mm) and 600 µl DMSO, in which the crystal can dissolve. The cryovials are placed again in the TissueLyser LT at a frequent of 45 Hz for 4 minutes to mix and dissolve the crystal completely in the DMSO. In figure 5.6 on the right, a cryovial with one (purple) skin biopsy punch is shown.

For every skin sample in the DSMO, twice 100 µl is pipetted in a microtiter plate. The concentration of the dissolved crystal in the 100 µl is measured by its absorbance of the specific wavelength of purple light. The higher the concentration of the crystal, the higher the amount of living cells in the biopsy punch sample.

Another way to get insight in damage of the skin is by histology. After every treatment, one biopsy punch sample is taken from the skin and placed in kryofix[6]. From every sample, 5 contiguous coupes of 25 µm thick are cut and stained with hematoxylin and eosin (H&E stain). This stain makes it possible to see the cells and fibers in the skin under the microscope.

---

[5]3-(4,5-Dimethylthiazol-2-yl)-2,5-diphenyltetrazolium bromide

[6]Kryofix is a fixative, a solution to preserve cell specimens for microscopic examination. Bacteria which are on the glass, will stay on the glass.

Chapter 6

Results of treatment on biological material

The results of the experiments described in chapter 5 are presented and analyzed in this chapter.

6.1 The effect of treatment on *S. aureus*

In this section the results of the treatment on *S. aureus* on glass, figure 5.4, are shown and analyzed. First, the efficiency of the ultrasonic bath is discussed. Second, the number of CFU per measurement are plotted in one graph: the CFU in the original dilution, the CFU on the untreated glasses and the CFU on the treated glasses. In another graph the two log reductions per set and the averaged log reduction are plotted. Third, these results are compared with results on the treatment of bacteria on culture plates.

6.1.1 Validation of the method

An ultrasonic bath is used to dislodge the bacteria from the glass. The efficiency of this ultrasonic bath is not known and may depend on the intensity of the treatment. Bacteria might secrete certain proteins when they are treated with a plasma and will stick better on the glass. The bacteria will therefore dislodge less efficiently or not at all when the treated glasses are placed in the ultrasonic bath.

This hypotheses is checked by analyzing the accumulation of bacteria on the glasses for different treatments, by using the dye, Acridine orange, which colors the bacteria. The 1 ml buffer PBS of every treated glass is replaced by 1 ml kryofix. After minimal 1 day in the kryofix, the glasses are flushed with

PBS and the dye is applied on the glasses. With a microscope the efficiency of the ultrasonic bath after different treatments can be compared qualitatively. For a treatment with higher intensity, treatments with a longer pulse width or a higher pulse frequency, the accumulation of bacteria on the glasses is indeed higher. For instance for a pulse frequency of 3500Hz, a huge number of bacteria on the glass can be seen, all the bacteria stayed on the glass, approximately the 1 million which were deposited on the glass. The result of the culture plates out of the stove is in agreement with this statement since no single colony was seen on the culture plates for this treatment. For the untreated glasses, no accumulation of bacteria was found on the glasses. All bacteria are dislodged from the untreated glass, when placed in the ultrasonic bath.

For all the results it is assumed that if bacteria are effected such by the plasma that they stick on the glass, they died. So if they would have loosened from the glasses in the ultrasonic bath it would not change the results from counting the culture plates.

6.1.2 Bacteria inactivation as a function of the pulse frequency

In figure 6.1 in the left the CFU per measurements in the solution of 1 ml PBS are shown, with in red the data from set 1 and in blue the data from set 2. The CFU on the untreated glasses is approximately four times smaller than the CFU in the original dilution. During the 20 minutes when the drop with bacteria is evaporating on the glass, a large amount of bacteria die. Partly due to osmosis and partly due to dehydration. Since the 4 to 5 drops with bacteria on every cover glass have not the same shape every time, the CFU counted for the same treatments differ more from each other than if they were exactly the same every time.

The averaged log reduction per set and per frequency is shown in the right graph in red and blue. These averaged log reductions are again averaged in green and the error bar is the standard deviation of the six individual measurements. The treatment with the plasma is very effective. The difference in CFU for the untreated glasses and treated glasses is very large, which leads to a high log reduction. For the log reduction, a significant difference between 500 Hz and 1500 Hz, and 2500 and 3500 Hz is visible.

6.1.3 Bacteria inactivation as a function of pulse width

The CFU per measurement are shown in the left graph of figure 6.2 . Even for

Figure 6.1: *Left the counted CFU in the solution of 1 ml PBS for every measurement and for the control and untreated cover glasses. Right the per set averaged log reduction for a frequency of 500, 1500, 2500 and 3500Hz in red and blue. In green the averaged log reduction for both sets are averaged again. The treatment was for 30 seconds, with a duty cycle of 10%, a pulse width of 10µs and a distance between the culture plates and the DBD of 1mm.*

Figure 6.2: *Left the counted CFU in the solution of 1 ml PBS for every measurement and for the control and untreated cover glasses. Right the per set averaged log reduction for a pulse width of 1, 4, 7 and 10µs in red and blue. The averaged log reductions for both sets are averaged again and are plotted in green. The treatment was for 30 seconds, with a duty cycle of 10%, a frequency of 1500Hz and a distance between the culture plates and the DBD of 1mm.*

Figure 6.3: *Left the counted CFU in the solution of 1 ml PBS for every measurement with the new setup and for the control and untreated cover glasses. Right the per set averaged log reduction for a pulse width of 1, 4, 7 and 10µs in red and blue. The averaged log reductions for both sets are averaged again and are plotted in green. The treatment was for 30 seconds, with a duty cycle of 10%, a frequency of 500Hz and a distance between the culture plates and the DBD of 1mm.*

the smallest pulse width of 1μs there is a strong inactivation of the bacteria due to the plasma treatment. In the graph on the right, an overall increase of the log reduction is visible for a higher pulse width. The difference in the log reduction for the two smallest pulse widths compared with the two highest pulse widths is significant.

6.1.4 The bacteria inactivation as a function of pulse width for the new setup

The measurements on different pulse widths with the old setup in subsection 6.1.3 are repeated for the new setup. In figure 6.3 the results of this measurement are shown. On the left the CFU in the solution, the CFU on the untreated glasses and the CFU on the treated glasses are given. In the right graph the log reduction, relative to the untreated glasses, is shown for the treatments with different pulse widths. No big differences are visible compared with the result in figure 6.2, although the frequency is 500 Hz instead of 1500 Hz. This is in agreement with subsection 6.1.2, where no significant difference was seen between treatments with both pulse frequencies. So, comparing both the log reduction for old and new setup, the properties of the discharge in the old and the new setup are not that different from each other.

6.1.5 Bacteria inactivation as a function of gap distance

On the left in figure 6.4 the number of CFU in the solution of 1 ml PBS are shown. For set 2 there is no data for a gap distance of 3 mm. The reason this measurement is not repeated for a second time, is because at this distance there was no plasma[1]. Without a plasma there is no significant difference between the untreated cover glasses and the treated glasses as can be seen in the left graph. In the right graph the averaged log reduction is given. There is a significant difference between the treatment at a distance of 1 mm and the other treatments, the difference of a distance of 1,5 and 2 mm has no significant effect on the effectiveness of the treatment.

6.1.6 Qualitative check with treatments on culture plates

The treatments of bacteria on glass with the old setup are checked qualitatively by direct treatment with the old setup of the culture medium covered

---

[1]The gap distance at which no plasma can occur, depends also on the length of the wire of the load, in this case, the length of the wire was 1.1 meter.
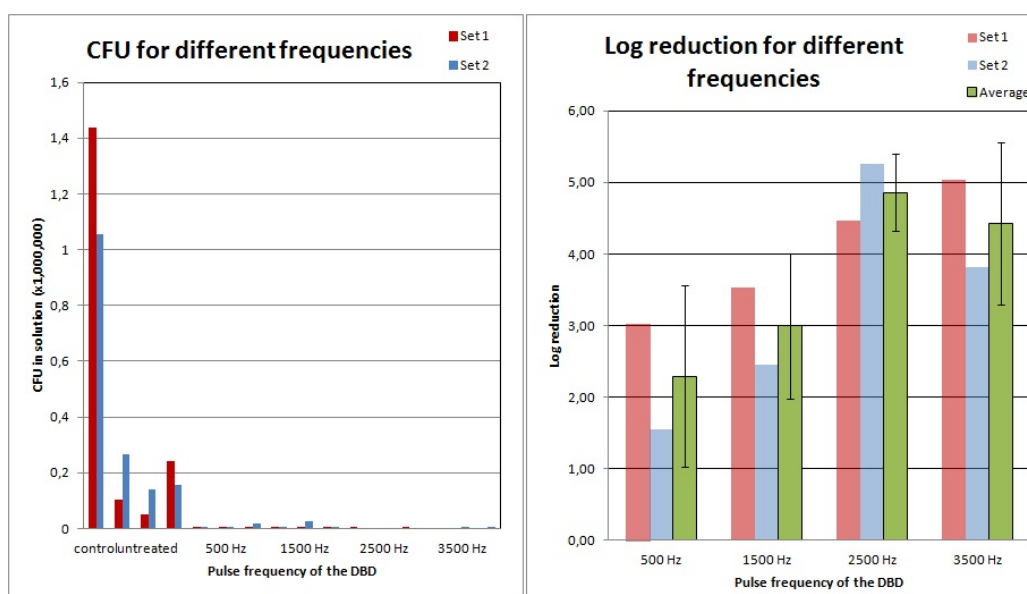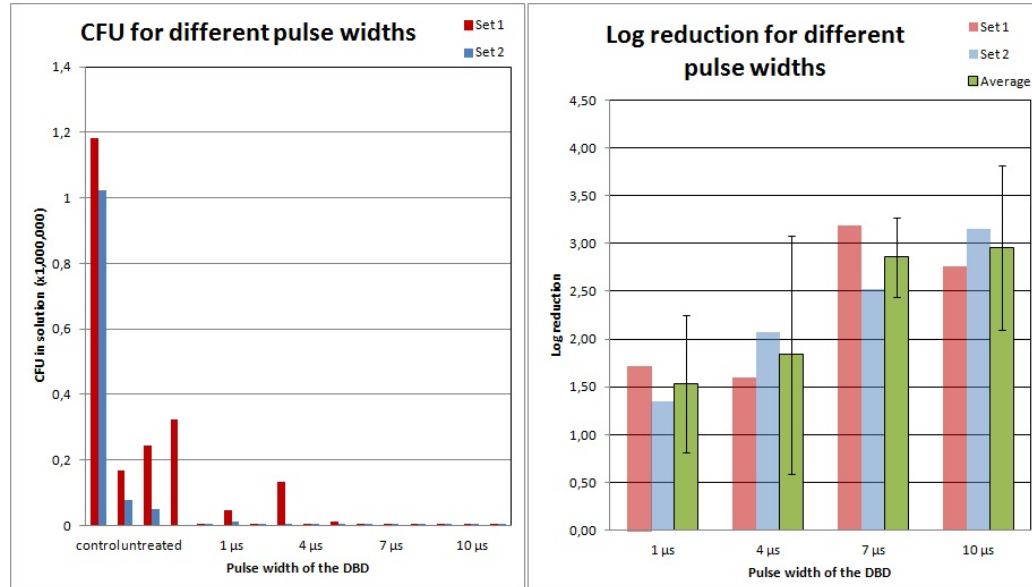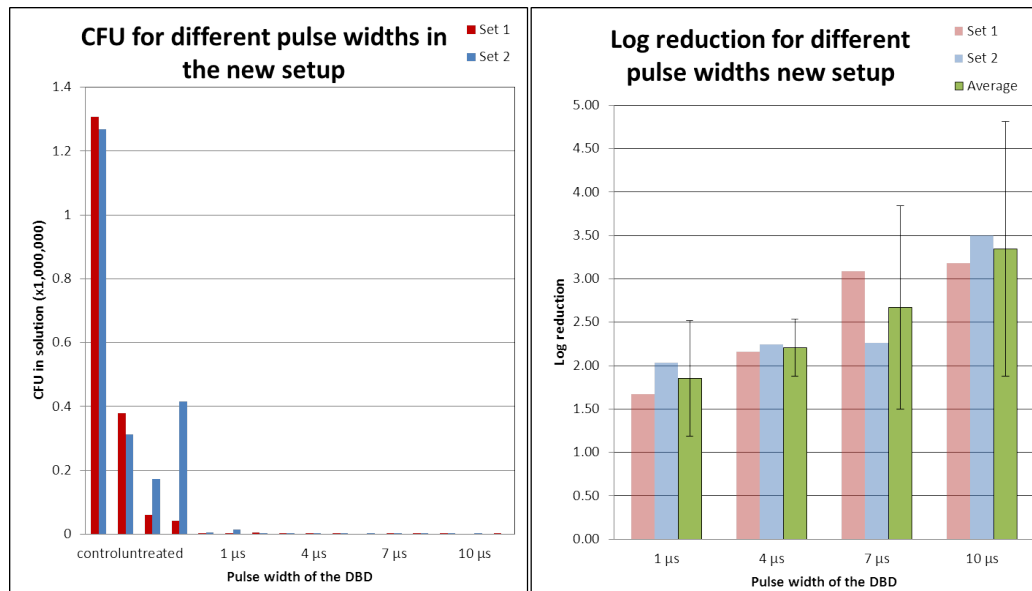
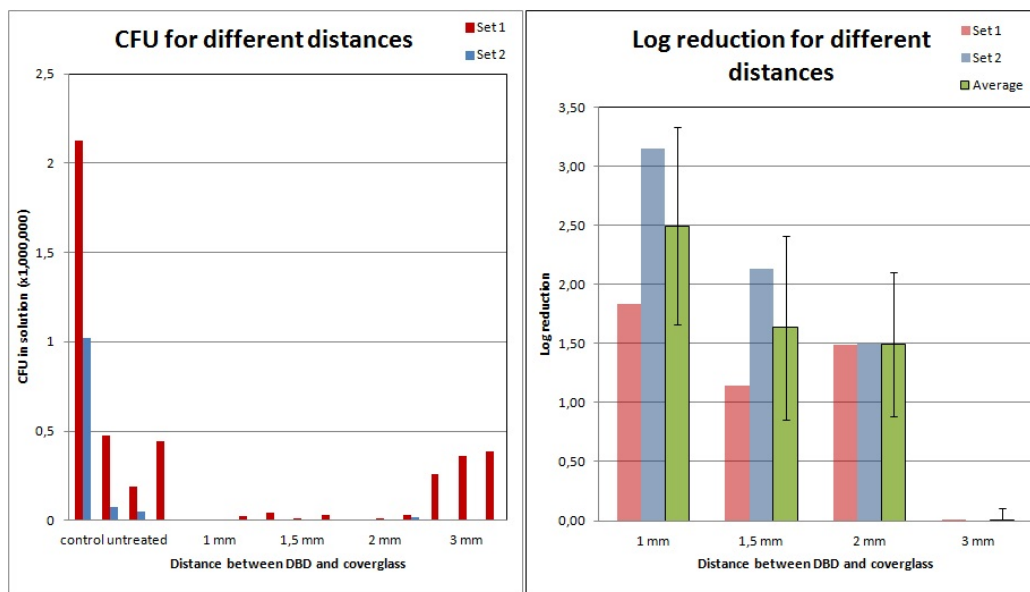**Figure 6.4:** *Left the counted CFU in the solution of 1 ml PBS for every measurement and for the control and untreated cover glasses. Right the per set averaged log reduction for a distance of 1, 1.5, 2 and 3 mm in red and blue. In green the averaged log reduction for both sets are averaged again. The treatment was for 30 seconds, with a duty cycle of 10%, a pulse width of 10µs and a pulse frequency of 1500Hz.*
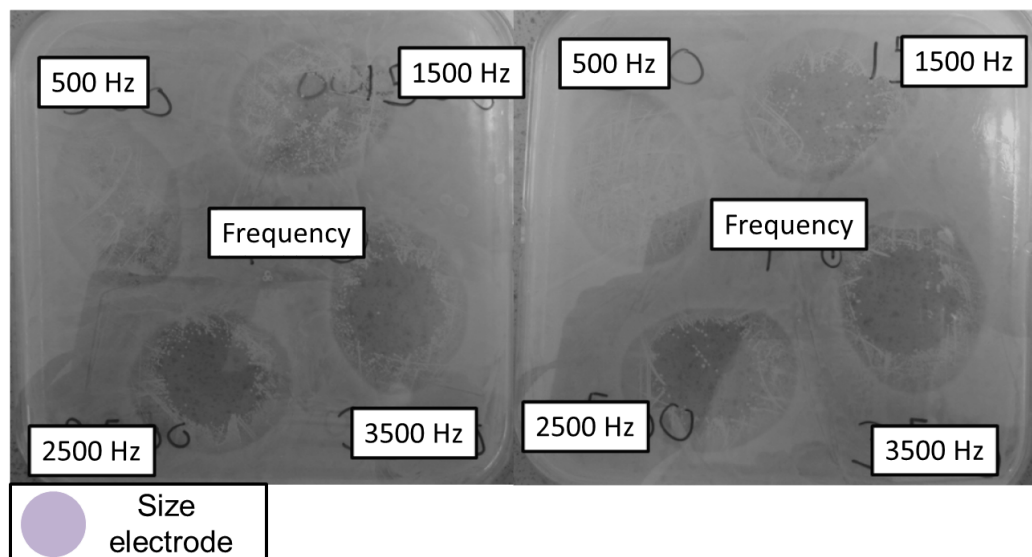
Figure 6.5: *Treatment of two culture plates with pulse frequencies of 500, 1500, 2500 and 3500 Hz. The treatment was for 30 seconds, with a duty cycle of 10%, a pulse width of 10µs and a fixed gap distance of approximately 1mm.*

by bacteria. In figure 6.5 the treatments for different frequencies, in figure 6.6 the treatments for different pulse widths, and in figure 6.7 the treatments with a gap distance of 1.5 and 2 mm are shown. The treatment with a gap distance of 1mm is visible in figure 6.5 for a frequency of 1500 Hz and in figure 6.6 for a pulse width of 10 µs.

If the three figures are compared with the results in the previous subsections, it seems that the log reduction on these culture plates is higher than the treatments on the cover glasses. On the culture plate $0.2 \cdot 10^9$CFU are spread out over a surface of $0.15 \cdot 0.15$ meter. So, on the direct treated surface area of the DBD, with a radius of 1 cm, we have around $3 \cdot 10^6$CFU. Roughly 10 till 200 CFU are counted in the area as large as the DBD for the treatments with a frequency of 1500Hz, a pulse width of 10µs and a distance of 1mm in figures 6.5 and 6.6. These values give a log reduction between 4.2 and 5.5, but the averaged log reduction in graph 6.1 and 6.2 are around 3. This difference in log reduction can be due to the large percentage of water in the culture plates: up to 99% is water. This composition of the culture plates may have electric properties which produce a more intense plasma. Another additional explanation may be the distribution of the bacteria: on the culture plates the bacteria are spread out. However, on the cover glass the bacteria are deposited in drops and therefore bacteria may be covered by others and are therefore shielded for some fluxes of the plasma. Finally, the
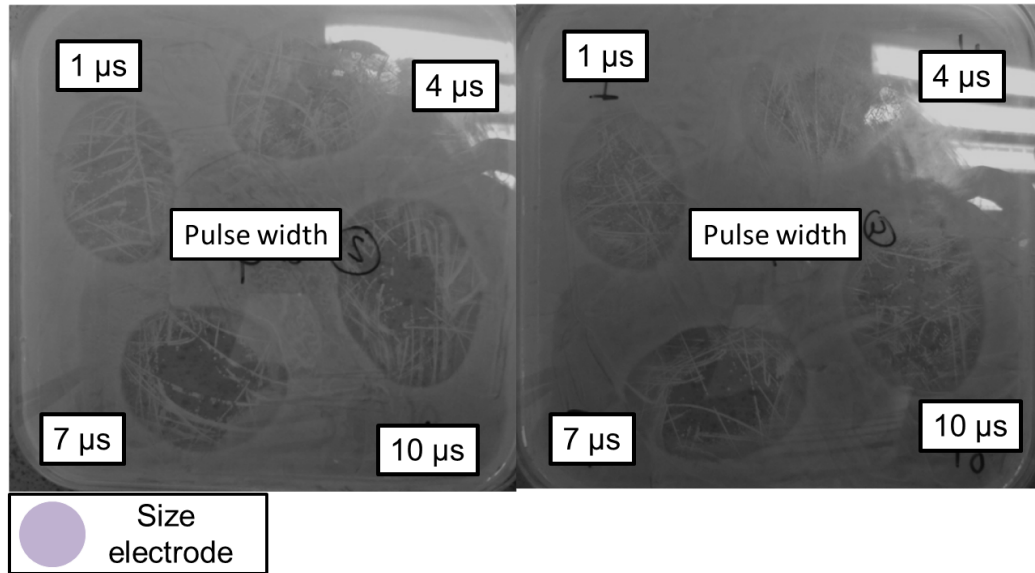
Figure 6.6: *Treatment of two culture plates with pulse widths of 1, 4, 7 and 10µs. The treatment was for 30 seconds, with a duty cycle of 10%, a frequency of 1500Hz and a fixed gap distance of approximately 1mm.*

Figure 6.7: *Treatment of two culture plates with a distance between the culture plates and the DBD of approximately 1.5 and 2mm. The treatment was for 30 seconds, with a duty cycle of 10%, a pulse width of 10µs and a pulse frequency of 1500Hz.*

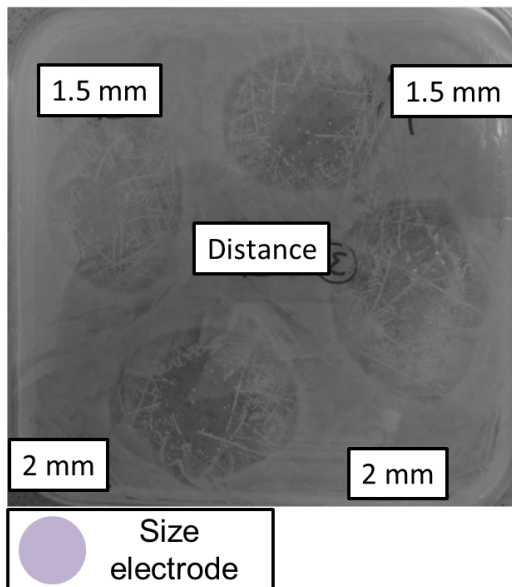medium in the culture plate is treated as well, so the chemical composition and pH of the culture medium may change. A different pH of the medium may inhibit the growth of the bacteria.

The relationships found in the quantitative results compared with the results on the culture plates give no big differences. The culture plates which are treated with different pulse widths, have like the results in subsection 6.1.3, a comparable kill for the treatments of 1 and 4µs and for the treatments of 7 and 10µs. In graph 6.4 and in figure 6.7 there is more kill for a distance of 1 mm and no clear differences in bacteria kill for the distances of 1.5 and 2 mm, this is in agreement with figure 6.4. For the frequency treatments the kill of bacteria is more efficient for a higher frequency like in figure 6.5. However, the difference in effectiveness for a treatment of 500 and 1500 Hz is present on the culture plates, but the difference was not significant for the treatments on the cover glass.

Now, for all the three figures, the active regions have an oval shape and not round, this is due to the fact that the culture plates are not completely leveled, they are a little bit tilted, since the grounded metal is bent. Also the treated surfaces are larger than the surface of the DBD. This means the inactivation is also indirect, no direct electric field or (V)UV effect.

6.2 The effect of treatment on the other Staphylococci

In figure 6.8 four square culture plates are shown, each with one of the four different staphylococci: *S. aureus*, *S. hominis*, *S. capitis* and *S. epidermis*. Each treatment with the old setup on one kind of bacteria was made twice and there was no difference in the culture plates for the same kind of Staphylococcus. The active radius is equal for all four Staphylococci, every treatment time leads to the same shape.

The difference in amount of CFU for the treated areas is very small for the different bacteria, maximum a factor of ten. The changes in previous found log reductions when treating an other staphylococcus than the *S. aureus* would therefore be negligible compared with the large standard deviation in the log reduction. Therefore the results found in the previous section are representative for all four bacteria which cause neonatal sepsis.
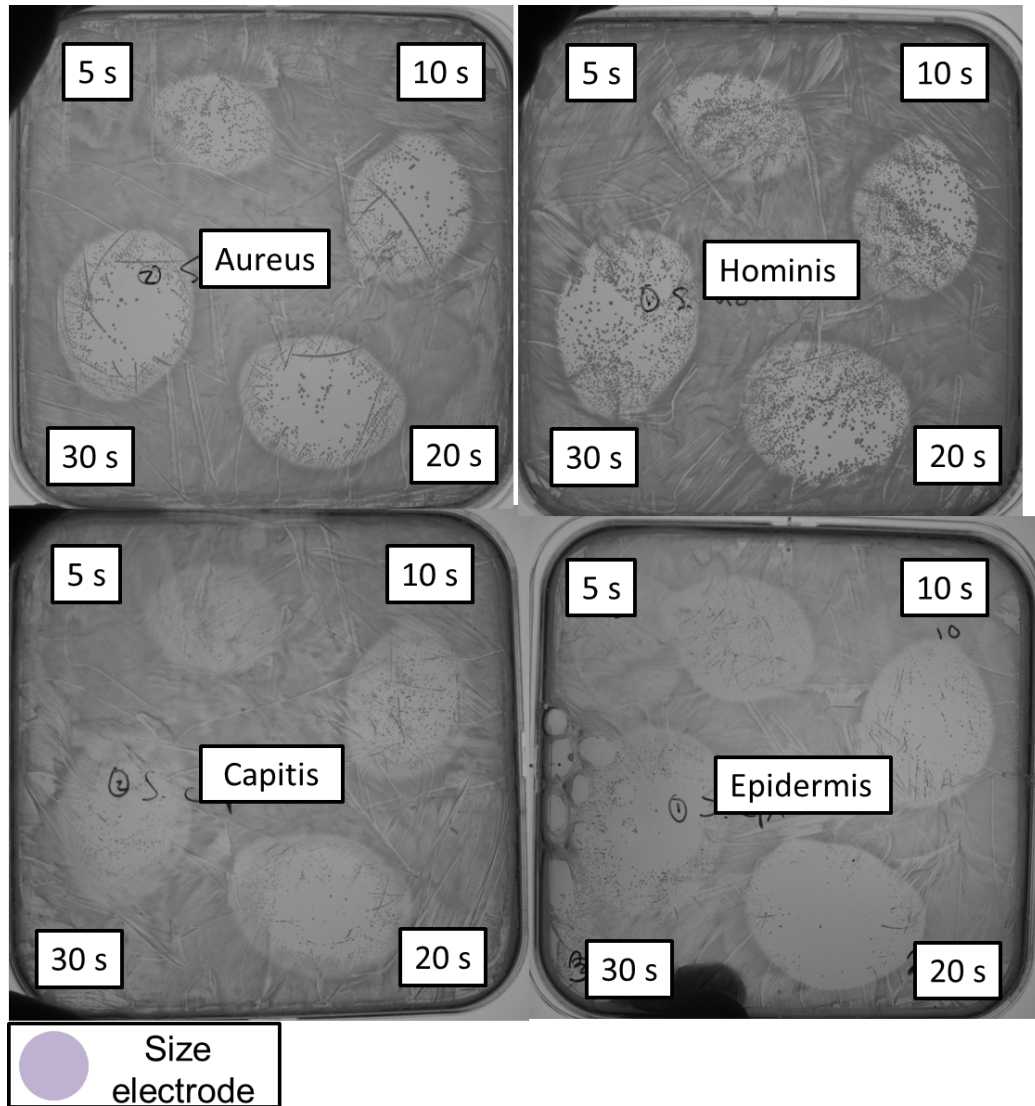
Figure 6.8: *Treatment of 15 by 15 culture plates with bacteria for 5, 10, 20 and 30 seconds. The bacteria on the left top is S. aureus, on the right top S. hominis, on the left bottom S. capitis and on the right bottom S. epidermis. The treatment was with a duty cycle of 10%, a pulse width of 10μs a pulse frequency of 1500Hz and with a distance between the culture plates and the DBD of approximately 1mm.*
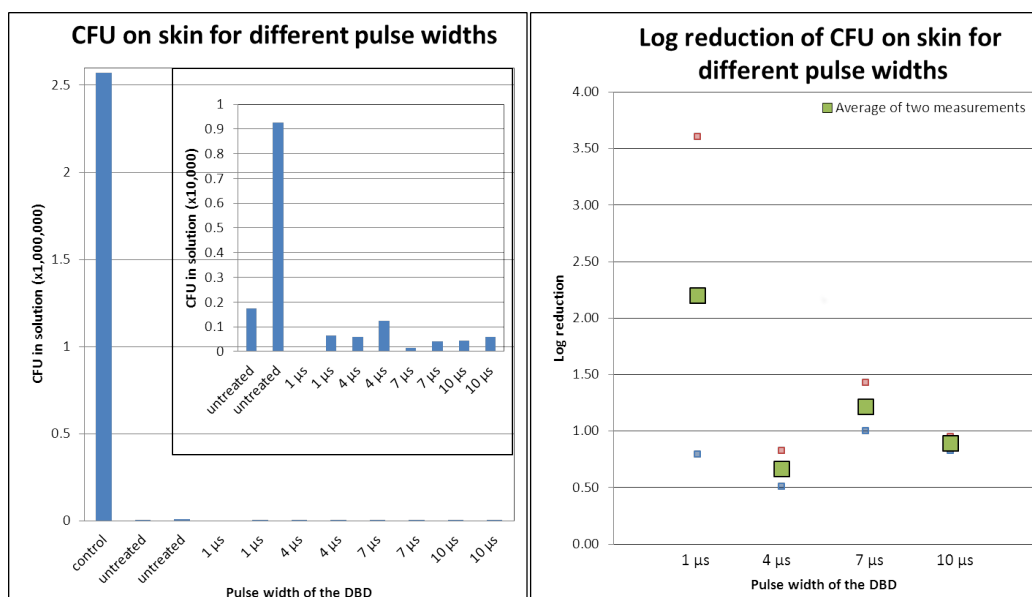
Figure 6.9: _On the left the CFU in the solution, the CFU on the untreated skin_
and the CFU on the treated skin with a pulse width of 1, 4, 7 and 10μs. On the
right the log reduction for two different measurements is shown per treatment in red
and blue. In green the average log reduction for the treatments with the different
pulse widths of 1, 4, 7 and 10μs are given.

6.3   Treatment with the new setup of donor skin infected with _S. aureus_

In this part the log reduction of bacteria on donor skin is given after treatment
with the new setup and the effect of the ex-vivo treatment on the skin is
discussed.

6.3.1   The in activation of bacteria on skin as function of the pulse width of the new setup

On the left in figure 6.9 the CFU in the solution, the CFU on the untreated
skin and the CFU on the treated skin are shown. The CFU on the untreated
skin are much lower than the CFU which are pipetted on the skin. One
reason may be the evaporation time of the drop, during this 1 hour, the
bacteria can die from osmosis or from dehydration. One other reason may
be the effectiveness of the metal beads in the cryovials. Not all bacteria may
be dislodged from the skin, when in the TissueLyser LT [93]. The number of
CFU for both untreated skin samples is very different from each other, the

amount of bacteria that die or the amount of bacteria which are dislodged from the skin may differ a lot per skin sample.

In figure 6.9 on the right, the log reduction for two different treatments, blue and red, and the average log reduction in green is shown. Since there are only two measurements performed, due to the limited availability of donor skin, no good statistics can be performed. However, it is clear that bacteria are inactivated by the treatment with plasma. The log reduction is smaller than in figure 6.3, although the electric properties of the skin lead to a higher power dissipation, as was shown in figure 4.22. The log reduction may be lower, since bacteria can be located in the pores of the skin and are shielded for some effects of the plasma.

6.3.2   The effect of treatment with the DBD on skin

Here the activity of skin cells after the treatment is discussed. In figure 6.10 the result of the treatment and MTT-assay, discussed in subsection 5.3.2 are shown. In red and blue the average activity of the five skin samples for one treatment are shown. In green the averaged activity for the 10 skin biopsy samples belonging to one pulse width treatment and the average activity of the 7 untreated skin biopsy samples is given.

There is no clear difference in the metabolic activity of the skin cells, between treated and untreated skin. It seems that for the treatment with a pulse width of 10 μs the activity of the cells is slightly higher than for the untreated case. This effect is observed in other investigations as well and not completely understood yet [33, 31, 41].

In figure 6.11 two microscope images of skin are shown. On the top an image of untreated skin is shown and on the bottom an image of treated skin is shown. In the bottom figure there is some visible damage. First some parts of the stratum corneum are gone, but this can be due to the cutting of the coupes. Second, the cells in the epidermis seem to have nuclear fading or shrinkage (karyolysis and pyknosis), which mainly occurs as a result of necrosis. Due to external trauma from the plasma, the cells in the epidermis died. Third, the transition between epidermis and dermis in the top figure is smooth, in the bottom figure the membrane, which is the separation between two layers, is degraded. Finally, the collagen is lighter in color and the structure is finer. In all the 5 contiguous coupes taken from this skin sample, the skin was damaged. In all the other treated skin samples, no damage is visible. There may be damage in this treated skin samples, but it depends on the position of the coupes whether these damaged parts are present in the coupes. The damage occurs in spots and relatively small. Since the damage in total is relatively small, no overall decrease in activity was seen for the
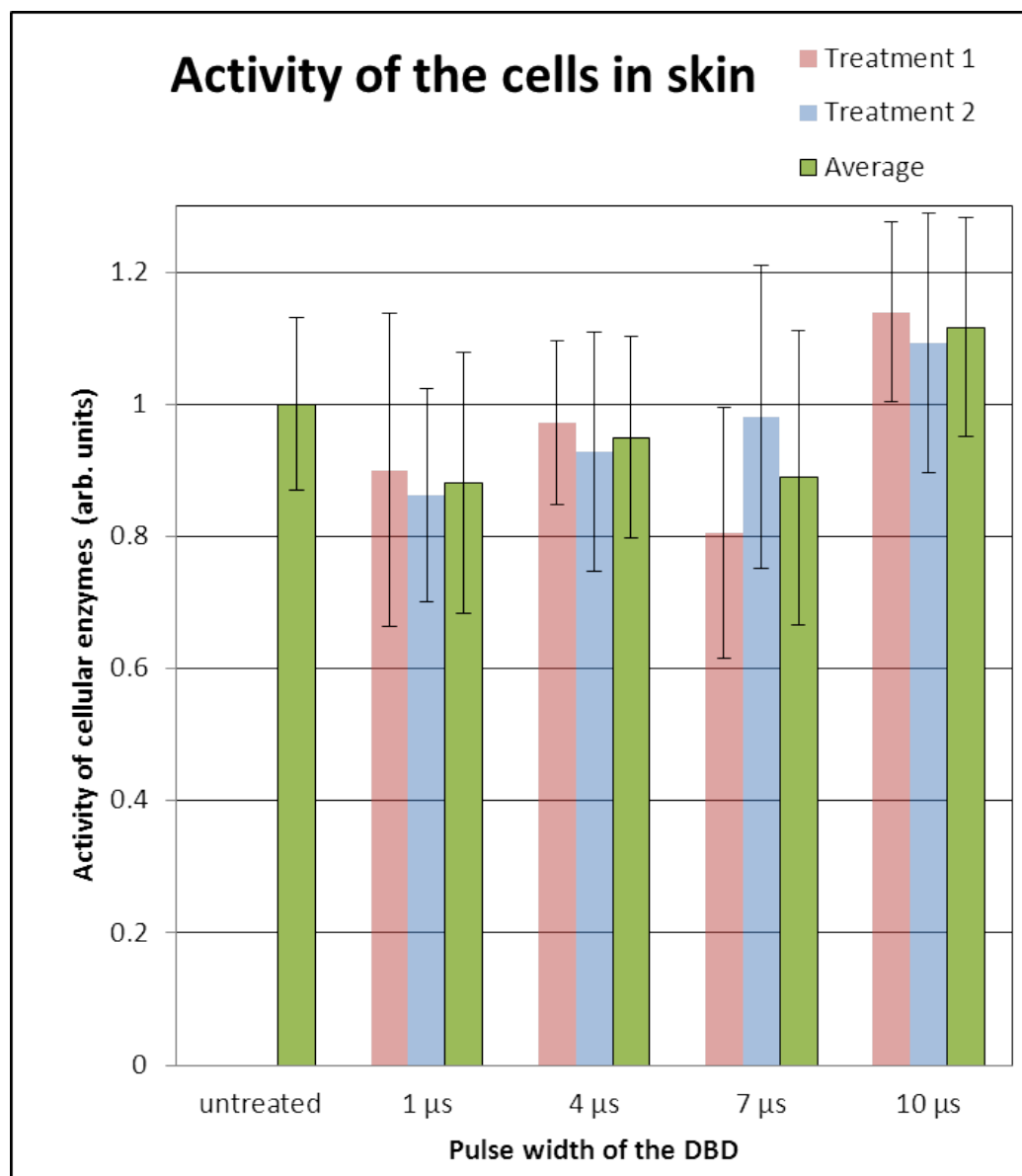
Figure 6.10: *The average activity of cellular enzymes for the skin biopsy samples. The activity of the cells for the untreated skin piece and for the treated skin pieces at a pulse widths of 1, 4, 7 and 10μs.*
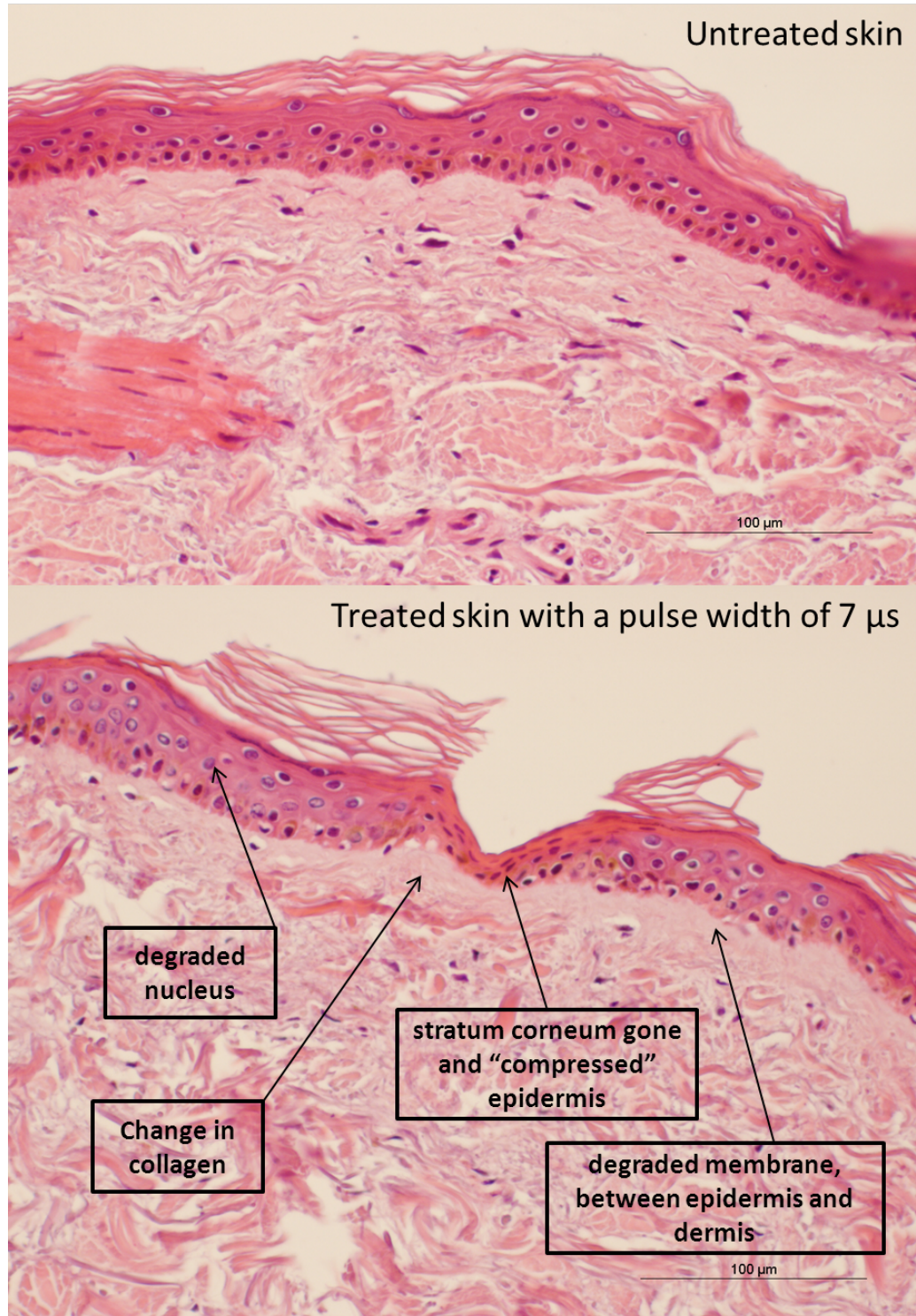
Figure 6.11: *On the top an image of the untreated skin and on the bottom an image of skin treated for 30 seconds, with a duty cycle of 10%, a gap of 1 mm, a pulse frequency of 500 Hz and a pulse width of 7 μs. The dark purple oval shapes are the nuclei of the cells and in pink the surrounding cytoplasm is visible. The treated skin has some visible damage.*

different treatments in the MTT assay. The position of the damaged areas
is probably linked to the position of the filaments. When one piece of skin
is a little bit higher a large number of filaments will hit this part of the skin
and this part will be damaged.

Part III

Discussion, Conclusion and Outlook

Chapter 7

Discussion and Conclusion

From chapter 6 it is clear that the treatments with the FE-DBD are very effective and uniform: almost all bacteria are killed. For the treatments direct on culture plates, the effective treated area is visibly larger than the size of the electrode. It seems that the bacteria are not only inactivated due to direct contact with the filaments, which are not uniformly distributed, but also due to interaction with the chemical species, probably ROS and RNS as discussed in subsection 1.4.2.4. Those chemical components reach the whole surface of the culture plates, the cover glass and also the skin and therefore reach all the bacteria. On skin the treatment is less effective than on cover glass, although the energy dissipated is higher, possibly since the bacteria can be located in pores.

The skin itself is damaged after treatment. The damage is not uniform, but occurs in spots. This indicates that the damage is not due to the chemical species (only). The damage is probably due to the impact of one or more filaments on the same position. On this position, damage is due to locally high electric fields or a lot of heat, possibly in combination with chemical species. The non uniform distribution of the filaments on the skin is due to irregularities in the skin, like hairs, folds in the skin, or pores and is hard to prevent in practice. The overall damage in the skin seems relatively small, since there was no visible drop in the metabolic activity of the skin cells after treatment with the plasma. Still, also small local damage in the skin is of course not desirable for the application. The stimulation of cell growth shown for a treatment with a pulse width of 10 μs is for this application, probably also not favorable.

The results for measurements with the Floating-Electrode Dielectric Barrier Discharge (FE-DBD) in chapter 4 and 6 can be compared. In figure 7.1 the combined results for the different pulse frequencies, different pulse widths
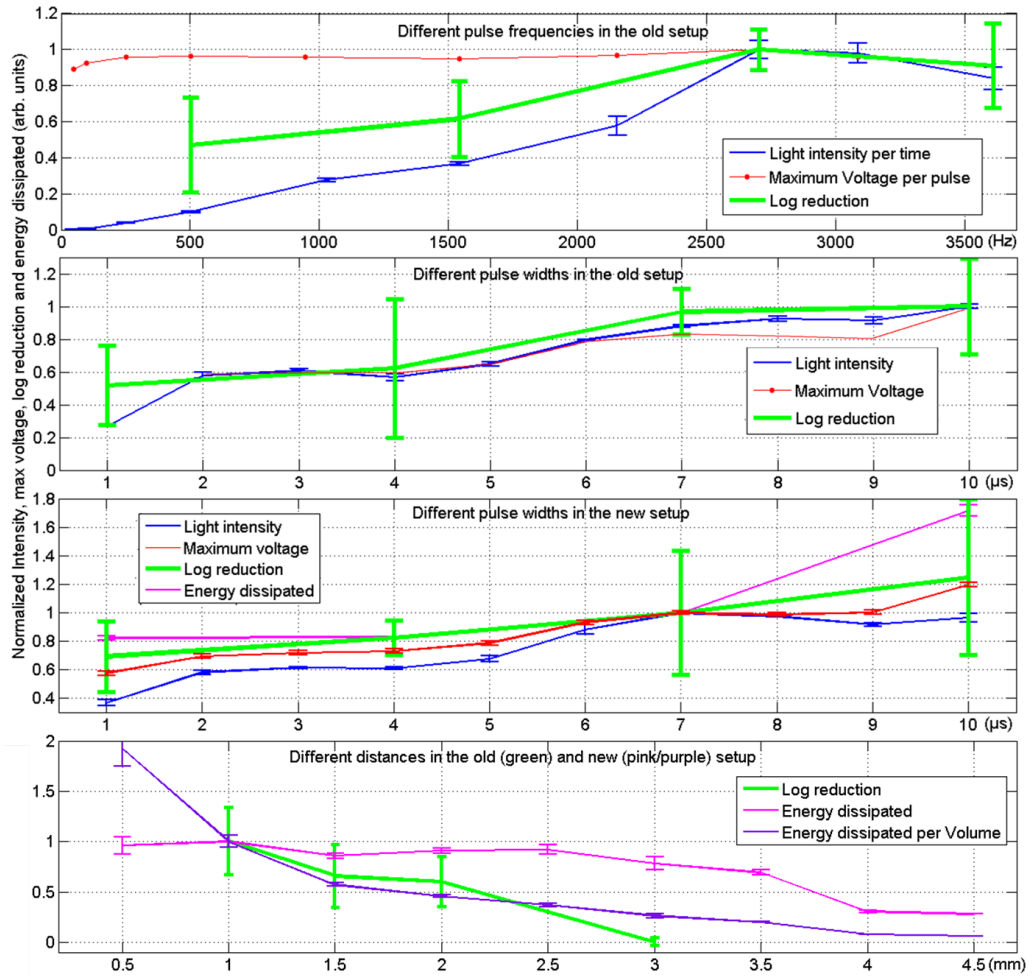
Figure 7.1: *The combined results from chapter 4 and 6 for different pulse frequencies, different pulse width and different gap distances. The normalized maximum voltage per pulse, the light intensity per time, the log reduction of S. aureus on cover glass and the energy dissipated per pulse (per volume) are shown in the graphs.*

and different gap distances are shown. The trend of the variables, the log reduction, the light emission, and the energy dissipated in the plasma, are the same. For a setting which generates more discharges per time unit, a higher pulse frequency or a longer pulse width, the power dissipated in the plasma is higher and more light is emitted. When there are more discharges, more chemical species, in specific, more ROS and RNS will be formed. As discussed above, these chemical species are probably causing the inactivation of bacteria. Therefore, more discharges lead to a higher log reduction.

In the top of figure 7.1 the results for different pulse frequencies in the old setup are shown. The normalized light intensity, the normalized log reduction and the normalized maximum voltage are plotted in the same figure. The maximum voltage is given per pulse and the other two variables are given per time unit. All three variables show the same trend as discussed in subsection 4.2.2, where the maximum is at a frequency of 2500 Hz. This trend is directly linked to the number of discharges which can be formed, as stated before.

Also for different pulse widths, the number of discharges is changing. The results for the measurements with different pulse widths for as well the old as the new setup are given in the two graphs in the middle in figure 7.1. The trends for light emission and maximum voltage for the old and the new setup are discussed in subsection 4.2.3 and 4.3.2 respectively. The energy dissipated in the plasma and the log reduction follow the same trend. Only the light intensity for a pulse width of 7 μs is too high compared with the other variables.

The bottom graph in figure 7.1 is showing the results for different gap distances: the log reduction, the energy dissipated in the plasma and the energy dissipated in the plasma per volume. The measurements for the log reduction are made with the old setup and the experiments to determine the energy dissipated in the plasma are performed with the new setup. Therefore the gap distance at which no plasma occurs is different. For the experiments regarding the log reduction, this gap distance is 3 mm and for the measurements to determine the energy dissipated in the plasma, this gap distance is 4 mm. In subsection 4.4.2 the small decreasing dissipation of energy for a higher gap distance is discussed. A large gap distance leads to a higher breakdown voltage, therefore less discharges will be formed for a larger gap distance. However, the properties of these discharges, listed in table 2.2, can change as well when changing the configuration as stated in subsection 2.1.1. Moreover, the energy dissipated is distributed over a larger volume when the gap distance is larger. Therefore the energy per volume will decrease with a faster rate[1], together with the log reduction.

---

[1]The energy losses in other parts of the load, which give an offset in the energy graph,

7.1   Critical remarks

There are a few side notes for the results obtained in chapter 4 and 6, they may be different in the real case. First of all, the skin used in the experiments was older than the skin of a neonate. This means that the stratum corneum of the skin, consisting of dead cells, is thicker. This has an influence on the electric properties of the skin, but more important, on the interaction of the plasma with the cells in the epidermis. The dead cells may protect the living cells in the skin from the influences of the plasma. When this protecting layer is thinner, the plasma may have a more detrimental effect. Also, every skin will be different, so the effectiveness of the treatment may differ per patient. Even though one plasma treatment may not have a direct influence on the metabolic activity of the skin cells in general, it still can have other short or long term effects, which are not excluded yet in this research. The DNA in the cells may be damaged for instance, which can lead to skin problems. In this research the treatment is only done once, in practice the treatment has to be repeated probably a few times a day, since the bacteria will grow back. The effects on skin may differ and will be more severe for a frequent treatment. Further, the temperature and humidity in the incubator are higher than the temperature and humidity during the experiments. The higher water concentration will lead to a different chemistry for the discharges and different power dissipation in the plasma. During the experiments the temperature and humidity was not monitored.

7.2   Design considerations for the FE-DBD

There are a few design considerations for the FE-DBD:

- Not only the discharges at the quartz surface are possible, discharges are possible in the whole load, since the kHz frequency is passing through the whole load. When the insulating wire is held, discharges will form between the hand and insulating wire. And if for instance an ungrounded metal is near the load, this metal will charge and discharge at once when touched. This leads to unwanted electric shocks. By grounding the surrounding metal surfaces, these shocks can be prevented.

- Both examples mentioned above have an influence on the total capacity of the load and therefore on the formation of the plasma at the quartz

will make this decrease smaller.

surface. To have the same plasma formation every time the FE-DBD is used, the load should not change. So, the insulating wire should be of the same length, but also the interaction with surrounding materials should not change.

- The pulse frequencies of the FE-DBD are within the range of hearing, this would increase stress for the premature child. The electric signal should be altered by for instance having less discharges per pulse and a higher pulse frequency or the other way around.

- Due to the EM-fields created by the plasma and the setup, the many monitoring devices in the incubator described in section 1.1 may be disturbed. Unwanted effects of the EM-fields may be overcome by a proper shielding of the device.

- The quartz material, which is essential to minimize the current going through the skin, may break. When there is a small air bubble between the quartz and the metal, it will grow due to high fields and eventually break the dielectric material. An arc discharge may be possible in this situation. This requires a good security system and a short use of the same load. In an other design this risk can be excluded.

- From the results it is clear that the distance has an influence on the plasma formation and therefore on the treatment. Since the skin is not flat but curved, it is difficult to have the same distance from the skin everywhere. The treatment with the FE-DBD will therefore not be equal in the whole area. A flexible DBD should be used.

- A different geometry than used in this research is needed. The skin around a catheter and underneath a tegaderm (transparent dressing) needs to be disinfected. The fluid within the catheter should not change in chemical composition, by interaction with the plasma.

- The skin around the opening has to be visible, the device should be transparent for instance. By looking at the skin, an infection in early state can be seen by a red color of the skin.

So, the applicability of this specific FE-DBD for preventing neonatal sepsis is not very promising. However, the use of a DBD or other plasma source to prevent neonatal sepsis may be much more promising. In the next chapter, an outlook in the research for the use of plasma to prevent neonatal sepsis is given.

Chapter 8

Outlook

From the previous chapter it is clear that the FE-DBD of Fridman et al. is not the desirable plasma device to prevent neonatal sepsis with premature children. Especially the detrimental effects on skin, due to the inhomogeneous discharges, are cause for concern. The focus in the close future should be on the development of a new plasma source that does not use the skin as second electrode. This allows a slightly uneven skin surface without affecting the plasma that is generated. From this research the indirect treatment, the effect of the chemical mix in contact with the substrate, seems to be adequate to inactivate the bacteria. In the development of this new plasma source the practical application should be kept in mind, to foresee and prevent issues as mentioned in section 7.2.

From this research it is once again shown that bacteria are inactivated by the treatment with a plasma source and that the effect on skin is, on first hand and after only one treatment, small. The bacteria which cause neonatal sepsis are probably killed by the interaction with the chemical mixture of the plasma. Which combination in this chemical mixture in humid air is responsible for the inactivation, which are the activity-responsible plasma species? What is the effect of the electric field in this inactivation process and is the inactivation the same without an electric field? What happens exactly in the bacteria, do they die due to a complicated pathways of signalling, or do specific species simply enter the cell directly which may lead to an instantaneous death? So, which kinetics are related to these processes? Which interactions are there between the plasma molecules and the biological matter and its individual bio macromolecules, like DNA, proteins, lipids and polysaccharides? [94, 95, 96]

The possible dangers should be identified and excluded. Like the production of ozone and its effect on the premature, but also the long term effects of treatment on skin. For instance DNA damage will lead to skin problems.

Experiments with premature-like skin have to be performed to exclude effects of the stratum corneum. The skin should not be damaged. The effect of the plasma on the skin growth has to be understood and it must be known to which extend a stimulation of growth is harmful. What are the consequences for a more frequent exposure to the plasma?

Effects of differences in the to be treated skin and a higher humidity of the air have to be researched. Are these difference negligible and if not, how can we tackle these differences? This can be done by for instance changing the power dissipated in the plasma. For different situations, the right treatment has to be known. This treatment can change in treatment time and frequency of the treatment, to reach a certain log reduction. What is the ideal combination of these two parameters?

Do premature born children not need to suffer from neonatal sepsis anymore in the future, due to skin disinfection with a plasma source? The fields of plasma physics, chemistry, biology and medicine should work together. People from these different disciplines should research if a safe and practical plasma device is possible and have to understand the complexity and find the answers to all questions mentioned above.

Bibliography

[1] Centraal Bureau voor de Statistiek CBS. bevolking. 1

[2] Welzijn en Sport Rijksinstituut voor Volksgezondheid en Milieu, Ministerie van Volksgezondheid. Vroeggeboorten. 1

[3] Perinatale Regristratie Nederland Stichting PRN. 1

[4] GE Healthcare. Giraffe incubator. 1.1

[5] A.J Lyon and C Oxley. Heatbalance, a computer program to determine optimum incubator air temperature and humidity. a comparison against nurse settings for infants less than 29 weeks gestation. *Early Human Development*, 62(1):33 – 41, 2001. 1.1

[6] M Abdiche; G Farges; S Delanaud; V Bach; P Villon; Jean Pierre Libert. Humidity control tool for neonatal incubator. *Medical, biological engineering, computing*, 36:241–5, 1998. 1.1

[7] K. Hammarlund and G. Sedin. Transepidermal water loss in newborn infants. vi. heat exchange with the environment in relation to gestational age. *Acta Paediatrica Scandinavica*, 71(2):191–196, 1982. cited By (since 1996)20. 1.1

[8] Adriaan Bink. *Bevochtiging van de Giraffe couveuse*. Intranet MMC, 2012. 1.1

[9] Majid Mirmiran and Ronald L. Ariagno. Influence of light in the nicu on the development of circadian rhythms in preterm infants. *Seminars in Perinatology*, 24(4):247 – 257, 2000. <ce:title>Chronobiology in the Newborn Period</ce:title>. 1.1

[10] Fanos V. Antonucci R, Porcella A. The infant incubator in the neonatal intensive care unit: unresolved issues and future developments. *Journal of Perinat Medicine*, 37:587–98, 2009. 1.1

[11] Lago P Arslan E Pisan P. Benini F, Magnavita V. Evaluation of noise in the neonatal intensive care unit. *American Journal of Perinatology*, 13:37–41, 1996. 1.1

[12] Wei Chen, I. Ayoola, S.B. Oetomo, and L. Feijs. Non-invasive blood oxygen saturation monitoring for neonates using reflectance pulse oximeter. In *Design, Automation Test in Europe Conference Exhibition (DATE), 2010*, pages 1530–1535, 2010. 1.1

[13] Ideas that work for life Ambu. Neonatal monitoring. 1.1, 1.4.1

[14] William W. Fox Richard A. Polin. *Fetal and Neonatal Physiology*, volume 1. W.B. Saunders Company, 1992. 1.1, 1.2, 1.3, 1.4.1

[15] Saakje P. da Costa. *Development of Sucking Patterns in Preterm Infants*. PhD thesis, Rijksuniversiteit Groningen, 2010. 1.1

[16] drug information online drugs.com. Umbilical venous catheter in newborns. 1.2

[17] Ivanka Ercegovic Branka Polic Luka Stricevic Ante Omazic Vesna Capkun Julije Mestrovic, Tanja Kovacevic. Use of central venous catheters in children. *Signa Vitae*, 1:20–24, 2006. 1.1

[18] Z. Stanga S. C. Bischoff P. Brass W. Hartl S. Muehlebach E. Pscheidl P. Thul O. Volk K. W. Jauch, W. Schregel and Working group for developing the guidelines for parenteral nutrition of The German Association for Nutritional Medicine. Access technique and its problems in parenteral nutrition, guidelines on parenteral nutrition, chapter 9. *German Medical Science*, 7, 2009. 1.1

[19] Hopkins CC Malt RA. Savage AP, Picard M. Complications and survival of multilumen central venous catheters used for total parenteral nutrition. *The British journal of Surgery*, 80:1287–90, October 1993. 1.1

[20] Wirtschafter DW. Powers RJ. Decreasing central line associated bloodstream infection in neonatal intensive care. *Clin Perinatol*, 37:247–72, 2010. 1.1, 1.3

[21] Simmer K Currie A Levy O Burgner D. Strunk T, Richmond P. Neonatal immune responses to coagulase-negative staphylococci. *Current Opinion in infectious diseases*, 20:370–5, 2007. 1.1

[22] D. Bakari C. Doi) E. Bingen Y. Aujard M. Rajguru, P. Mariani-Kurkdjian. Bacterial colonization of umbilical (uvc) and central (cvc) venous catheters in infant newborns. 1.1

[23] Julian Lewis Martin Raff Keith Roberts Peter Walter Bruce Alberts, Alexander Johnson. *Molecular Biology of the Cell, fifth edition*. Garland Publ Co, November 2007. 1.2, 1.4.2.1

[24] beta Microbe world. Meet the microbes, bacteria, what they look like. 1.3

[25] Centers for disease control and prevention. Publik health image library. 1.3

[26] C. G. Gemmel. Coagulase negative staphylococci. *J. Med. Microbiol.*, 22285-295, 1986. 1.2

[27] Gerhard Pulverer. Coagulase-negative staphylococci. In Wadstram, editor, *Pathogenesis of Wound and Biomaterial-Associated Infections*, pages 299–308. Springer London, 1990. 1.2

[28] R.N.C.; Carol Van de Rostyne A.N.P.; Grace Schmidt R.N.C.; Kelley OLeary R.N. Jack Jacob, M.D.; Deb Sims. Toward the elimination of catheter-related bloodstream infections in a newborn intensive care unit (nicu). *The Joint Commission Journal on Quality and Patient Safety*, 37(5):211–16, 2011. 1.2, 1.3

[29] Stoll BJ, Hansen NI, Adams-Chapman I, and et al. Neurodevelopmental and growth impairment among extremely low-birth-weight infants with neonatal infection. *JAMA*, 292(19):2357–2365, 2004. 1.3

[30] Verboon-Macciolek MA et al. Van den Hoogen A, Brouwers AJ. Improvement of adherence to hand hygienepractice using a multimodal intervention program in a neonatal intensive care unit. *J. Nurse. Car Qual.*, 26:22–29, 2011. 1.3

[31] G. Morfill G.E. Nosenko T. Shimizu T. van Dijk J. Zimmermann J.L. Kong, Michael G. Kroesen. Plasma medicine: an introductory review. *Net Journal of Physics*, 11:26, 2009. 1.4, 1.4.1, 1.4.2, 1.4.2.2, 6.3.2

[32] Julia Heinlin, Gregor Morfill, Michael Landthaler, Wilhelm Stolz, Georg Isbary, Julia L. Zimmermann, Tetsuji Shimizu, and Sigrid Karrer. Plasma medicine: possible applications in dermatology. *JDDG: Journal der Deutschen Dermatologischen Gesellschaft*, 8(12):968–976, 2010. 1.4

[33] Gregory Fridman, Gary Friedman, Alexander Gutsol, Anatoly B. Shekhter, Victor N. Vasilets, and Alexander Fridman. Applied plasma medicine. *Plasma Processes and Polymers*, 5(6):503–533, 2008. 1.4, 1.5, 3.1, 3.2, 6.3.2

[34] M. Laroussi. Nonthermal decontamination of biological media by atmospheric-pressure plasmas: review, analysis, and prospects. *Plasma Science, IEEE Transactions on*, 30(4):1409–1415, 2002. 1.4, 1.4.2, 1.4.2.2

[35] Gregory Fridman, Marie Peddinghaus, Manjula Balasubramanian, Halim Ayan, Alexander Fridman, Alexander Gutsol, and Ari Brooks. Blood coagulation and living tissue sterilization by floating-electrode dielectric barrier discharge in air. *Plasma Chemistry and Plasma Processing*, 26:425–442, 2006. 10.1007/s11090-006-9024-4. 1.4, 1.4.1, 1.6, 1.5

[36] Gary Friedman Danil Dobryinin, Gregory Fridman and Alexander Fridman. Physical and biological mechanisms of direct plasma interaction with living tissue. *New Journal of Physics*, 11:26, 2009. 1.4, 1.4.2.2, 1.5

[37] David B Graves. The emerging role of reactive oxygen and nitrogen species in redox biology and some implications for plasma applications to medicine and biology. *Journal of Physics D: Applied Physics*, 45(26):263001, 2012. 1.4, 1.1

[38] Bender C Koban I Hübner NO Kramer A. Matthes R, Bekeschus S. Pilot-study on the influence of carrier gas and plasma application (open resp. delimited) modifications on physical plasma and its antimicrobial effect against pseudomonas aeruginosa and staphylococcus aureus. *GMS Krankenhhyg Interdiszip*, 7:7, 2012. 1.4

[39] G Y Park, S J Park, M Y Choi, I G Koo, J H Byun, J W Hong, J Y Sim, G J Collins, and J K Lee. Atmospheric-pressure plasma sources for biomedical applications. *Plasma Sources Science and Technology*, 21(4):043001, 2012. 1.4.1

[40] Thomas von Woedtke Marcel Hähnel Manfred Stieber Klaus Dieter Weltmann, Eckhard Kindel and Ronny Brandenburg. Atmospheric-pressure plasma sources: Prospective tools for plasma medicine. *Pure Appl. Chem.*, 82:1223–1237, 2010. 1.4.1

[41] Roxana Silvia Tipa. *Plasma in wound healing*. PhD thesis, Eindhoven : Technische Universiteit Eindhoven, juni 2012. 1.4.1, 1.4.2, 6.3.2

[42] Yukinori Sakiyama, David B Graves, Hung-Wen Chang, Tetsuji Shimizu, and Gregor E Morfill. Plasma chemistry model of surface microdischarge in humid air and dynamics of reactive neutral species. *Journal of Physics D: Applied Physics*, 45(42):425201, 2012. 1.4.1, 1.4, 1.4.2.4, 4.5.2

[43] X Lu, M Laroussi, and V Puech. On atmospheric-pressure non-equilibrium plasma jets and plasma bullets. *Plasma Sources Science and Technology*, 21(3):034005, 2012. 1.4.1, 1.5

[44] Natalia Yu Babaeva and Mark J Kushner. Intracellular electric fields produced by dielectric barrier discharge treatment of skin. *Journal of Physics D: Applied Physics*, 43(18):185206, 2010. 1.4.1, 1.6, 1.4.2.3

[45] G E Morfill, T Shimizu, B Steffes, and H-U Schmidt. Nosocomial infections - a new approach towards preventive medicine using plasmas. *New Journal of Physics*, 11(11):115019, 2009. 1.4.1

[46] C.A.J. van Gils. Investigation of the mechanisms of bacterial inactivation induced by a cold atmospheric pressure plasma jet for burn wound treatment. Master's thesis, Eindhoven University of Technology, August 2012. 1.4.1, 1.4.2

[47] M. Golkowski, C. Golkowski, J. Leszczynski, S.R. Plimpton, P. Maslowski, A. Foltynowicz, Jun Ye, and B. McCollister. Hydrogen-peroxide-enhanced nonthermal plasma effluent for biomedical applications. *Plasma Science, IEEE Transactions on*, 40(8):1984 –1991, aug. 2012. 1.4.1

[48] M Laroussi. Non thermal decontamination of biological media by atmospheric pressure plasmas: review, analysis and prospects. *IEEE Trans. Plasma. Sci.*, 30:1409–15, 2002. 1.4.1

[49] M Kuchenbecker, N Bibinov, A Kaemlimg, D Wandke, P Awakowicz, and W Via. Characterization of dbd plasma source for biomedical applications. *Journal of Physics D: Applied Physics*, 42(4):045212, 2009. 1.4.1

[50] H. Ayan, G. Fridman, A.F. Gutsol, V.N. Vasilets, A. Fridman, and G. Friedman. Nanosecond-pulsed uniform dielectric-barrier discharge. *Plasma Science, IEEE Transactions on*, 36(2):504–508, 2008. 1.4.1

[51] WebMD. Skin problems and treatments health center. 1.7

[52] J. A. Bittencourt. *Fundamentals of Plasma Physics*. Springer, 2004. 1.4.2

[53] Alan J. Lichtenberg Michael A. Lieberman. *Principles of Plasma Discharges and Materials Processing, 2nd edition*. Wiley, April 2005. 1.4.2

[54] Lubert Stryer John L. Tymoczko, Jeremy M. Berg. *Biochemistry*. W.H.Freeman & Co, 2007. 1.4.2.1

[55] Q. S. Yu, C. Huang, F.-H. Hsieh, H. Huff, and Yixiang Duan. Bacterial inactivation using a low-temperature atmospheric plasma brush sustained with argon gas. *Journal of Biomedical Materials Research Part B: Applied Biomaterials*, 80B(1):211–219, 2007. 1.4.2.1

[56] Charles Polk. Biological applications of large electric fields: some history and fundamentals. *Plasma Science, IEEE Transactions on*, 28(1):6–14, 2000. 1.4.2.3

[57] Robert Susil, Dejan Šemrov, and Damijan Miklavcic. Electric field-induced transmembrane potential depends on cell density and organizatio. *Electromagnetic Biology and Medicine*, 17(3):391–399, 1998. 1.4.2.3

[58] Victor J Thannickal and Barry L Fanburg. Reactive oxygen species in cell signaling. *American Journal of Physiology-Lung Cellular and Molecular Physiology*, 279(6):L1005–L1028, 2000. 1.4.2.4

[59] Palwinder K Mander, Aiste Jekabsone, and Guy C Brown. Microglia proliferation is regulated by hydrogen peroxide from nadph oxidase. *The Journal of Immunology*, 176(2):1046–1052, 2006. 1.4.2.4

[60] David A Wink, Ingeborg Hanbauer, Murali C Krishna, William DeGraff, Janet Gamson, and James B Mitchell. Nitric oxide protects against cellular damage and cytotoxicity from reactive oxygen species. *Proceedings of the National Academy of Sciences*, 90(21):9813–9817, 1993. 1.4.2.4

[61] Guy C Brown and Vilmante Borutaite. Nitric oxide inhibition of mitochondrial respiration and its role in cell death. *Free Radical Biology and Medicine*, 33(11):1440–1450, 2002. 1.4.2.4

[62] Ursula Rauen, Tongju Li, Iosif Ioannidis, and Herbert de Groot. Nitric oxide increases toxicity of hydrogen peroxide against rat liver endothelial cells and hepatocytes by inhibition of hydrogen peroxide degradation. *American Journal of Physiology-Cell Physiology*, 292(4):C1440–C1449, 2007. 1.4.2.4

[63] H.-E. Wagner, R. Brandenburg, K.V. Kozlov, A. Sonnenfeld, P. Michel, and J.F. Behnke. The barrier discharge: basic properties and applications to surface treatment. *Vacuum*, 71(3):417 – 436, 2003. Symposium on Plasma Surface Engineering at the Spring Meeting of the German Physical Society, Regensburg, Germany, March 11-15 2002. 2, 2.1, 2.1.1, 2.2

[64] Ashok Kumar Vijay Nehra and H K Dwivedi. Atmospheric non-thermal plasma sources. *International Journal of Engineering*, 2. 2.1

[65] Kogelschatz, U., Eliasson, B., and Egli, W. Dielectric-barrier discharges. principle and applications. *J. Phys. IV France*, 07:C4–47–C4–66, 1997. 2.2, 2.2

[66] Sander Nijdam. *Experimental Investigations on the Physics of Streamers*. PhD thesis, Technische Universiteit Eindhoven, februari 2011. 2.1.1, 2.1.3, 2.1.3, 2.1.3.1

[67] Leonard B. Loeb and John M. Meek. The mechanism of spark discharge in air at atmospheric pressure. i. *Journal of Applied Physics*, 11(6):438–447, 1940. 2.1.1

[68] Ulrich Kogelschatz. Dielectric-barrier discharges: Their history, discharge physics, and industrial applications. *Plasma Chemistry and Plasma Processing*, 23:1–46, 2003. 2.1.1

[69] E.M. van Veldhuizen S. Nijdam, G. Wormeester and U. ebert. Probing background ionization: Positive streamers with varying pulse repetition rate and with a radioactive admixture. *J. Phys. D: Appl. Phys.*, 44:17, 2011. 2.1.3

[70] I A Kossyi, A Yu Kostinsky, A A Matveyev, and V P Silakov. Kinetic scheme of the non-equilibrium discharge in nitrogen-oxygen mixtures. *Plasma Sources Science and Technology*, 1(3):207, 1992. 2.1.3.1

[71] N.L. Aleksandrov and E.M. Bazelyan. Ionization processes in spark discharge plasmas. *Plasma Sources Schi. T.*, 8:285, 1999. 2.1.3.1

[72] A.V. Levchenko V.A. Bityurin, G. Yu. Alekseev. Pulsed positive corona for flue gas cleaning. mathematical model and computer code of chemical and gasdynamical decay of streamer channel, September 1992. 2.1.3.1

[73] Tomoyuki Murakami, Kari Niemi, Timo Gans, Deborah O'Connell, and William G Graham. Chemical kinetics and reactive species in atmospheric pressure helium-oxygen plasmas with humid-air impurities. *Plasma Sources Science and Technology*, 22(1):015003, 2013. 2.1.3.1

[74] The hitran database. 2.4

[75] J. Michael Hollas. *Modern spectroscopy*. Wiley, 4th edition, 2004. 2.1.4

[76] Relative Permittivity Dielectric constant. www.engineeringtoolbox.com. 2.3

[77] J. G. Stinstra M. J. Peters and I. Leveles. *Modeling and Imaging of Biolelectrical Activity: Principles and Applications*. Springer, 2004. 2.3

[78] S Gabriel, R W Lau, and C Gabriel. The dielectric properties of biological tissues: Iii. parametric models for the dielectric spectrum of tissues. *Physics in Medicine and Biology*, 41(11):2271, 1996. 2.3

[79] Leonard B. Loeb and J. M. Meek. The mechanism of spark discharge in air at atmospheric pressure. ii. *Journal of Applied Physics*, 11(7):459–474, 1940. 2

[80] home.earthlink.nl. Gaseous breadown & paschen's law, Februari 2004. 2.2

[81] T.C. Manley. *The Electric Characteristics of the Ozonator Discharge*, volume 84. J. Electrochem. Soc., 1943. 2.2.1.1

[82] J D Jackson. *Classical Electrodynamics*. New York: Wiley, 1975. 3.1.4

[83] Agilent Technologies. http://www.home.agilent.com. 3.2

[84] information unlimited Amazing. http://www.amazing1.com/. 3.2

[85] solutions in spectroscopy Avantes. http://www.avantes.com. 3.3.1

[86] Stanford Computer Optics. http://www.stanfordcomputeroptics.com. 3.3.2

[87] J. R. Janesick. *Scientific charge-coupled devices*. SPIE Press, 2001. 3.3.2

[88] Innovation with Integrity Bruker. www.bruker.com. 3.4

[89] David A. Naylor and Margaret K. Tahic. Apodizing functions for fourier transform spectroscopy. *J. Opt. Soc. Am.*, 24(11):3644–3648, November 2007. 8

[90] Matthew J Pavlovich, Hung-Wen Chang, Yukinori Sakiyama, Douglas S Clark, and David B Graves. Ozone correlates with antibacterial effects from indirect air dielectric barrier discharge treatment of water. *Journal of Physics D: Applied Physics*, 46(14):145202, 2013. 3.4.1.1, 4.5.2

[91] K V Kozlov, R Brandenburg, H-E Wagner, A M Morozov, and P Michel. Investigation of the filamentary and diffuse mode of barrier discharges in n 2 /o 2 mixtures at atmospheric pressure by cross-correlation spectroscopy. *Journal of Physics D: Applied Physics*, 38(4):518, 2005. 4.1.2

[92] Team UCL. Igem 2010. 5.1

[93] Qiagen. http://www.qiagen.com/. 5.3.1, 6.3.1

[94] Mahmoud Y. Alkawareek, Qais T. Algwari, Sean P. Gorman, William G. Graham, Deborah O'Connell, and Brendan F. Gilmore. Application of atmospheric pressure nonthermal plasma for the in vitro eradication of bacterial biofilms. *FEMS Immunology & Medical Microbiology*, 65(2):381–384, 2012. 8

[95] Kai Masur Deborah O Connell Steffen Emmert Antoinette Killian Julia Zimmermann Theresa A. Freeman, David Graves. Workshop: Plasma to plasma! Lorentz center, Januari 2013. 8

[96] K.-D. Weltmann, M. Polak, K. Masur, T. von Woedtke, J. Winter, and S. Reuter. Plasma processes and plasma sources in medicine. *Contributions to Plasma Physics*, 52(7):644–654, 2012. 8

[97] A. V. Pipa, J. Koskulics, R. Brandenburg, and T. Hoder. The simplest equivalent circuit of a pulsed dielectric barrier discharge and the determination of the gas gap charge transfer. *Review of Scientific Instruments*, 83(11):115112, 2012. A

Dankwoord

Na een klein jaar onderzoek ben ik trots om deze scriptie te presenteren. Mede dankzij een grote groep mensen heb ik dit project kunnen uitvoeren. Hierbij wil ik dan ook de mogelijkheid aangrijpen om al deze mensen te bedanken.

Ten eerste wil ik natuurlijk mijn directe begeleider Gerrit bedanken, dat hij in zijn volle schema als vakgroepleider en decaan toch altijd een moment kon vinden om samen met mij mijn bevindingen te bespreken. Ik ben heel dankbaar dat bij veel van deze momenten ook Peter aanwezig was om kritisch op de zaken in te gaan. Verder wil ik Sidarto bedanken dat hij me heeft begeleid bij alle medisch aspecten en Bouke voor het begeleiden bij en bediscussieren van alle biologische aspecten. Bedankt dat jullie alle vier zo goed met mij hebben meegedacht en goed naar mijn verslag hebben gekeken.

Veel dank aan Ab, Loek, Gerard en Huib voor de hulp bij al mijn technische obstakels, de ontwerpen en de reperaties. Hierbij kunnen zeker niet de mensen van EPC ontbreken, Paul, Jovita en Rob heel erg bedankt voor het repareren van mijn gesneuvelde power generator en het meedenken. En Evert, bedankt voor de ICT ondersteuning en de verre ritjes helemaal naar Beverwijk.

Ook veel andere mensen bij EPG hebben altijd klaar gestaan om met mij mee te denken, bedankt Paulien, Ronny, Eddie, Sander, Bram, Sven, Arij, Tiny en Chris. Ook de mede studenten in mijn kantoor waren vaak bereid om mee te denken en soms mee te ontspannen, dankjewel Ben, Leroy, Paul en Luuk. In het bijzonder bedank ik Thomas, dat hij tijd heeft gestoken in mij te leren werken met de FTIR spectrometer.

Ten slotte wil ik natuurlijk niet de lunch vergeten, waar ik elke dag met veel plezier naar toe ben gegaan. De goede en gezellige gesprekken met alle collegae die hier gevoerd werden zal ik zeker niet snel vergeten.

Appendix A

Derivation of the dissipated power

In this appendix the circuit in figure 2.5 is used to find the way to determine the power dissipated in the discharge [97]. During a discharge there is an electric current, called the plasma current. Besides the plasma current, there is a current running through the air gap, i_{air} which is indicated in figure 2.5. This current is given by

$$i_{air}(t) = C_{air} \frac{dV_{air}(t)}{dt} \,, \tag{A.1}$$

where $V_{air}(t)$ is now the voltage through the air gap when there is a discharge, this voltage can be determined as follows

$$V_{air}(t) = V_{total}(t) - \frac{Q(t)}{C_{d1,2}} \,, \tag{A.2}$$

where $C_{d1,2}$ is the capacity of the two dielectric surfaces in series. If equation A.2 is substituted in equation A.1 with $\frac{dQ(t)}{dt} = i(t)$ the result is given by

$$i_{air}(t) = C_{air} \left(\frac{dV_{total}(t)}{dt} - \frac{i_{total}(t)}{C_{d1,2}} \right). \tag{A.3}$$

In order to calculate the power in the plasma, the current through the plasma needs to be determined. From the electric circuitry, the value of the current through the discharge is can be calculated by subtracting the current through the air from the total current, $i_{plasma}(t) = i_{total}(t) - i_{air}(t)$. From this and using equation A.3 the plasma current is written as

$$i_{plasma}(t) = \left(1 - \frac{C_{air}}{C_{d1,2}}\right) i_{total}(t) - C_{air} \frac{dV_{total}(t)}{dt} \,, \tag{A.4}$$

or can be rewritten with equation 2.15 in the form

$$i_{plasma}(t) = \frac{1}{1 - \frac{C_{total}}{C_{d1,2}}} \left(i_{total}(t) - C_{total} \frac{dV_{total}(t)}{dt} \right).$$ (A.5)

For the average power in the plasma P the energy $E(t)$ coupled in the discharge is used

$$P = E(T)/T\,,$$ (A.6)

$$E(t) = \int_0^t i_{plasma}(t) V_{air}(t) dt\,,$$ (A.7)

this latter equation can be rewritten by combining V_{air} ,equation A.2, and equation A.5 which gives

$$E(t) = \int_0^T \frac{1}{1 - \frac{C_{total}}{C_{d1,2}}} \left[V(t)i(t) - C_{total}V(t)\frac{dV(t)}{dt} - \frac{Q(t)}{C_{d1,2}}i(t) + \frac{Q(t)}{C_{d1,2}}C_{total}\frac{dV(t)}{dt} \right] dt\,,$$ (A.8)

with $i(t) = i_{total}(t)$ and $V(t) = V_{total}(t)$. The second and third term are equal to zero for one whole period T:

$$\int_0^T \left[V(t)\frac{dV(t)}{dt} \right] dt = \frac{1}{2} \left[V^2(T) - V^2(0) \right] = 0 \text{ and}$$

$$\int_0^T \left[Q(t)i(t) \right] dt = \int_0^T \left[Q(t)\frac{dQ(t)}{dt} \right] dt = \frac{1}{2} \left[Q^2(T) - Q^2(0) \right] = 0\,.$$

The latter term in equation A.8 can be rewritten by integration by parts as following

$$\frac{C_{total}}{C_{d1,2}} \left[Q(T)V(T) - Q(0)V(0) - \int_0^T V(t)dQ(t) \right] = -\frac{C_{total}}{C_{d1,2}} \int_0^T V(t)i(t)dt\,.$$ (A.9)

With the latter term combined with the first term, the energy dissipated in the discharge is simplified in the form

$$E(t) = \frac{1}{1 - \frac{C_{total}}{C_{d1,2}}} \left[1 - \frac{C_{total}}{C_{d1,2}} \right] \int_0^T V(t)i(t)dt\,,$$ (A.10)

which gives the following relation for the energy dissipated in a whole period:

$$E(t) = \int\limits_{0}^{T} i_{plasma}(t) V_{air}(t) dt = \int_{0}^{T} V(t) i(t) dt \, . \qquad (A.11)$$

Appendix B

Current peaks

In figure B.1 the voltage signal is shown in blue and a signal shot current signal is given in red for a pulse frequency of 2500 Hz and 3500 Hz. There are more and higher current peaks for a pulse frequency of 3500 Hz. The measured current signal depends on the moment a shot is taken and is not fixed
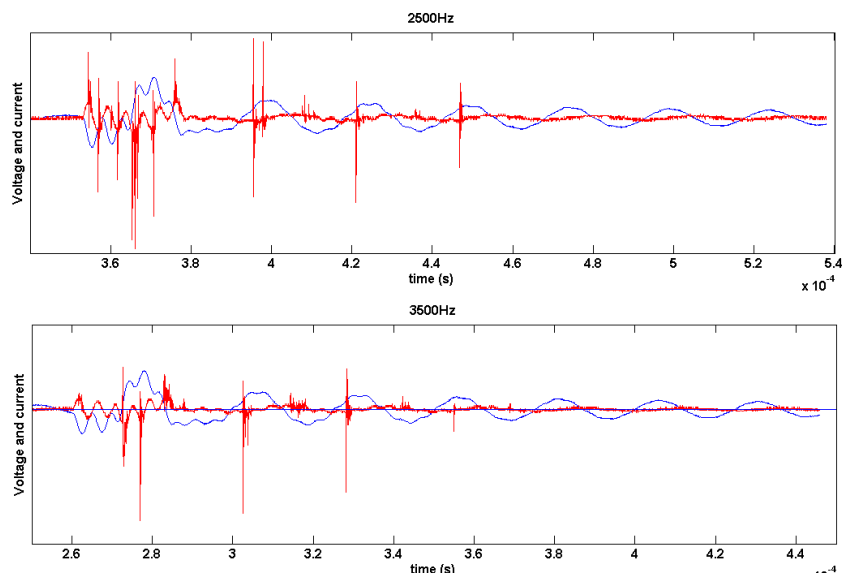

Figure B.1: *In blue the voltage signal and in red a single shot current signal. In top figure the pulse frequency is 2500 Hz and on the bottom this frequency is 3500 Hz.*